Title
Insights into DDX3X function and interactions in protein synthesis

Author
Wilkins, Kevin

Publication Date
2023

Peer reviewed|Thesis/dissertation

Insights into DDX3X function and interactions in protein synthesis

by
Kevin Wilkins

DISSERTATION
Submitted in partial satisfaction of the requirements for degree of
DOCTOR OF PHILOSOPHY

in

Biomedical Sciences

in the

GRADUATE DIVISION
of the
UNIVERSITY OF CALIFORNIA, SAN FRANCISCO

Approved:

DocuSigned by:
Hani Goodarzi
FDD44359FCC6487...

Hani Goodarzi

Chair

DocuSigned by:
Stephen Floor
DocuSigned by:
Hiten D. Madhani
DocuSigned by:
Melanie Ott
F950E29C571B493...

Stephen Floor

Hiten Madhani

Melanie Ott

Committee Members

This dissertation is dedicated to

Marina Mazzù

and

Liliana Naldini

for they inspired me to pursue knowledge

ma per seguir virtute e canoscenza

ACKNOWLEDGMENTS

Scholars are said to be able to see further for they stand on the shoulders of giants. I am fortunate to count some of said giants among my mentors, colleagues, friends, and family. In this section I would like to express my gratitude for all those who have contributed to this work and supported me through the years.

The paramount share of the recognition for the work presented here must be given to my dissertation advisor, Dr. Stephen Floor. It is an obvious understatement to say that nothing in this dissertation would have come about without his scientific, professional, and emotional support. Stephen excels as an empathetic and valuable mentor, both to students in his own lab as well as countless trainees from across the university who regularly seek his valued guidance and feedback. If I can retain a just a fraction of his commitment to academic and scientific rigor, intellectual curiosity, resilience, open and sincere communication, and understanding I shall consider myself a great scientist and human. I first met Stephen at the annual BMS retreat in Tahoe when I was a bright-eyed but unseasoned first-year student, and he was a mint-condition poster-wielding faculty member trying to attract students to his new lab. I was immediately and easily impressed by his intelligence, curiosity, knowledgeably, approachability, kindness, and sense of humor. Ever since, my reputation of him has only increased and I am continuously inspired both by his unparalleled scientific acumen as well as his boundless generosity of spirit and commitment towards his mentees and peers. I am truly grateful to him for the opportunity to join his lab, and I feel privileged to be the first in what I am confident will be long line of students to receive his invaluable mentorship.

When I first rotated in the Floor Lab, it was comprised by not much more than some empty benches, a few brand-new centrifuges, lots of inherited old instruments, and the talented Bao Thai. A mere 5.5 years later the lab has grown both in people, equipment, joviality, technical expertise, sense of community, and scientific achievement. Such growth is both a testament to Stephen's leadership and his ability to recruit great people and foster a positive environment, as well as a credit to the lab members who all, without fail, are talented, smart, amiable, and excellent lab citizens. From all, I have learned much and to all, without exceptions, I deeply indebted. I hope I have contributed to make the fun, rigorous, collaborative environment that it is today. To those currently in it and the many that will come, I can only wish a time as enjoyable and stimulating as mine was. I am immensely grateful to postdoctoral scholars Drs. Srivats Venkataramanan, Yizhu Lin, and Lorenzo Calviello, who have mentored and guided me from the very beginning of my dissertation work and have my time in the lab so formative and enriching. I have also had the pleasure to mentor Till Schroeder and Emily Ehsan; I can only hope they have learned from me as much as I have from them.

The true greatness of UCSF lies not in its rich history, vintage campus, nor plentiful scientific breakthroughs, but in its people. The collaborative and amicable environment, filled with a relaxed and unpretentious California attitude without comprising scientific rigor or hard work, is what attracted me to it and what many years later sustains my admiration. I am extremely grateful to the BMS program and all its directors, with special appreciation towards Demian Sainz, Ned Molineaux, Meredith Miner, for making it a welcoming and engaging environment and an excellent academic home. I also want to thank Drs. Michael McManus and Alex Pollen for giving me the chance to rotate in their

labs and for mentoring me freshman year. I would also like to thank Drs. Diane Baber, Licia Selleri, Danica Fujimori, Jonathan Weissman, Peter Walter, Shaeri Mukherjee and the many other faculty members on whose guidance and expertise I relied so heavily. I would like to thank our collaborators, including Drs. Jezrael Lafuente Revalde, Michelle Arkin, Debra Silver and Elliot Sherr, and the Parnassus Flow Cytometry core for the contributions and feedback in our partnership in the study of DDX3X.

I would be remiss not to acknowledge the tremendous scientistic mentorship I have received predating my time at UCSF. I would like to thank Dr. Daniela Tomatis for helping me cultivate my passion for biology in High School. I am extremely grateful to Dr. David Hyde for allowing me to join his lab for three years at the University of Notre Dame and providing me the opportunity to realize researching biology in a lab was indeed for me. I also want to thank the rest of the Hyde Lab and in particular Dr. Ryne Gorsuch for mentoring me and for teaching me, on the very first day in lab, that “90% of what we do in lab fail, but that 10% is worth the struggle”. I wish to acknowledge the mentorship, both scientific as well as personal, by the other amazing members of the faculty at Notre Dame, in particular Drs. Michelle Whaley, Patricia Champion, Rebecca Wingert, Gary Belovsky, Michael Ferdig, and Shaun W. Lee.

My deepest gratitude and appreciation to the many dear and wonderful friends that made my time in graduate school not merely bearable but enriching and amazing. My cohort, in particular Dr. Irene Chen, Jennifer Umhoefer, David Shin, Rachel Nakagawa, for sharing in the highs and lows of the UCSF and BMS experience, as well as being companions in the discovery and enjoyment of the amazing city that is San Francisco. A heartfelt thank you to Dr. Andrew Mancini for convincing me to come here, for being my

semi-official BMS mentor, and for sharing in many adventures. The laughter, support, and exploits, I have shared with Dr. Francesca Aloisio are too many to recounter but will forever be among my most cherished memories from my time at UCSF. Non-scientists are what keep us grounded, and I for that I thank Marcus Isaksson and Jane Fountain, respectively the best skier and best baker I have the honor to know. A special mention must be given to Kyle Kisor – the best roommate, friend, adventure buddy, and fellow student I could have ever asked for. I am profoundly grateful for all the amazing people, either in Torino, from Notre Dame, or in San Francisco I am privileged to call my friends. Finally, Tyler Nelson has made last few challenging months of graduate school so enjoyable with his unwavering support and deep kindness.

Everything I have ever achieved I ultimately owe to my family, my bedrock and source of joy and direction. My grandparents, Leo and Catherine Wilkins, have always proven steadfast exemplars and loving supporters. My father, John Wilkins, has always inspired me for his commitment to his beliefs. My *nonno*, Luigi Mazzù, for introducing me to the beauty of the natural world and encouraging my exploration of it. My *nonna*, Liliana Naldini, for her unconditional and steadfast encouragement and love, and for inspiring me with her boundless wisdom and knowledge. To my mom, Marina Mazzù, for being my role model and guiding star throughout my whole life. Her boundless love, hard work, adventurous spirit, resourcefulness, good nature, sense of humor, insightful mind, and love of knowledge inspire me every day. My sisters, Laura and Elena, have always bestowed upon me unconditional love and genuine support and have greatly enriched my life both in laughter and tenderness. I am fortunate to receive so much love and support from them as well as from the rest of my family.

CONTRIBUTIONS

This thesis work was performed under the direct supervision of Dr. Stephen Floor. Dissertation committee members Drs. Hani Goodarzi, Melanie Ott, Hiten Madhani, and Peter Walter provided invaluable expertise and input throughout this work.

Chapter 2 is a methods paper which I wrote together with Stephen Floor as a chapter of the 673th Volume of Methods In Enzymology, and describes *in vitro* and in cell assay strategies to probe the translational activity of RNA helicases. It has been adapted and reprinted largely as it appears in:

> Wilkins, K. C., Venkataramanan, S., & Floor, S. N. (2022). Lysate and cell-based assays to probe the translational role of RNA helicases. In *Methods in Enzymology*. Academic Press. https://doi.org/10.1016/bs.mie.2022.03.032

Chapter 3 is adopted from a manuscript being submitted for publication:

> Wilkins, K. C., Schroeder, T., Gu, S., Lafuente Revalde, J., Floor, S. N., (2023) A novel reporter for helicase activity reveals insights into DDX3X mechanism in translation. *In preparation*

"The scanning model now seems to admit of so many more possibilities than it was originally conceived to do"

From a letter from Dr. Harold Varmus to Dr. Marilyn Kozak

Harold E. Varmus Papers, 101584926X95

Insights into DDX3X function and interactions in protein synthesis

Kevin C. Wilkins

ABSTRACT

Protein synthesis is the most energy expensive process in the cell and a crucial component of most biological processes, and its dysregulation can lead to many human diseases, ranging from neurodegeneration to cancer. During translation initiation, the first and rate limiting step in protein synthesis, the small subunit of the ribosome scans the 5' untranslated region (5′ UTR) of an mRNA to identify a start codon and commence translation elongation. By unwinding and modulating secondary structures and other RNA features present in the 5′ UTR, RNA helicases can regulate ribosome scanning and start codon selection. This dissertation presents an approach to measure the effect of RNA helicases on mRNA translation initiation by employing *in vitro* transcribed 5′ UTR luciferase reporters in either an *in vitro* or a cell-based assay. These methods can be used to investigate how the perturbation of a helicase affects translation initiation at the 5′ UTR level to obtain insights into both normal and pathological conditions. This dissertation also explores the role and function of a specific RNA helicase of the DEAD-box family, DDX3X, which regulates the translation of human transcripts containing complex 5′ UTRs. Despite DDX3X's involvement in several diseases, particularly in medulloblastoma and neurodevelopment disorders, several questions abouts its function, interactions, and mRNA targets remain unanswered. We developed the helicase activity

reporter for translation (HART), a reporter that uses DDX3X-sensitive 5′ UTRs to measure DDX3X-dependent translational activity. Through SHAPE-MaP analysis, we determined the secondary structure of these 5′ UTRs and used HART to investigate the features that render them sensitive to DDX3X. Additionally, we investigated the association of DDX3X with the ribosome during scanning and identified residues 38-44 of DDX3X as potential mediators of its interaction with the translational machinery. HART revealed that both DDX3X 38-44ala and the helicase-defective mutant DDX3X R534H exhibit deficiencies in promoting translation on DDX3X-sensitive 5′ UTRs. These findings suggest DDX3X plays a crucial role in unwinding RNA structures during translation initiation through its interaction with the translational machinery. We also establish HART as a robust, lentivirally encoded, and adaptable reporter of DDX3X function.

TABLE OF CONTENTS

LIST OF FIGURES

LIST OF TABLES

LIST OF ABBREVIATIONS

5′ UTR – 5′ untranslated region

ATP – Adenosine triphosphate

AUX – Auxin, Indole-3-acetic acid

BFP – Blue fluorescent protein

CLIP – Cross-linking immunoprecipitation

CRISRP – Clustered regularly interspaced short palindromic repeats

CRISPRi – CRISPR interference

CMV - Cytomegalovirus

CTE – C-terminal extension

DMSO – Dimethylsulfoxide

eGFP – enhanced green fluorescent protein

eIF – Eukaryotic initiation factor

FLuc – Firefly luciferase

GC-content– Guanine-Cytosine content

HART – Helicase activity reporter for translation

hPGK - human phosphoglycerate kinase 1 promoter

IRES – Internal ribosomal entry site

lncRNA – long non coding RNA

MFE – Minimum free energy

mRNA – Messenger RNA

NAI - 2-methylnicotinic acid imidazolide

NTE – N-terminal extension

ORF – Open reading frame

PCR – Polymerase chain reaction

Puro – Puromycin

RLuc – Renilla luciferase

rRNA – Ribosomal RNA

RBP – RNA binding protein

SHAPE – Selective 2'-hydroxyl acylation analyzed by primer extension

siRNA – Small interfering RNA

SSFV – Spleen focus-forming virus

TISU – Translation Initiator of Short 5′ UTR

uAUG – Upstream AUG

UCOE – Ubiquitous Chromatin Opening Element

uCTG – Upstream AUG

uORF – Upstream open reading frame

WT – Wild type

CHAPTER 1

INTRODUCTION

RNA helicases in translation

mRNA translation and protein synthesis are at the cornerstone of biology, constituting a complex process that underpins the very essence of life. As the most energy-consuming endeavor within a cell (Buttgereit & Brand, 1995; Kafri et al., 2016; Rolfe & Brown, 1997), this orchestrated dance of molecular machinery transform genetic information into functional proteins, the foundation of all cellular activity (Hershey et al., 2019; Sonenberg & Hinnebusch, 2009).

Through regulation of protein synthesis the cell tailors its proteomic toolkit to meet changing environmental cues and internal demands (Hershey et al., 2019; Sonneveld et al., 2020). Strategies such as modulation of translation factors, differential mRNA isoforms, selective mRNA degradation, ribonucleoprotein complex formation, and microRNA-mediated repression, cells can swiftly respond to changing conditions, optimize energy usage, ensure precise regulation of biological processes, both preserving homeostasis as well as engage in development (Gebauer & Hentze, 2004; Mitschka & Mayr, 2022; Roux & Topisirovic, 2018; Wilkie et al., 2003).

This vital and complex molecular dance is not without its perils, as missteps or dysregulation in mRNA translation can contribute to diseases, ranging from neurodegenerative disorders, to cancers, metabolic syndromes, and more (Bhat et al., 2015; Blagden & Willis, 2011; Jishi et al., 2021; L. J. Lee et al., 2021). Unraveling the intricate links between mRNA translation, protein production regulation, and disease

offers tantalizing prospects for gaining a better understanding of human biology as well as therapeutic interventions.

A key role in regulation of mRNA translation is played by RNA helicases, which unwind and rearrange RNA molecules, often by utilizing ATP hydrolysis (Bohnsack et al., 2023; Bourgeois et al., 2016). Their function is modulating aspects of RNA structure and enabling proper mRNA processing, nuclear export, splicing, translation, and degradation, as well as ribosome biogenesis. By unzipping complex RNA secondary structures, RNA helicases grant access to key functional regions, modulate ribonucleoprotein assembly, and facilitate the passage of RNA through the ribosome. Additional roles for this class of proteins can be found in biological contexts as diverse as viral replication or response to cellular stress. As regulators and chaperones of RNA, these proteins participate in the molecular choreography that allows for proper cell functioning.

Studying the behavior and function of RNA helicases requires the developmental dn use of reliable methods and protocols that probe their effect on RNA. Chapter 2 of this dissertation describes assays to study the ability of helicases to promote translation initiation on the 5' untranslated region (5′ UTR) of given mRNA transcripts. The chapter describes the design and in vitro translation of 5′ UTR, as well as their employment in a lysate-based *in vitro* or a transfection-based in cell assay.

DDX3X: structure and function

DEAD-box RNA helicases are found in all eukaryotic cells and play important roles in a wide ranging set of biological functions (Linder & Jankowsky, 2011). These helicases are characterized by highly conserved core, constituted by two very similar domains that

resemble the bacterial recombination protein recombinase A (RecA) separated by a linker region. The core itself contains 12 conserved sequence motifs, including motif II, which includes the Asp-Glu-Ala-Asp residues (DEAD) that inspires the family's name (Tanner & Linder, 2001; Taschuk & Cherry, 2020; Wurm et al., 2021). The two RecA-like domains form a cleft which binds RNA on one side and binds and hydrolyses ATP on the other side, with the various motifs mediating one of both of these functions (Linder & Jankowsky, 2011; Tanner & Linder, 2001). Binding to ATP increases affinity for RNA while ATP hydrolysis allows for release.

Helicases of this family have been observed to act not as processive helicases, but rather as RNA clamps whose binding can destabilize RNA duplexes, although the exact mechanism is still under investigation (Hilbert et al., 2009; Linder & Jankowsky, 2011; Sengoku et al., 2006; Song & Ji, 2019). DEAD-box RNA helicases play integral roles in virtually all stages of RNA life, including transcription, editing, processing, splicing, ribosome biogenesis, nuclear export, translation, decay, stress granule regulation, assembly and remodeling of ribonucleoprotein complexes, as well as recognition and modulation or viral RNA (Andrisani et al., 2022; De Colibus et al., 2022; Kwon et al., 2022; Linder & Jankowsky, 2011; Sarkar & Ghosh, 2016; Tanner & Linder, 2001; Weis & Hondele, 2022). Given their wide-ranging functions in the cells make RNA helicases also implicated and relevant in several human diseases, in particular various cancers, developmental disorders, autoimmune diseases, and viral infection (Andrisani et al., 2022; Samir & Kanneganti, 2022; Tabassum & Ghosh, 2023).

DDX3X is a member of the DEAD-box RNA helicase family and is involved in various cellular processes, including transcription, splicing, nuclear export, translation

initiation, stress granule regulation and RNA degradation. Dysfunction of DDX3X is associated with human diseases, including neurodevelopmental disorder (Gadek et al., 2023; Lennox et al., 2020; Levy et al., 2023), inflammation (Samir et al., 2019), viral replication and infection (Hernández-Díaz et al., 2021; Soto-Rifo et al., 2013; Yedavalli et al., 2004), and several cancers, in which DDX3X has been observed to act both as a tumor suppressor and oncogene (Epling et al., 2015; Secchi et al., 2022).

Recent studies have highlighted its role in promoting translation of certain human transcripts during (Calviello et al., 2021; Oh et al., 2016; Phung et al., 2019; Ryan & Schröder, 2022). CLIP studies have observed DDX3X associating preferentially with the 5′ UTR of transcripts (Calviello et al., 2021; Gong et al., 2021; Valentin-Vega et al., 2016). This suggests a role in translation initiation, potentially akin to that of eIF4A, also a member of the DEAD-box family, which unwinds secondary structures in the 5′ UTR to allow for scanning of the smaller subunit of the ribosome through its association with the other members of the eIF4F complex, eIF4E and eIF4G (Andreou & Klostermeier, 2013; Harms et al., 2014; Marintchev et al., 2009; Parsyan et al., 2011). DDX3X itself, as well as its yeast homolog Ded1, has been suggested to associate with eIF4F components (Gulay et al., 2020; Gupta et al., 2018; Hilliker et al., 2011; Ryan & Schröder, 2022; Soto-Rifo et al., 2012) as well as the ribosome (Calviello et al., 2021; Guenther et al., 2018), but the exact characterization of these interactions as well as dynamics and their functional valence during translation initiation are unknown. Chapter 3 of this dissertation seeks to elucidate the interaction between DDX3X and the translational machinery and its impact on DDX3X's ability to promote ribosome scanning.

Unlike eIF4A, which drives overall translation and whose inhibition leads to a general decrease in translation (Galicia-Vázquez et al., 2012; Sonenberg & Hinnebusch, 2009), DDX3X has been observed to regulate only a subset of human mRNAs (Calviello et al., 2021). Understanding which human transcripts are dependent on DDX3X for their proper translation and what features they possess causes this DDX3X-sensitivity is an important step in understanding its role in translation. While factors such as 5′ UTR GC content and G-quadruplexes have been identified as contributing to DDX3X-sensitivy, the lack of clear consensus sequences from CLIP experiments suggests that DDX3X-sensitive is not driven by sequence, but possibly by structure (Calviello et al., 2021; Ryan & Schröder, 2022; Valentin-Vega et al., 2016). Other observations, such as DDX3X's role in unwinding 5′ proximal structures (Soto-Rifo et al., 2012), have yet to be tested in a systematic fashion. Chapter 3 of this dissertation characterizes DDX3X-sensitive 5′ UTRs and investigates the structural underpinnings of DDX3X-dependence during translation. Additionally, it describes the employment of sensitive 5′ UTRs for the creation of a reporter of DDX3X function, which can be employed for further systematic investigations of both 5′ UTR features that confer sensitivity as well as the effect of DDX3X perturbations on translation.

CHAPTER 2

LYSATE AND CELL-BASED ASSAYS TO PROBE THE TRANSLATIONAL ROLE OF RNA HELICASES

Kevin C Wilkins[1,2], Srivats Venkataramanan[1], Stephen N Floor[1,3]

[1]Department of Cell and Tissue Biology, University of California, San Francisco, San Francisco, California 94143, USA

[2]Graduate Division, University of California, San Francisco, San Francisco, California 94143, USA

[3]Helen Diller Family Comprehensive Cancer Center, University of California, San Francisco, San Francisco, California 94143, USA

ABSTRACT

Translation initiation is the first step in protein synthesis, during which the small subunit of the ribosome scans the 5' untranslated region (5′ UTR) of an mRNA to identify a start codon and commence translation elongation. By unwinding and modulating secondary structures and other RNA features present in the 5′ UTR, RNA helicases can regulate ribosome scanning and start codon selection. This chapter presents an approach to measure the effect of RNA helicases on mRNA translation initiation. 5′ UTR luciferase reporters are transcribed *in vitro* and employed in either of two assays. The *in vitro* assay translates the reporters in a cell-free whole-cell lysate system, which allows for greater biochemical manipulation and tighter control over confounding effects. In the alternative

cell-based approach, the reporters are transfected and translated in living cells, which provides a more physiological setup. Either method can be used to investigate how the perturbation of a helicase, such as changes in protein levels or mutations, affects translation initiation at the 5′ UTR level. The chapter also discusses alternative approaches, troubleshooting, and further applications of these methods. These assays will provide insights on the role of helicases and other translational factors as regulators of the proteome both in physiological and diseased settings.

INTRODUCTION

Translation regulation

The translation of messenger RNA (mRNA) into protein is a fundamental and tightly regulated process. Canonical cap-dependent translation starts with the recruitment of the 40S ribosome subunit and associated factors, collectively known as the 43S pre-initiation complex (PIC), to the 5′-cap of an mRNA. Recruitment is mediated by cap-binding protein eIF4E that, together with scaffolding protein eIF4G and RNA helicases, comprises the eIF4F complex. Once bound near the 5′-cap, the 43S PIC travels along the 5′ untranslated region (5′ UTR) in the 5′-3’ direction until it reaches a start codon where it is joined by the 60S large ribosomal subunit and translation elongation commences. Known as ribosome scanning, the process of the ribosome moving along a 5′ UTRs intensely regulated.

The 5′ UTR contains features that regulate protein production from the open reading frame (ORF) by altering the rate of ribosome scanning and start codon selection (Hinnebusch et al., 2016; Leppek et al., 2018). Hairpins, RNA secondary structures, G-

quadruplexes, pseudoknots, and other features can alter translation by slowing down ribosomes, preventing them from reaching the main start codon altogether, or promoting use of an alternative start codon (Hinnebusch et al., 2016; Leppek et al., 2018). Upstream open reading frames (uORFs) result from initiation at start codons before the main ORF start codon. Upstream initiation generally decreases but, more infrequently, can also increase protein production at the main ORF depending on the arrangement of the start codons and reading frames (Calvo et al., 2009; Hinnebusch et al., 2016). The strength of the Kozak sequence environment around the start codon, both of the main ORF and of the uORFs, can drastically alter their usage (Kozak, 2002). Secondary structures can stimulate usage of a uORF through proximity, which causes ribosomes to dwell longer on a start codon and initiate elongation (Kozak, 1990). Other regulatory features in 5′ UTRs include RNA modifications, RNA binding protein (RBPs) binding sites, and long non-coding RNAs (lncRNAs), which can form ribonucleoprotein complexes or interact with other RNA molecules (Leppek et al., 2018). Understanding the complex 5′ UTR regulatory network is essential for a complete picture of how protein production is regulated.

RNA helicases

One class of proteins that have an important role in modulating and interacting with 5′ UTR regulatory features are RNA helicases. The family of RNA helicases contains multiple subfamilies, some of which function as processive helicases and others function as distributive RNA chaperones (Fairman-Williams et al., 2010); we refer to this entire group as RNA helicases in this method. eIF4A, a member of the eIF4F complex and one of the canonical initiation factors, is a crucial DEAD-box RNA helicase whose role is to

unwind secondary structures in 5′ UTR to allow for ribosome progression (Iwasaki et al., 2016; Leppek et al., 2018; Pestova & Kolupaeva, 2002). The related DEAD-box RNA helicase DDX3X is similarly implicated in resolving secondary structures ahead of ribosome scanning (Calviello et al., 2021; Nashchekin et al., 2006; Sharma & Jankowsky, 2014; Soto-Rifo et al., 2012). The DExH-box RNA helicase DHX29 has also been shown to be required for proper translation of highly structured 5′ UTRs (Parsyan et al., 2009; Pisareva et al., 2008). Whether DHX29 acts by unwinding mRNA or by modulating the ribosomal RNA or a combination of both is under active investigation (Sweeney et al., 2021). Another example is provided by DHX36, which has been shown to resolve G-quadruplexes within the 5′ UTR in order to promote proper translation (Murat et al., 2018; Sauer et al., 2019). Given the importance of tightly regulating protein synthesis, it is unsurprising that many helicases involved in mRNA translation are also implicated in several diseases, particularly in cancer (Cai et al., 2017; Fuller-Pace, 2013a; Hao et al., 2020; van Voss et al., 2017; Zhao, Mao, Zhao, et al., 2016). Developing methods to functionally interrogate RNA helicases during protein production is an essential step to advancing the understanding of their role in health and disease.

Characterizing the direct role of individual RNA helicases on mRNA translation in mammalian cells presents challenges. Perturbing a given helicase to observe its role on translation in cells can be difficult, since any secondary effects on translation, transcription, or other RNA processing steps can act as confounding factors. Additionally, targeting a helicase that affects translation can alter the proteome which can indirectly affect protein production. Small molecules can be effective ways to perturb activity (Iwasaki et al., 2016; Naineni et al., 2020), but achieving specificity can be hard since

there are many similar RNA helicases (Arrowsmith et al., 2015; Calviello et al., 2021; Floor, Barkovich, et al., 2016). These challenges can complicate studies observing the direct effects of the helicase on the mechanism of translation. Reconstituted systems, particularly in yeast, have been fundamental to avoid these issues and have been an excellent source of mechanistic insight into translation initiation (Acker et al., 2007; Aitken et al., 2016). An alternative option are mRNA reporter-based *in vitro* translation assays which can measure the effects of perturbing a given helicase on translation. Such assays have also been used for other RNA binding proteins and translation factors, such as eIF3 (A. S. Y. Lee et al., 2015), as well as investigating translation by transcript isoforms (Floor & Doudna, 2016).

In this chapter, we present a protocol to measure the effect of helicases on mRNA translation. We describe how to transcribe mRNA luciferase reporters *in vitro* and how to employ them in both an *in vitro* and an *in cell* translation assay. These assays can be used to observe the effects of the perturbation of a given helicase on protein production. Observing how mutations of a given helicase, as well as alterations of its protein levels, impact translation initiation on 5′ UTRs can provide insight on its function as a regulator or protein levels as well as its malfunction in disease systems. We also outline the advantages and the limitations of the *in vitro* and *in cell* systems compared to in vivo investigations. Finally, we discuss troubleshooting, adaptations of protocol for further experiments and alternative strategies.

BEFORE YOU BEGIN

List of reagents

The reagents used in this study, including manufacturer or origin, and identifying numbers, can be found in Table 2.1.

Equipment

- Cell culture equipment and reagents
- GloMax Explorer plate reader (Promega) or equivalent
- Thermocycler
- Water bath (can also use thermocycler or thermomixer)
- Opaque 96-well plates, sterile (PerkinElmer – 6005688 or equivalent)

RNA reporters

The RNA reporters employed in this assay contain a 5′ UTR followed by a Renilla luciferase ORF (Calviello et al., 2021; Floor & Doudna, 2016; Iwasaki et al., 2016). Plasmids and full sequences are available on Addgene (Addgene ID 182638 for the minimal 5′ UTR reporter and ID 182639 for an example of an experimental 5′ UTR reporter). Other luciferases could also be used in place of Renilla. Transcription is driven by a bacteriophage T7 promoter and terminated via run-off transcription following 60 adenosine nucleotides encoded in the template downstream of the stop codon to mimic polyadenylation (Figure 2.1 A). The 5′ UTR of each reporter is chosen based on the biological question of the experiment, for example 5′ UTRs that are

sensitive to the perturbation of a given helicase or translational factor. In Calviello et al., the 5′ UTRs employed were selected among those known to be translationally controlled by DDX3X (Calviello et al., 2021). Additionally, this assay also employs a control reporter, which we refer to here as the minimal 5′ UTR reporter. As the name suggests, it possesses a minimal 8 nucleotide 5′ UTR. During data analysis, the signal of all other reporters is normalized to the signal of this control reporter to account for variations in the translational activity of the different lysates. This reporter can be modified or adapted for future experiments to obtain a control that is non-sensitive or the least sensitive as possible to the biological perturbation that is investigated.

Cells and lysates

The *in vitro* assay (step 2.2) measures the luciferase signal from RNA reporters translated for 1 hour in an enriched whole-cell lysate reaction (see Figure 2.1 B). The lysate is obtained by growing and lysing cells and then supplementing it with additional reagents (A. S. Y. Lee et al., 2015). This protocol and the papers referenced have been tested and optimized for HEK 293T, HCT-116, and HeLa cells (Calviello et al., 2021; A. S. Y. Lee et al., 2015; Venkataramanan et al., 2021). Other cells may also be employed but may require optimization and may not achieve the desired signal.

The *in cell* assay (step 2.3) measures the luciferase signal from RNA reporters transfected into cells (see Figure 2.1 C). This assay has been optimized for the same cell lines as step 2.2; using other cell types may require optimization. Because the luciferase measurement protocol requires lysis in a small volume, adherent cells are recommended.

Suspension cells may need to be removed from their media for lysis and this may prove unfeasible or compromise the strength of the signal.

Note: The relative advantages and disadvantages of the two assays are discussed in at the end of this chapter.

Perturbation of the helicase

Each experiment should include a control condition and one or more experimental conditions in which the helicase (or the translational factor) of interest is perturbed. For example, the assay can be run with cells expressing wild-type versus a mutant helicase, or cells expressing normal protein levels versus depletion. Chemical inhibition or inducible degron tags may prove advantageous, when possible, due to the rapid impact on translation before compensatory effects can occur. When using gene knockout or depletion with CRISPRi or siRNA, it is possible that some effects may be secondary in nature.

STEP-BY-STEP METHOD DETAILS

This protocol is composed of three sections. Step 2.1 describes the *in vitro* transcription of mRNA reporters (Rio, 2011). These can be used in either the *in vitro* translation assay (step 2.2) or the *in cell* translation assay (2.3) or other assays (Bai et al., 2013; Calviello et al., 2021). Quantification and statistical analysis for both assays are described in the section “Quantification and statistical analysis”. The advantages and limitations of each assay are described in at the end of this chapter, in section “Advantages and limitations”.

2.1 *IN VITRO* TRANSCRIPTION, CAPPING, AND 2'-O METHYLATION OF LONG RNAS

This protocol is for *in vitro* transcription of long RNAs off plasmid or PCR product templates (see Figure 2.1 A) (Rio, 2011). The template is purified and the size verified by running an agarose gel, and transcription occurs via a T7 promoter with a fixed 3' polyA tail encoded in the template (typically A60). Following this protocol, the RNA will be ready for transfection into mammalian cells (step 2.3) or *in vitro* translation (step 2.2) (Bai et al., 2013; Calviello et al., 2021). Significant amounts of template are necessary: at least 1 µg of template per 100 µL reaction; ideally closer to 5 µg of template, especially for very long templates. Use RNase sensitive protocols and reagents for all steps of this procedure.

PCR amplification of template

1. The DNA template is amplified using the following primers:

Reverse template primer	TTT TTT TTT TTT TTT TTT TTT TTT TTT TTT TTT TTT TTT TTT TTT TTT TTT TTT TTT TTT CTG CAG
Forward template primer	CGG CCA GTG AAT TCG AGC TCT AAT ACG ACT CAC TAT AGG

Note: The reverse primer ensures 60 thymidine residues are present on the template. This primer is used to amplify any 3’ UTR that has a

constant 3' hexanucleotide region but can be modified for higher efficiency PCR by extending the complementarity region if only one 3' UTR is being used.

2. Assemble the following PCR reaction. Prepare one reaction (total volume of 100 µL) for each of the RNAs you are transcribing.

Reagent	**Amount per 100 µL rxn**
HF buffer	20 µL
dNTP	2 µL
Forward template primer (100 µM)	0.5 µL
Reverse template primer (100 µM)	0.5 µL
Phusion polymerase	1 µL
Template (50 ng total)	10 µL
water	66 µL

3. Run PCR with a two-step protocol:

1) 98 ºC melting for 2 minutes
2) 98 ºC melting for 30 seconds
3) 67 ºC annealing for 30 seconds
4) 72 ºC annealing/extension for 3 minutes
5) Repeat steps 2, 3 and 4 for 30 cycles
6) 10 minute final extension time.

Note: Steps 2 and 3 can be also done with different PCR kits and polymerases. Regardless of which PCR kit is used, step 4 is used to check if you have the right product.

4. Run the PCRs on a native agarose gel, verify the size of the template band(s), and gel extract with a Qiagen DNA gel extraction kit (alternatively, other gel purification kits can be used). **Note**: The size of the template PCR product will be the length of the RNA reporter construct including primers. It should be 1098bp + length of the 5′ UTR for the plasmid cited in section “Before you begin: RNA reporters” but will differ if the luciferase or other transcribed regions change.
5. You have now obtained the DNA template that will be used for RNA transcription.

In vitro transcription of RNA

Note: This protocol employs purified T7 polymerase at 1 mg/mL (Rio, 2013). It is possible to transcribe the RNA by using alternative kits, such as the MEGAscript™ T7 Transcription Kit (AMB13345) and following manufacturer instructions. If using an alternative kit, assemble transcription and skip to step 5.

1. Assemble a 10X transcription buffer:

300 mM Tris-Cl, pH 8.1
250 mM MgCl2
0.1% Triton X-100
20 mM spermidine
DTT

2. Assemble ACGU solution by mixing adenosine, cytidine, guanosine, uridine 5′-triphosphate disodium salt hydrates at 25 mM each. **Critical**: Ensure solution of nucleoside triphosphates is adjusted to pH 7. **Note**: The solution can be stored long term at -20 ºC.
3. Warm all reagents for step 4 except T7 polymerase and Superase:IN to room temperature. **Note:** Adding cold spermidine to template can cause precipitation of the template.

4. Assemble the transcription reaction by mixing the following in a tube at room temperature. If you are transcribing more than one RNA, assemble a master mix, split it into different tubes, and add the templates separately. **Note**: This reaction can be run in either a 1.5 mL tube or a PCR tube.

Reagent	**100µL reaction (µL each)**
Template (from step 2.1.1)	1 to 5 g
ACGU (25 mM)	30 µL
10X txn buffer (RT)	10 µL
DTT (1M)	2 µL
MgCl2 (1M)	1 µL
T7 polymerase (1 mg/mL)	10 µL
Superase:IN	1 µL
RNase-free H2O	Up to 100

1. Incubate at 37 °C in a stable incubator - a water bath, stable dry incubator, or PCR thermocycler. Warm rooms and heat blocks can have higher variability in temperature that may decrease reproducibility.
2. Wait one hour and check the reactions - they should be somewhat cloudy from pyrophosphate precipitation. If they are, add 1 µL of 1 mg/mL pyrophosphatase to each. ***Note:*** *Reactions that are not cloudy might also have worked, although it is less likely. You can proceed* with

the protocol and check if non-cloudy reactions were successful with a glyoxal gel.

3. Allow the reactions to proceed for 3-4 hours.
4. Add 1 µL of RQ1 RNase-free DNase to each reaction and incubate at 37 °C for 30 minutes to digest the template.
5. Precipitate transcription products by adding 200 µL 0.3M NaOAc pH 5.2, 1 µL GlycoBlue and 750 µL 100% EtOH to each reaction. **Note**: If the reactions were run in a 1.5 mL tube, add these directly to the tube. If the reactions were run in a smaller tube, add these to a new 1.5 mL tube and then transfer the reactions into the tube.
6. Incubate at -80 °C for >1 hour to overnight.

   Pause point: The samples can be kept at stored at -80 °C for months.

Resuspending EtOH precipitated RNA

1. Pellet precipitations by centrifugation at 16,000 g at 4 °C for 25 minutes.
2. Remove supernatant with a pipette and discard.
3. Wash with 500 µL -20 C° 70% EtOH.
4. Centrifuge at 16,000 g at 4 C° for 5 minutes.
5. Remove supernatant with a pipette and discard.
6. Quick-spin and remove residual ethanol with a P20 pipet.
7. Allow pellet to air dry for 5 minutes **Note:** Do not overdry as this can impact recovery.
8. Resuspend pellet in 100 µL 50 mM EDTA.

9. Purify RNA with Zymo RNA Clean & Concentrator 25 column following the small RNA removal protocol and elute in 30 µL RNase-free H_2O.
10. Measure concentration of RNA on a nanodrop or Qubit or other assay.

Quality control: glyoxal gel

1. RNA molecules will fold intramolecularly and may not run according to their sequence length in a native gel. Chemical modification of adenine, cytidine, and guanosine bases by glyoxal reduces intramolecular secondary structure, promoting size-dependent migration of RNA molecules without using formamide or other denaturing gels.
2. Add 2 µL of the NorthernMax™-Gly Sample Loading Dye to 2 µL of each RNA. Add 5 µL of the dye to 5 µL of the RNA ladder. Incubate reactions for 30 min at 50 °C (Rio, 2015).
3. Run samples on an 1% agarose gel. Make the gel and run it in 0.5X TBE buffer. **Critical**: Ensure the gel and the running buffer are made from RNase free water to prevent RNase contamination.
4. Check size of the products.
5. If degradation products are apparent on the agarose gel, use image quantification software to quantify the band corresponding to full-length product and use this to determine concentration in combination with nanodrop readings.

6. Alternatively, if significant truncated products are present purify the full-length product by agarose gel purification using the Zymo Agarose Gel Zymoclean kit (R1011).

Capping and 2'-O-Methylation

1. Dilute 20 µg of RNA in 26 µL RNase-free H_2O in a PCR tube.
2. Prepare a 4 mM stock of SAM (supplied with Vaccinia kit) in RNase-free H_2O from the supplied 32 mM stock.

   Note: SAM is labile and should not be freeze-thawed repeatedly. If reusing SAM supplied in a kit, aliquot on first thaw to avoid freeze-thaws. Degraded SAM will interfere with proper mRNA capping and reduce translation efficiency.

3. Assemble a master mix according to the following recipe.

Reagent	**per 40 µL reaction**
10X NEB capping buffer	4 µL
10 mM GTP	2 µL
4 mM SAM	2 µL
NEB Vaccinia capping enzyme	2 µL
NEB 2'-O-Me transferase	2 µL
RNasin	2 µL

4. Add 14 µL of the master mix to each PCR tube from step 1.
5. Incubate at 37 C° for 60 minutes.
6. Purify over a Zymo Clean and Concentrator 25 column following the small RNA removal protocol and elute in 30 µL RNase-free H_2O.
7. **Optional:** Run a second glyoxal gel as in step 2.1.27 to verify your RNAs are the correct size.

2.2 *IN VITRO* TRANSLATION ASSAY

The RNA reporters transcribed in 2.1 can be used in an *in vitro* translation assay. In this assay, the transcribed reporters are translated for one hour in whole-cell lysate. The luciferase produced is then measured (see Figure 2.1 B). The whole-cell lysate, while not perfectly reproducing the biology of a living cell, presents the opportunity to easily manipulate the reaction by adding or removing chemical compounds, proteins, or other factors. In addition, the optimized *in vitro* reaction provides a short timeframe (which reduces unwanted secondary effects) and a high translation signal.

Materials

Lysis Buffer

10 mM Hepes, pH 7.6
10 mM KOAc
0.5 mM MgOAc2
5 mM DTT
Complete EDTA-free protease inhibitor (1 tablet per 10mL buffer)
(make in RNase-free water and keep on ice)

Note: The buffer can be stored at 4 ºC, but the protease inhibitor must be added fresh.

Making the lysate

1. Grow cells in 15 cm plates, making 5-10 plates at a time. **Note:** Do not let cells reach high confluency levels since this inhibits translation. Actively replicating cells are best suited for this protocol.
2. Treat your cells to obtain cells with the desired helicase perturbation and the appropriate control cells (as discussed in section “Before you being: Cells and lysates”). **Note:** For example, cells expressing WT or mutant helicase can be used to create a WT and mutant lysates. Alternatively, cells expressing normal levels and knock-out for the helicase of interest can be used to obtain lysates. See section “Before you being: Perturbation of the helicase”.

3. Trypsinize the cells by adding 4 mL trypsin to each plate and stop by adding 4 mL complete media and move into a conical tube.
4. Spin 1 minute at 1000 g, 4 C° to pellet.
5. Wash the pellet with PBS and transfer to a 1.5 mL microcentrifuge tube.
6. Spin down the pellet and remove the PBS.
7. Add equal volume of Lysis Buffer to the pellet. **Note**: The volume of Lysis Buffer added needs to match the pellet approximately 1:1. To obtain this, check the volume of the pellet at the bottom of the 1.5 mL tube by eye and add the equal amount of Lysis Buffer. To ensure all lysates are made the same way, you can weigh all the pellets first. Add the Lysis Buffer to the first tube, and then adjust the amount of Lysis Buffer added to the other tubes in proportion to the weight.
8. Dissolve the pellet by pipetting up and down, do not vortex.
9. Incubate the tubes on ice for 45 minutes. This induces hypotonic swelling in the cells.
10. Homogenize the cells. This is done by aspirating slowly the lysate into a 1 mL syringe with 26G (subq) needle. Then, push the lysate out quickly with the needle against the side of the tube. Repeat 13 times.

Note: Squirting the cells through the needle and against the tube helps completely break down the cell membranes, which were previously made fragile by the hypotonic swelling.

11. Check under light microscope for disruption with trypan blue (blue nuclei signify lysis). Disrupt until ~95% is done.
12. Centrifuge the tubes at 14000 g for 1 min, 4 ºC to remove cell debris and nuclei.
13. Collect the supernatant. These are the lysates for the assay.

    Note: any antibody depletion or other biochemical manipulations to the lysate can be performed at this step.

14. Aliquot and flash freeze the lysate in liquid nitrogen. Put at -80 ºC. **Note**: An aliquot of the lysate (diluted into lysate buffer 10:1) can be run on a western blot.

    Pause point: The lysates can be stored at -80 ºC.

Running the assay

1. Each RNA assay will be run as three technical replicates; the number of total reactions will be the number of RNAs times three. **Note**: If you do more than eight total replicates, it is easiest to run the assay in a 96-well PCR plate, and then image it on a 96-well opaque flat-bottom plate.

2. For each RNA, mix in a tube:

Reagent	**1 replicate**
100mM ATP	0.042 µL
10mM GTP	0.105 µL
1M Creatine Phosphate	0.105 µL
7.5U/µL Creatine phosphokinase	0.03 µL
1 M Hepes pH7.5	0.05 µL
0.1 M DTT	0.1 µL
40 mM MgOAc	0.25 µL
2 mM KOAc	0.25 µL
1mM amino acids	0.04 µL
Spermidine (.02295M)	0.056 µL
Murine RNAse inhibitor	0.125 µL
Lysate	2.5 µL
(Usually 100-200ng) RNA	1.348 µL

Note: The concentration of MgOAc and KOAc may require optimization based on the control 5′ UTR and/or the cell type used. It is recommended to test ranges of 25-150 mM for the MgOAc and ranges 1-3 mM for the KOAc.

Note: To minimize variability, we recommend making a 3X master mix for each RNA construct, and then splitting into three replicates.

Note: The concentration of RNA needed to obtain enough signal will vary by 5′ UTR construct since different 5′ UTR have different translational activity. Optimization might be required for each construct. Initial values can range from 20 to 200 ng total RNA per replicate.

3. Incubate for 1 hour at 30 ºC (PCR Block).
4. Transfer the content of the 96-well PCR plate into a 96-well opaque flat-bottom plate. **Note**: Make sure the plate is opaque and compatible with luciferase luminescence measurement.
5. Image the luciferase signal. **Note**: Luciferase measurement protocols will vary based on the kit and apparatus used. **Example**: For the Renilla Luciferase Assay System (Promega) measured on a GloMax Explorer luminometer (Promega) **Steps:** 1) Transfer each reaction to a well in a 96-well plate 2) add lysis buffer to each well 3) leave 15 minutes on rocker 4) place in machine and follow machine measurement protocol.

2.3 *IN CELL* TRANSLATION ASSAY

The RNA reporters transcribed in **2.1** can also be used for an *in cell* assay. In this assay, transcribed reporters are transfected into living cells that produce luciferase protein for 24 hours, which is then measured (see Figure 2.1 C). The longer incubation time for the translation step compared to the *in vitro* assay in step **2.2** may leave more time for non-translation related confounding effects to take place. On the other hand, it provides a more physiologically relevant system since it takes place in living cells instead of lysate.

Grow cells and transfect

1. Grow cells in a sterile 96-well opaque flat-bottom plate.

Critical: This plate will be used for the whole experiment, including growing cells, transfecting them with reporter RNAs, and measuring the luciferase signal. Make sure the plate is compatible with the luminometer (in particular, the plate must be opaque to prevent signal leaking between wells).

Note: Since the plate is opaque, it is not be possible to observe the cells under a microscope during the experiment. To obviate this issue, we recommend plating a “mirror” 96-well transparent culture plate in parallel with the same number of cells and transfecting them in the same manner as in the experimental plate. These cells will be able to be observed and will mirror the conditions of the cells used for the experiment. Alternatively, cells can be grown and transfected in a transparent culture plate. Cells will then

be lysed, and the lysate moved to the opaque plate for luciferase measurement.

2. Plate cells at ~80% confluency. **Note:** Confluency and plating timeline may need to be optimized based on cell type.
3. After 48 hours, transfect cells with a mixture of 10 ng *in vitro* transcribed firefly luciferase (Fluc) RNA with a minimal 5′ UTR and between 50–200 ng renilla luciferase RNA (Rluc) downstream of selected 5′ UTRs using the TransIT mRNA Transfection Kit (Mirus Bio) per manufacturer's instructions.
4. Lyse cells 24 hours post transfection.
5. Measure luciferase values with the Dual-Luciferase Reporter Assay System (Promega) on a GloMax Explorer luminometer (Promega) or similar instrument, following manufacturer's instructions.

2.4 QUANTIFICATION AND STATISTICAL ANALYSIS

For the *in vitro* translation assay (section 2.2)

1. The data obtained from the plate reader will consist of a luminescence value for each replicate. **Note**: These values are dimensionless (See table 2.2).
2. Inspect the luminescence values to ensure there is sufficient signal to analyze the results. Typical successful experiments have ranged from luminescence values in the 10^3 to 10^8 range. Observe if there are large differences between neighboring wells – note that luminescence will bleed from high signal wells into lower signal wells. Multiple order-of-magnitude signal differences should be avoided between neighboring wells.

3. Divide the Renilla luminescence value of each replicate by the average value of the replicates obtained from the same lysates as that well and the control RNA reporter. This step normalizes the values of all RNA reporters to that of the control RNA reporter translated with the same lysate. This returns values for each reporter and condition that are normalized to the control and helps account for differences in translational activity of each lysate (See step 1 in table 2.2).
4. Secondly, divide the resulting value for each replicate by the average value of all replicates for the same RNA reporter for the control lysate. This step will return the relative signal obtained for each reporter with that of the same reporter in the control lysate. **Note**: The values for all reporters in the control lysates will be equal to 1, while the values for the reporters with the experimental lysates will represent level of translation relative to the control (See step 2 in table 2.2).
5. Following the above steps, the average value of all replicates of mRNA reporters in control lysates are normalized to 1. The impact of the perturbation of an RNA helicase on translation of a given mRNA is the difference between the experimental lysate versus the control. **Note**: The values for the control mRNA reporters will average to 1 across all lysates, since they are the normalization factor. This reflects the in-built assumption of this assay that the control reporter is insensitive to perturbations of the helicase. This assumption can be tested using an orthogonal luciferase, but there may be perturbations that impact all translation.
6. Statistical analysis can be run for each reporter to compare the values of the replicates in each lysate relative to the other lysates. For the example provided,

statistical significance between conditions was calculated with an unpaired two-tailed *t*-test.

7. Finally, the data can be visualized, for example using a box plot with data points (See Figure 2.2).

For the *in cell* translation assay (section 2.3)

1. Normalize the Renilla luciferase signal in each well by dividing it by the Firefly luciferase signal from the same well. This is done to control for cell number, transfection efficiency, and basal translation levels of each well.
2. The resulting values obtained for each well are then divided by the average of the values of the wells with control cells.
3. The average value of all replicates of the mRNA reporters transfected in the control cells will be equal to 1. The average values of the replicates of a given mRNA reporter transfected in the treated cell will reflect the translational level relative to the control. **Note**: The values for the control mRNA reporters will average to 1 across all cells, since they are the normalization factor. This reflects the in-built assumption of this assay that the control reporter is insensitive to perturbations of the helicase.
4. Statistical analysis can be run for each reporter to compare the values of the replicates in each cell treatment relative to control and other treatments. For the example, statistical significance between conditions was calculated with an unpaired two-tailed *t*-test.
5. Finally, the data can be visualized, for example using a bar graph. (See Figure 2.2)

3. Expected Outcomes

The luciferase luminescence values will change both depending on the intrinsic translation level of different reporter constructs and the perturbations to RNA helicases. Reporters with decreased luciferase levels upon helicase perturbation depend on the helicase of interest for efficient translation, while reporters with increased luciferase levels are inhibited by the helicase of interest. Some helicases that operate during translation initiation like eIF4A will likely be overall promoters of translation (Linder & Jankowsky, 2011; Sen et al., 2015), although they might inhibit translation of a subset of transcripts (Calviello et al., 2021). It is important to note that reporters might behave differently to knockdown vs missense mutations of helicases (Calviello et al., 2021; Lennox et al., 2020).

ADVANTAGES AND LIMITATIONS

Advantages

The mRNAs reporter, as constructed, isolates a specific part of the mRNA on which the effect of the helicase can be determined. In the case of the reporters described here, they differ solely in their 5′ UTR, hence the impact that is measured on translation can be attributed to translation initiation. The reporters in this protocol are transcribed, capped, and polyadenylated mRNA *in vitro*. This allows isolating the effect of the helicase on translation alone, without having to account for potential effects during DNA or pre-mRNA processing.

The short 1 hour translation timeframe of *in vitro* assay allows for tight control and focuses the assay predominantly on translation. The time constraint limits the possibility

of secondary effects due to proteome changes and RNA-processing steps in which the helicase might be involved. The protocol, which has been optimized to increase translational output, allows for increased signal. Additionally, conducting the assay in a whole-cell lysate makes it amenable to manipulations that might be impossible in a cell system. This includes the addition of drugs, purified proteins, and reagents that are hard to deliver in cells or the removal of factors from the lysate with IP or similar techniques. Biochemical manipulation of the lysate can be performed, such as immunodepletion of factors, addition of recombinant proteins, or addition of compounds that are not cell permeable.

Compared the *in vitro* assay, the *in cell* assay offers more physiological relevance since translation occurs within living cells. For example, our prior work identified a difference in *CCNE1* 5′ UTRtranslation between in vitro and in cell experiments, which could be caused by cell cycling (Calviello et al., 2021).

Limitations

There are situations where reporters do not recapitulate native regulation (Mitschka & Mayr, 2021). Another factor to take in account is that the reporters contain a limited amount of the mRNA of interest (in this case the 5′ UTRs), which might exclude other important regulatory features and miss important biological information. Additionally, given the overexpression of the reporters and/or the helicase, the stoichiometry of factors in the assay might differ from physiological conditions. Finally, given how data normalization is conducted, is necessary to find control 5′ UTRs that are not regulated by helicase of interest, which may not always be possible.

The *in vitro* assay is more removed from the biology of the cells, since it lacks important features of the cells such as the cell wall, organelles, and the cell cycle. Similarly, the whole-lysate reaction is composed of diluted cytoplasm and additional reagents, providing for an environment that may differ in composition and stoichiometry from physiological conditions. Finally, there can be substantial variability in specific activity between batches of lysate, although the normalization to the control reporter is designed to minimize this noise.

The timeframe of *in cell* assay is significantly longer than for the *in vitro* assay, which may lead to a greater opportunity for secondary effect downstream of the perturbation of the helicase to act as confounding factors. Additionally, there is a greater possibility that the helicase might affect the mRNA reporters by non-translational means, such as through mRNA nuclear shuttling or mRNA decay. This assay tends to give lower signal compared to the *in vitro* assay, given the fact that lacks the additional reagents that optimize and boost its translational output. Additionally, given the inefficiency of transfection, it requires higher amounts of mRNA.

OPTIMIZATION AND TROUBLESHOOTING

Poor or no signal:

- *In vitro* transcription is a delicate procedure, and improperly transcribed mRNA, the transcription of an incorrect isoform, or insufficient levels of reporter may result in poor or no signal. Ensure to run a glyoxal gel to control the size, integrity, and amount of product. Ensure that all reagents are free from RNase which will degrade the reporters.
- Another possibility is low signal whole-cell lysate which is not translationally active. This might result from the lysate having been collected when the cells were too confluent (as this inhibits translation), the frozen lysate being too old or having been freeze-thawed too many times, or the use of cell lines that are not optimal for translation.

The experimental signal matches the control

- A lack of differences between the measurement obtained by the experimental and the control conditions may be due to the control 5′ UTR (or control mRNA element) being sensitive to the perturbation of the helicase to the same degree as the experimental 5′ UTR. To solve this problem, select a different control 5′ UTR that is likely to be the least sensitive to regulation by the helicase of interest. Another solution is to employ a firefly reporter as internal control (as described in step 2.3). It may be useful to employ an internal ribosomal entry site (IRES) to drive the translation of the internal control firefly reporter, as many IRESs require different and often fewer translation factors and may not be sensitive to the helicase of interest (Pisarev et al., 2005).

The *in vitro* data does not match the *in cell* data:

- The data collected with the *in vitro* assay (step 3.2) may not match up with that collected with the *in cell* assay (step 3.3), even if the same reporters and same experimental conditions are employed. This might be due to non-translation related processes (such as mRNA export or decay) or other secondary effects of the helicase. These may be occurring in the *in cell* setup but may not have the time to take place in the short time span of *in vitro* assay. Additionally, it may be caused by the involvement of biological features of the cell, such as organelles or the cell cycle, that are lost in the whole-cell lysate setup. Finally, the amount of mRNA per reaction/cell, the confluency and translational potential of cells, and other variables might be different between the two assays.

ALTERNATIVE METHODS/PROCEDURES

In addition to the translational assays here presented, there are several alternative methods to measure the translational effect of a given helicase:

- Ribosome profiling is a powerful technique that can provide genome wide and transcript specific information on the translational effect of RNA helicases (Calviello et al., 2021; Ingolia et al., 2019). This technique maps all footprints of actively translating ribosomes onto the transcriptome, allowing to detect changes in translation due to the perturbation of a helicase (Guenther et al., 2018).
- Other techniques that measure global translation include polysome profiling, 35S methionine, FUNCAT, or puromycin staining (Aryanpur et al., 2019;

Dieterich et al., 2010; Goodman et al., 2012; Guenther et al., 2018; Murat et al., 2018). Combined with the appropriate experimental setup, these methods can provide insight in the effects of helicases on the translatome.

- For the impact of helicases on the translation of specific proteins, methods such as fluorescence-based reporters in cells, western blotting, or direct measurement of protein levels can be employed. The use of translation inhibitors can test whether the changes observed are translationally mediated.
- Rabbit reticulocyte lysate and wheat germ extract are well established and highly efficient *in vitro* eukaryotic protein synthesis systems that can be employed to translate reporters in a cell-free context (Chong, 2014). While these systems may have less physiological relevance for the investigation of human helicases compared to the protocols described in section 2.3, they may be more robust and more amenable for certain reporters and experimental setups. These systems also generally have higher specific activity.

SUMMARY AND CONCLUSION

As the first step of protein synthesis, translation initiation is fundamental and tightly regulated process in every cells. Helicases play an important role by modulating and interacting with the 5′ UTR and its many structural features. In particular, several helicases unwind complex secondary structures, such as hairpins and g-quadruplexes, or modulate uORF selection allowing for proper regulation of ribosome scanning. Gaining insight of how helicases affect translation will unlock a more complete understanding of their role as regulators of the proteome both in physiological and diseased settings.

This chapter explores helpful ways to investigate the effect of helicases on mRNA translation initiation. Starting with *in vitro* transcribed, capped, and polyadenylated luciferase 5′ UTR reporters allows for assays that restrict probing to the aspect of translation itself, removing confounding effects such as DNA and RNA processing. Two assays are described in this chapter: an *in vitro* approach, with employs the mRNA reporters in a cell-free whole-cell lysate system, and an *in cell* approach, in which the reporters are transfected into living cells. Either method can be used to investigate how translation initiation at 5′ UTR is affected by RNA helicases. While the *in vitro* method offers tighter controls and fewer confounding effects, the *in cell* approach can offer a more physiologically relevant setup.

Although the protocol described here measures the effect of helicases on translation initiation by using 5′ UTR reporters, it is adaptable to further use. Other mRNA features, such as the 3'UTR, individual regulatory elements and structures, ORF features, or even point mutations in the mRNA can be used as reporters in the same fashion. Similarly, this protocol can be used to investigate not only the translational role of helicases, but of any protein or factor with translational implication, including chemicals compounds.

ACKNOWLEDGMENTS

The authors wish to thank Malvika Tejura and Bao Thai for their contributions. This work was supported by the National Institutes of Health DP2GM132932 and R01NS120667 (to S.N.F.) and the California Tobacco-Related Disease Research Grants Program 27KT-0003 (to SNF) and T30DT1004 (to KCW). S.N.F. is a Pew Scholar in the Biomedical Sciences, supported by The Pew Charitable Trusts.

FIGURES

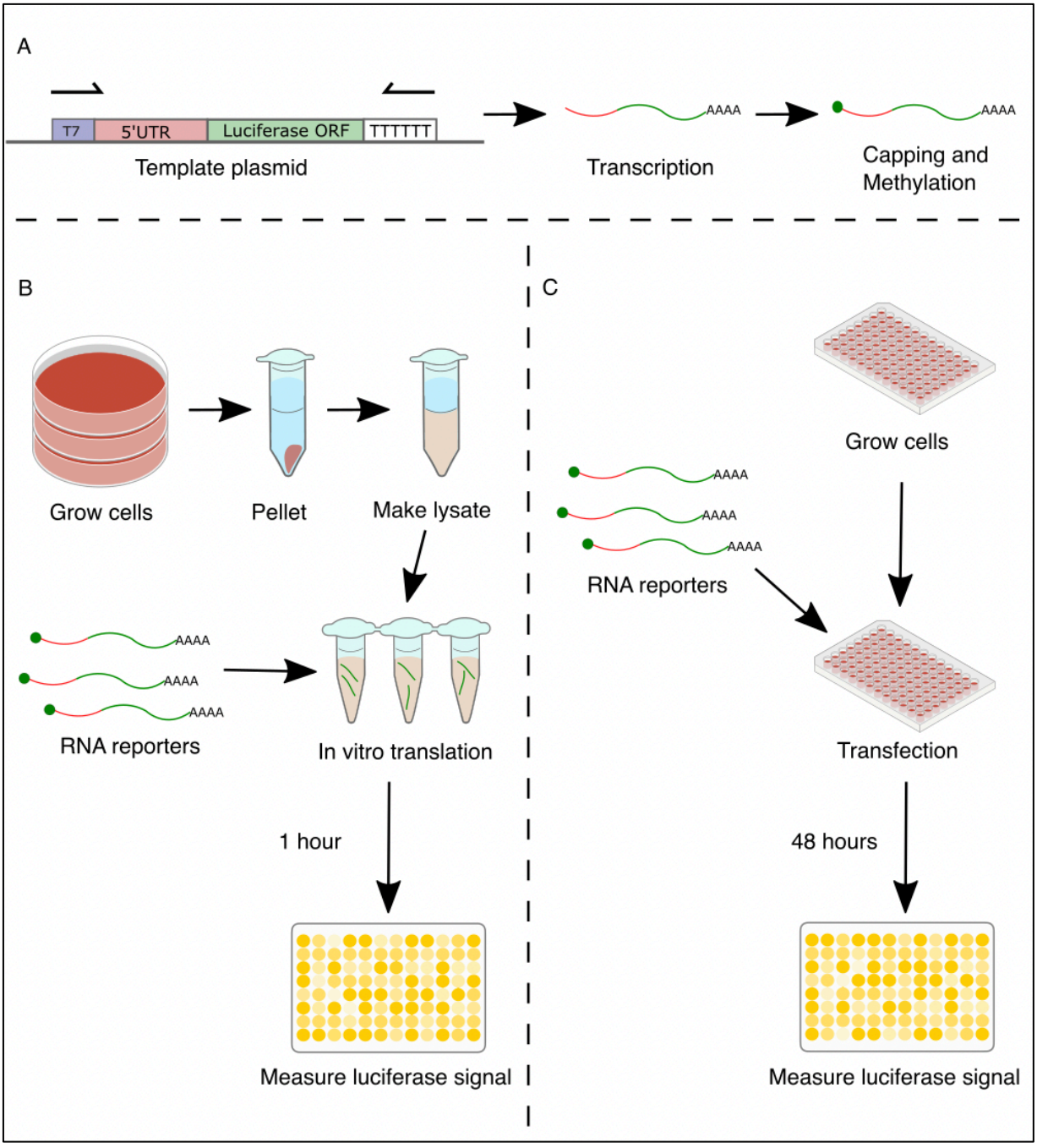
A
T7
5'UTR
Luciferase ORF
TTTTTT
Template plasmid
Transcription
AAAA
Capping and
Methylation
B
Grow cells
Pellet
Make lysate
RNA reporters
In vitro translation
1 hour
Measure luciferase signal
C
Grow cells
RNA reporters
Transfection
48 hours
Measure luciferase signal

Figure 2.1 Schematic of the transcription of the reporters and the in vitro and in vivo translation assays. A) In vitro transcription of RNA reporters. The template plasmid contains a T7 promoter followed by a 5′ UTR (either the control or a 5′ UTR of interest), followed by the luciferase open reading frame (ORF) and a string of Adenosines. PCR on this plasmid is used to obtain the template DNA containing the reporter. The DNA is then used to transcribe the RNA reporters. The reporters are then capped and methylated. B) *In vitro* assay. Cells are grown, pelleted, and lysed to obtain the whole-cell lysate. The lysate is enriched and combined with the mRNA reporters in a 1 hour translation reaction. The reactions are moved to an opaque plate and the luciferase signal is measured. C) *In cell* assay. Cells are grown in an opaque plate. The mRNA reporters are transfected into the cells. After 24 hours, the media is removed and the cells are lysed, and the luciferase signal is read on an imager.

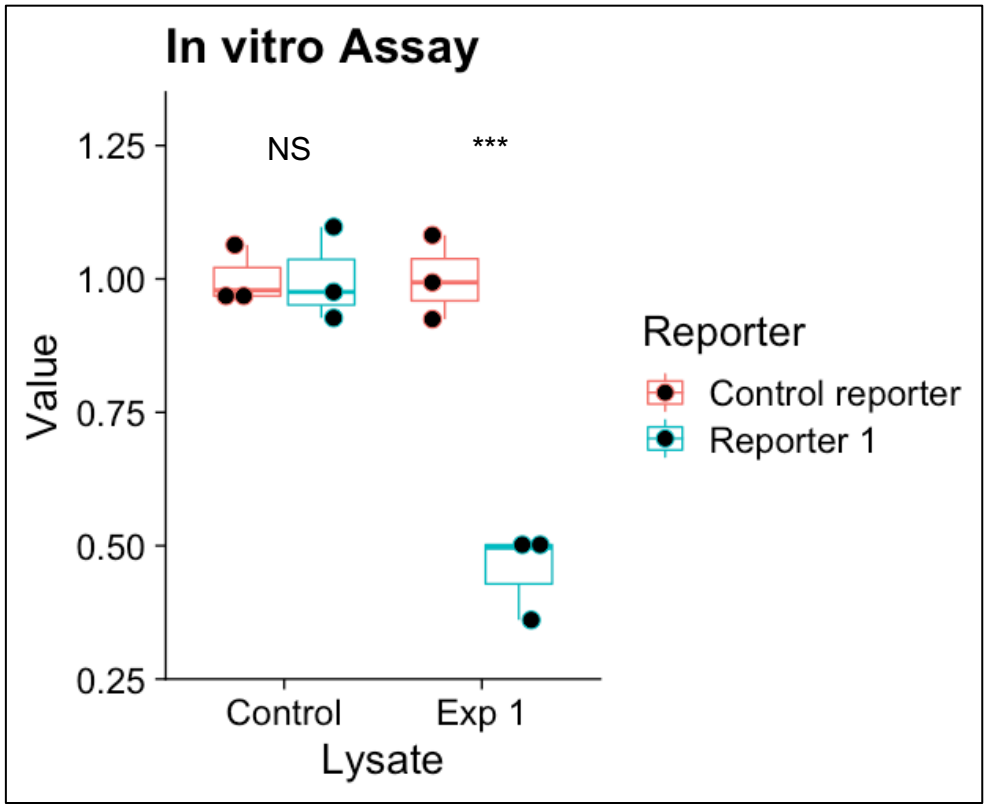

Figure 2.2 Data visualization for the translation assay. The final values data obtained from normalization in Table 2.2 can be plotted. Both the control and experimental reporters will give final normalized values of 1 with the control lysate since they are the values on which the normalization is calculated. This is also true for the value of the control reporter in the experimental lysate. This graph shows that the translation of the experimental reporter goes down in the lysate experimental lysate compared to the control lysate. The dots represent the three technical replicates. Statistical significance was calculated with an unpaired two-tailed *t*-test (*** = P<0.005).]

TABLES

Table 2.1 List of reagents. This table contains the list of reagents used in this chapter, including the name, manufacturer or source, and identifying number.

Reagent	Source	Identifier
2'-O-methyltransferase (enzyme, buffer, SAM)	NEB	M0366S
Adenosine 5′-triphosphate disodium salt hydrate	Sigma-Aldrich	A7699
Cytidine 5′-triphosphate disodium salt	Sigma-Aldrich	C1506
Guanosine 5′-triphosphate sodium salt hydrate	Sigma-Aldrich	G8877
Uridine-5'-triphosphate trisodium salt	Sigma-Aldrich	U6750
1mM Amino Acids	Promega	L4461
ATP	Sigma-Aldrich	A26209
cOmplete™, Mini, EDTA-free Protease-Inhibitor-Cocktail	Merck	4693159001
Creatine Kinase (CK) from rabbit muscle	Merck	10127566001
Creatine Phosphate	Merck	10621714001

Reagent	Source	Identifier
DTT	Gold Bio	DTT500
EDTA 500 mM, pH 8.0	Teknova	E0308
EtOH	VWR	V1101
GlycoBlue™ Coprecipitant	Ambion/ThermoFisher	AM9516
Hepes pH 7.6	Gold Bio	H-400
KOAc	Sigma-Aldrich	P5708
MgCl2	Sigma-Aldrich	M2670
MgOAc2	Sigma-Aldrich	M5661
Murine RNAse inhibitor	NEB	M0314S
NaOAc pH 5.2	Fisher Scientific	P171-500
NorthernMax™-Gly Sample Loading Dye	Ambion/ThermoFisher	AM8551
RNase-free DNase	Promega	M6101
RNasin Ribonuclease Inhibitor	Promega	N2611
Spermidine	Sigma-Aldrich	S2626
Superase:IN	Ambion/ThermoFisher	AM2696
TBE 10X Concentrate	VWR	E442
T7 polymerase (1 mg/mL)		
Tris-Cl, pH 8.1	Gold Bio	T-095-100
Triton X-100	Sigma-Aldrich	T8787

Reagent	Source	Identifier
Vaccinia capping enzyme system (enzyme, buffer, SAM, GTP)	NEB	M2080S
Zymo Clean & Concentrator 25 columns	Zymo Research	D4033
Promega Dual Glo	Promega	E2920
Renilla Luciferase Assay System	Promega	E2820

Table 2.2 Quantification and Statistical Analysis. The raw data obtained from the plate reader will consist of numerical luciferase luminescence value for each technical replicate. The averages that need to be calculated for step 1 are shown. Step 1) The raw value of each replicate is divided it by the average value of the replicates obtained from the same lysate as with the control RNA reporter. This normalizes each replicate's value to the baseline translational activity of its lysate. The averages that need to be calculated for step 2 are shown. Step 2) The intermediate resulting value for each replicate was divided by the average value of all replicates obtained with the same RNA reporter for the control lysate. This step will return the signal obtained for each reporter relative to the same reporter in the control lysate.

	Lysate - control						**Lysate – experimental condition 1**					
	Reporter: control			**Reporter 1**			**Reporter: control**			**Reporter 1**		
Replicate:	**1**	**2**	**3**	**1**	**2**	**3**	**1**	**2**	**3**	**1**	**2**	**3**
Raw values	225000	230000	250000	380000	400000	450000	470000	505000	550000	320000	440000	450000
	average is 235000						*average is 508333*					
Step 1	*divide by 235000*			*divide by 235000*			*divide by 508333*			*divide by 508333*		
	0.957	0.979	1.064	1.617	1.702	1.915	0.925	0.993	1.082	0.630	0.866	0.885
	average is 1			*average is 1.7446*								
Step 2	*divide by 1*			*divide by1.7446*			*divide by 1*			*divide by 1.7446*		
Final values	0.957	0.979	1.064	0.927	0.976	1.098	0.925	0.993	1.082	0.361	0.496	0.507
	average is 1			*average is 1*			*average is 1*			*average is 0.4547*		

CHAPTER 2

A NOVEL REPORTER FOR HELICASE ACTIVITY REVEALS INSIGHTS INTO DDX3X MECHANISM IN TRANSLATION

Kevin C. Wilkins[1,2], Till Schroeder[1], Sohyun Gu[1], Jezrael Lafuente Revalde[3], Stephen N. Floor[1,4]

Affiliations

[1] Department of Cell and Tissue Biology, University of California, San Francisco, San Francisco, California 94143, USA

[2] Graduate Division, University of California, San Francisco, San Francisco, CA, United States

[3] Department of Pharmaceutical Chemistry, University of California, 600 16th Street, San Francisco, California 94143, United States

[4] Helen Diller Family Comprehensive Cancer Center, University of California, San Francisco, San Francisco, California 94143, USA

ABSTRACT

DDX3X regulates the translation of human transcripts containing complex 5′ untranslated regions. In this study, we developed a reporter called HART that uses DDX3X-sensitive 5′ UTRs to measure DDX3X-dependent translational activity. Through SHAPE-MaP analysis, we determined the secondary structure of these 5′ UTRs and used

HART to investigate the features that render them sensitive to DDX3X. Additionally, we studied the association of DDX3X with the ribosome during scanning and identified residues 38-44 of DDX3X as potential mediators of its interaction with the translational machinery. HART revealed that both DDX3X 38-44ala and the helicase-defective mutant DDX3X R534H exhibit deficiencies in promoting translation on DDX3X-sensitive 5′ UTRs. These findings suggest DDX3X plays a crucial role in translation initiation through its interaction with the translational machinery, and establish the HART reporter as a robust, lentivirally encoded measurement of DDX3X-dependent translation in cells.

INTRODUCTION

DDX3X is a ubiquitously expressed RNA-helicase involved in almost all stages of RNA metabolism (Sharma & Jankowsky, 2014; Soto-Rifo & Ohlmann, 2013), including transcription (Chao et al., 2006; Saikruang et al., 2022), RNA export (Lai et al., 2008; Yedavalli et al., 2004), pre-mRNA splicing (Merz et al., 2007; Zhou et al., 2002), translation (Calviello et al., 2021; Shih et al., 2008; Soto-Rifo et al., 2012; Venkataramanan et al., 2021), microRNA expression (Hk et al., 2016; Nussbacher & Yeo, 2018), and viral RNA interactions (Heaton et al., 2023; Rao et al., 2021). By influencing gene expression, RNA localization, and RNA stability, DDX3X impacts cellular functions and responses, including cellular homeostasis (Tsai et al., 2017), stress granule regulation (Shih et al., 2012; Valentin-Vega et al., 2016), cell stress (Oh et al., 2016; Samir et al., 2019), cell signaling (Sharma & Jankowsky, 2014), the immune response (Soulat et al., 2008; Szappanos et al., 2018), and embryonic development (C.-Y. Chen et al.,

2016; Lennox et al., 2020). Alterations to *DDX3X* are linked to several human diseases, including cancer, viral infection, inflammation, and developmental disorders (Gadek et al., 2023; Mo et al., 2021; Sharma & Jankowsky, 2014).

DDX3X is a member of the DEAD-box RNA helicase family and hydrolyzes ATP to unwind RNA molecules and remodel RNA-protein complexes (Linder & Jankowsky, 2011). DDX3X shows high conservation with its yeast homolog Ded1 and form a clearly defined subfamily (Fairman-Williams et al., 2010). DDX3X/Ded1 helicases are characterized by a conserved helicase core domain which contains nine conserved motifs involved in ATP binding, hydrolysis, and RNA interaction (Linder & Jankowsky, 2011; Sharma & Jankowsky, 2014). While the helicase core is highly conserved across the DEAD-box family, the N- and C-termini are more variable (Floor, Condon, et al., 2016; Linder & Jankowsky, 2011). These termini are involved in protein-protein interactions and subcellular localization, but their role is yet to be fully understood (Sharma & Jankowsky, 2014).

DDX3X is thought to play a role in translation by unwinding RNA secondary structures and remodeling RNA-protein complexes. DDX3X/Ded1 are suggested to interact with components of the translation initiation complex, including the eIF4F complex (eIF4E, eIF4G, and eIF4A), to promote ribosome binding to the mRNA's 5' cap structure and enhance the recruitment of ribosomes to the mRNA (Guenther et al., 2018; Gulay et al., 2020; Gupta et al., 2018; Sharma & Jankowsky, 2014; Shih et al., 2012). As opposed to eIF4A, a generalist necessary for global translation, DDX3X has been observed to act as a specialist helicase, required for the proper translation of a subset of the human mRNAs (Calviello et al., 2021; Linder & Jankowsky, 2011). This specialized role could

derive from DDX3X/Ded1's higher RNA unwinding capability compared to eIF4A, suggesting that DDX3X might be required to resolve complex and highly structured 5′ UTRs (Gao et al., 2016).

Several aspects of DDX3X's activity during ribosome scanning and translation are still incompletely understood. The 5′ UTR features that confer dependency on DDX3X are an active area of study. Further, while DDX3X has been observed to interact with helix 16 of the 18S rRNA, a component of the small ribosomal subunit (Calviello et al., 2021) the function and extent of its association with the ribosome and other translation factors is still unclear. Given the substrate-dependency of DDX3X's role in diseases, a better picture of such variables is necessary for insights into the broader landscape of translation regulation and its implications in health and disease.

DDX3X exhibits a dual role in cancer, acting either as a tumor suppressor or an oncogene, depending on the context and the specific mRNA transcripts it regulates during translation (Fuller-Pace, 2013a; Secchi et al., 2022; Zhao, Mao, Zhou, et al., 2016). Examples of oncogenic behavior include high DDX3X expression being associated with poor prognosis in non-small-cell lung cancer (NSCLLC) and head and neck squamous carcinoma (HNSCC) (H.-H. Chen et al., 2018; Heerma van Voss et al., 2015; Stransky et al., 2011; van Voss et al., 2017). In HNSCC, DDX3X promotes translation of ATF4 and other oncogenic mRNAs, although the exact mechanism is unknown (H.-H. Chen et al., 2018). Conversely, DDX3X acts as a tumor suppressor in cancers like medulloblastoma, colorectal cancer, and non-small-cell lung cancer, where its loss is associated with increased colony formation and invasiveness (Fuller-Pace, 2013a; C.-H. Lee et al., 2014; Oh et al., 2016; Zhao, Mao, Zhou, et al., 2016).

The diverse behavior of DDX3X in cancer, functioning as both an oncogene and a tumor suppressor, is likely attributed to specific mutations within DDX3X and the distinctive structural characteristics of the 5′ UTRs of mRNA molecules present in different cell types or cancer subtypes. These variations in transcriptional substrates can give rise to distinct translational outcomes for various oncogenes or tumor suppressors, contributing to the progression of cancer (H.-H. Chen et al., 2018; Kozak, 1991). Identifying the mechanism of DDX3X function in translation and the features of mRNA transcripts it regulates will help provide insights into cancer progression and potential therapeutic targets.

DDX3X's role in mRNA processing and translation has been linked to several other diseases. DDX3X-related is a neurodevelopmental disorder is a type of global developmental delay (GDD) associated with structural brain defects in which DDX3X mutants with RNA helicase activity cause induce ectopic RNA-protein granules in neural progenitors and neurons and impair translation (Gadek et al., 2023; Hoye et al., 2022; Lennox et al., 2020). DDX3X is essential in the replication of several viruses, such as HIV-1 or HCV, and is implicated in in host-virus interaction, viral replication, antiviral responses, and immune evasion (Hernández-Díaz et al., 2021). Analyzing the transcriptional substrate context influenced by DDX3X in translation provides critical insights into the on the key genes, pathways, biological processes, and pathogenesis of intellectual disability and viral infections. Given the lack of current effective therapies to treat DDX3X(Gadek et al., 2023), this knowledge can aid in the development of targeted

therapeutic strategies to restore normal translation control and mitigate the detrimental effects of DDX3X dysregulation in these diseases.

In this chapter, we created a helicase activity reporter for translation (HART) to measure the translational activity of DDX3X. We characterized the structures and features of DDX3X-dependent 5′ UTRs and employed HART to dissect this sensitivity to DDX3X. We then identified residues in the N-terminus of DDX3X that interact with the ribosome and used HART to determine that this interaction is important for DDX3X's role in translation. Together, our work advances the understanding of the mechanism of DDX3X-dependent translation and creates a versatile reporter with potential implications in both further dissection of DDX3X function and drug discovery.

RESULTS

Creating a reporter for the translational activity of DDX3X

To better understand the mechanism of DDX3X, we created a reporter for the translational activity of DDX3X. We first identified human transcripts whose proper translation is dependent on DDX3X. Prior work showed that the loss of DDX3X caused a decrease in ribosome density on a subset of transcripts, including ODC1, RAC1, and HMBS (Calviello et al., 2021). The 5′ UTRs of these transcripts require DDX3X for efficient translation *in vitro* and in cells (Wilkins et al., 2022). We define these sequences as DDX3X-sensitive 5′ UTRs and reasoned we could use them as the foundation of a reporter for DDX3X translation activity in cells (Figure 3.1 A).

We incorporated four different DDX3X-sensitive 5′ UTRs into a construct we called helicase activity reporter for translation (HART, Figure 3.1 B). HART is a lentiviral plasmid

built around a dual promoter, containing a copy of human PGK (hPGK) and mini CMV, which is an efficient bidirectional promoter in cells and *in vivo* (Amendola et al., 2005). We used hPGK to direct transcription of a DDX3X-sensitive 5′ UTR followed by the open reading frame (ORF) of the fluorescent protein mCherry. The mini CMV promoter was used to direct transcription of a DDX3X-insensitive 5′ UTR followed the ORF of eGFP to act as an internal control. The DDX3X-insensitive 5′ UTR consists of a short 9 nt sequence (CTAGCCACC) which was previously used as a control in cellular and *in vitro* assays of DDX3X-sensitive translation (Calviello et al., 2021). To better detect changes in protein levels, we fused mCherry to the ornithine decarboxylase (ODC) degron (d4), which confers a protein half-life of 4 hours (Yen et al., 2008). In the HART reporter, mCherry protein levels are a proxy for translation of DDX3X-sensitive transcripts, while eGFP protein levels are independent of DDX3X changes and act as an internal control. The mCherry/eGFP ratio, which we refer to as the HART ratio, is thus a readout of DDX3X's ability to promote translation.

To validate the reporter system, we assessed the impact of DDX3X loss on the HART ratio. We depleted endogenous DDX3X using an inducible degron system in the male colorectal cancer HCT 116 cells (Calviello et al., 2021; Natsume et al., 2016). Treating the DDX3X degron cells with auxin for 48 hours results in near complete degradation of DDX3X protein (Figure 3.1 E). We transduced HART into the DDX3X degron cells and treated them with auxin for 48 hours. Flow cytometry measurements of the ratio of mCherry to eGFP signal identified a significant decrease in auxin-treated cells compared to the DMSO-treated control in HART constructs containing HMBS, ODC1, or RAC1 but not RPLP1 5′ UTRs (Figure 3.1 C, Figure 3.2 A). These results were in line with

previous in cell and *in vitro* translation assays (Calviello et al., 2021; H.-H. Chen et al., 2015; Perfetto et al., 2021). Notably, there was no difference in eGFP fluorescence levels between auxin-treated cells and controls, while mCherry levels exhibited significant differences, demonstrating that the change in HART ratio between treatments was driven by the DDX3X-sensitive 5′ UTR (Figure 3.2 B-C). Microscopy measurements were consistent with flow cytometry, confirming the reliability and generalizability of HART-ODC1 and HART-RAC1 (Figure 3.1 F). Overall, these results collectively demonstrated the effectiveness of HART as a reporter for evaluating DDX3X's impact on translation initiation.

Structural probing of the RAC1 and ODC1 5′ UTRs

DDX3X is necessary for the proper translation of several human mRNAs, but the precise understanding of which 5′ UTR structures and features render a given transcript sensitive to DDX3X remains incomplete. Prior work has implicated upstream start codons, RNA structure, GC content, and other mRNA features as important in DDX3X-based regulation (Calviello et al., 2021; H.-H. Chen et al., 2015; Lai et al., 2016; Soto-Rifo et al., 2012). However, experimental evidence of RNA structure in DDX3X-sensitive mRNAs is limited. To gain deeper insights into the elements that confer DDX3X sensitivity to the RAC1 and ODC1 5′ UTRs, we used SHAPE-MaP structure probing to experimentally determine their secondary RNA structures (Smola et al., 2015; Smola & Weeks, 2018). We transcribed the RAC1 and ODC1 5′ UTRs and the luciferase ORF *in vitro* using T7 polymerase (Calviello et al., 2021; Wilkins et al., 2022). RNA was then folded, probed with NAI or DMSO as control, reverse transcribed, and sequenced. Mutation profiles and

SHAPE reactivity were measured using SHAPE-MaP and used to generate SHAPE-constrained RNA secondary structures using SHAPEmapper (Figure 3.3 A-D).

The SHAPE-MaP constrained structure for RAC1 is complex, comprising a 152 bp long structure and a 23 bp stem loop (Figure 3.3 A-B). The RAC1 5′ UTR has predicted free energy of -97.20 kcal/mol and 79% GC content. The RAC1 SHAPE-MaP result obtained *in vitro* is similar to the one obtained in cells (Figure 3.4 A-B) or via *in silico* predictions using RNAfold (Figure 3.4 C). The ODC1 5′ UTR also showed a highly complex structure, with a long 376 bp structure with several smaller hairpins branching off it and a shorter 107 bp structure, with an overall free energy of -251.70 kcal/mol (Figure 3.3 C-D) and a 69% GC content. These *in vitro* probing results are overall similar to an RNAfold prediction (Figure 3.4 D).

The presence of large stem loops and overall high complexity of these 5′ UTRs could impede efficient translation initiation in the absence of the unwinding and remodeling activity of helicases (Pisareva et al., 2008). DDX3X may be crucial in resolving these stable stem loops and enabling mRNA accommodating into the small ribosomal subunit or scanning across the 5′ UTR to identify the translation start site. Previous work has suggested that Ded1, the yeast homolog, has a higher unwinding activity than eIF4A, which may position Ded1/DDX3X as a specialist helicase required to unwind particularly complex structures (Gao et al., 2016).

Dissection of RAC1 and ODC1 DDX3X-sensitivity

We next sought to determine which regions of the ODC1 and RAC1 5′ UTRs contribute to DDX3X-sensitivity. We created HART constructs with five equal size

deletions tiling the 5′ UTRs of both RAC1 (Figure 3.5 A and B) and ODC1 (Figure 3.5 A and E). The HART ratio was used to measure the translation efficiency of deletion constructs in HCT-116 degron cells after 48 hours of auxin or DMSO treatment.

Deletions of the 79-117, 118-157, and 158-197 regions of the RAC1 5′ UTRs residues conferred similar DDX3X-sensitivity compared to full length wildtype. However, deletion of residues 1-39 led to diminished sensitivity, while deletion of residues 40-78 showed an even further reduction to the point where there was no statistical difference between cells treated with auxin or DMSO. The 1-39 and 40-78 deletions overlap the large structure in the RAC1 5′ UTR, suggesting that unwinding of this structure by DDX3X is important in translational regulation of the 5′ UTRs (Figure 3.5 B). This is consistent with prior work that identified an important role for cap-proximal RNA structures in DDX3X-dependent translation (Soto-Rifo et al., 2012). Notably, *in silico* folding predicts the Δ40-78 RAC1 5′ UTRs possess the lowest free energy among all the deletions, suggesting that a less stable structure exhibits decreased sensitivity to DDX3X (Figure 3.6). In contrast, we find that deletions in the ODC1 5′ UTR do not impact DDX3X sensitivity, suggesting its overall GC content or structure may be sufficiently complex that no single deletion removes a requirement for DDX3X (Figure 3.5 G). Taken together, we find that DDX3X sensitivity is mediated by regions within some but not all DDX3X-sensitive mRNAs.

The 38-44 residues of DDX3X contribute to its association with the translational machinery

The dynamics of DDX3X unwinding of 5′ UTR structures during ribosome accommodation and/or scanning are currently unknown. One possibility is that DDX3X unwinds structures ahead of ribosome scanning independently and untethered from the ribosome or other ribosome-associated factors, in a *trans* mechanism. Alternatively, it is possible that DDX3X is bound to the ribosome or associated factors during scanning and that it unwinds 5′ UTRs while tethered, in a *cis* fashion. The *cis* scenario would be like the behavior of related DEAD-box RNA helicase eIF4A which associates with the ribosome during scanning (Brito Querido et al., 2020). Some evidence for the *cis* model is provided by iCLIP data, which suggests that DDX3X binds to the helix 16 of the 18S rRNA in the small subunit of the ribosome, which is located near the mRNA entry channel (Calviello et al., 2021). Interestingly, a similar result was also found in yeast, where iCLIP identified helix 16 as crosslinking with Ded1, the yeast homolog of DDX3X (Guenther et al., 2018).

While helix 16 is a potential location of binding of DDX3X to the ribosome, it is unknown what part of the DDX3X protein is responsible for this interaction. DDX3X contains two RecA-like domains that make up the helicase core. The helicase core is flanked by the N-terminal extension (NTE) and the C-terminal extension (CTE), which are essential for helicase activity (Epling et al., 2015; Floor, Condon, et al., 2016). Finally, the N-terminus and the C-terminus are present at the extremities of the protein and contain several regions conserved across the DDX3X/Ded1 subfamily and divergent regions (Figure 3.7 A), although (Sharma & Jankowsky, 2014).

DDX3X could interact with the translational machinery through the functional core, one or both termini, or multiple locations. One factor that suggests this interaction is happening in the termini is the possible conservation of this binding between DDX3X and its yeast homolog Ded1 (Guenther et al., 2018). Taken together, these data indicate that the N- and C- termini of DDX3X play a functional role and may mediate interaction with the ribosome.

To determine which regions in DDX3X interact with the translation machinery, we transduced HEK 293T cells with FLAG-tagged full length DDX3X or a truncated 132-607 mutant, and conducted FLAG immunoprecipitation. WT, but not 132-607, co-precipitated small ribosomal subunit protein RPS11 and eIF4A, suggesting a loss of interaction with the translation machinery for the truncated mutant (Figure 3.8 A).

Having identified the N- and C-termini as locations potentially mediating binding to the ribosome, we then attempted to narrow down the location of the ribosome-binding domain. We made constructs of FLAG-tagged DDX3X with alanine substitutions across termini residues conserved across the DDX3X family, including amino acids 14-21, 38-44, and 600-603 (Figure 3.8 B). These constructs were transduced into HEK 293T cells from which RNase-treated lysates were obtained and used for FLAG immunoprecipitation. DDX3X WT co-purified with the small ribosomal subunit protein RPS11 and translation factors eIF4E and eIF4A, which are associated with the scanning ribosome (Kumar et al., 2016). Conversely, the different mutants lost interaction with these proteins to different degrees. Both 14-21 and 600-603 mutant showed a similar ability to pull down eIF4E and eIF4A, but a reduced ability to pull down RPS11. The helicase deficient mutant R534H pulled down RPS11 to the same degree as wild type,

but lost interaction with eIF4E and eIF4A. Finally, the mutant with alanine substitutions spanning the 38-44 residues, which we refer to as 38-44ala, presented the most severe difference from wild type, with greatly reduced copurification of RPS11, eIF4E, and eIF4A (Figure 3.7 B, Figure 3.8 B). This suggests that the 38-44 residues of DDX3X are involved in mediating the interaction with the ribosome, whether directly or indirectly through other intermediary proteins.

The 38-44 residues (YIPPHLR) are conserved across the DDX3X/Ded1 subfamily but absent in other DEAD box proteins (Sharma & Jankowsky, 2014). This sequence has been previously identified as potential eIF4E-binding region because it is reminiscent of the consensus eIF4E-binding YXXXXLΦ found in several eIF4E-binding proteins such as the 4EBPs and eIF4G (Figure 3.7 C). substitution of Tyr38 or Leu43 to alanine partially ablated co-immunoprecipitation of DDX3X and eIF4E in HeLa lysate (Shih et al., 2008), in a fashion similar to our own observation of the lack of co-precipitation between 38-44ala and eIF4E. We hence decided to test whether these residues mediate DDX3X's indirect interaction with ribosome via direct binding to eIF4E.

To directly test whether the 38-44 region of DDX3X interacts with eIF4E, we used NMR spectroscopy. We purified ^{15}N labeled *S. cerevisiae* eIF4E, which shares the core conserved peptide binding site with human eIF4E (Joshi et al., 2004). The ^{15}N HSQC spectrum of eIF4E bound to m7GTP was well-dispersed, indicating a stable, folded protein (Figure 3.7 D). Addition of 1 mM of a peptide comprising human 4E-BP1 amino acids 51-67 elicited dramatic chemical shift changes (Figure 3.7 E), consistent with the known interaction between 4E-BP1 and eIF4E. In contrast, addition of a peptide comprising human DDX3X amino acids 33-51 caused minimal chemical shift

perturbations (Figure 3.7 F). We therefore conclude that human 4E-BP1 binds to *S. cerevisiae* eIF4E, but that DDX3X amino acids 33-51 does not directly interact with *S. cerevisiae* eIF4E.

The lack of co-immunoprecipitation between mutant DDX3X and ribosomal proteins could be due to altered protein localization. To test this possibility, we used microscopy to determine the localization of the different DDX3X variants. HEK 293T cells were transduced with different DDX3X-FLAG constructs, fixed, and stained for anti-DDX3X and the nuclear marker DRAQ7. DDX3X protein was broadly cytoplasmic, and neither the R534H mutation, nor 38-44ala, nor the double mutant 38-44ala/R534H altered this localization compared to WT (Figure 3.7 G). We have therefore identified the 38-44ala residues as contributors to the interaction between DDX3X and the ribosome or its associated factors, though likely not substantively through direct interactions with eIF4E.

Ribosome-association plays a role in DDX3X function

Having identified a DDX3X mutant that impacts its association with the ribosome, we next investigated the effect of losing this interaction on the DDX3X's translational activity. HCT-116 degron cells were transduced with both the HART construct and DDX3X-FLAG-BFP, either WT or helicase defective R534H, 38-44ala, or the double mutant 38-44ala/R534H. FACS was used to obtain a triple-positive population for mCherry, eGFP, and BFP. These cells were treated with auxin for 48 hours and flow cytometry was used to measure the HART ratio.

The HART-ODC1 ratio of auxin-treated cells co-transduced with WT DDX3X was increased compared to parental cells, although not to the same level as control DMSO-

treated cells. This suggests the exogenous DDX3X partially rescued the translation defect caused the loss of endogenous DDX3X. Instead, transduction of R534H nor 38-44ala nor the double mutant 38-44ala/R534H not only did not rescue the effect, but further decreased the HART ratio compared to uninfected cells suggesting a dominant effect (Figure 3.9 A). Results for HART-RAC1 showed no increase nor decrease in HART ratio in WT, 38-44ala, or R534H/38-44ala cells compared to uninfected, while infection R534H did show a statistically significant decrease compared to uninfected cells (Figure 3.9 B).

For both reporters, The R534H mutation seems to have a negative effect across 5′ UTRs. This is in line with DDX3X helicase mutations acting as dominant negative in translation assays as well as in human disease (Calviello et al., 2021; Epling et al., 2015; Gadek et al., 2023; Lennox et al., 2020). In contrast, the 38-44 mutant seems to have a dominant negative effect on ODC1 but a neutral effect on the RAC1 reporter. Interestingly, in both cases the dual mutant R534H/38-44ala followed the pattern of 38-44ala, suggesting that loss of association with the ribosome or associated factors is dominant over helicase mutations in the context of translation. This can be explained in the *cis* model of DDX3X activity, where interaction with the ribosome is necessary for its role in translation. The helicase defective DDX3X R534H mutants has a dominant negative effect on transcripts but the 38-44ala mutation rescues the effect. These results suggest that interaction with the ribosome or associated factors plays a role in the translational activity of DDX3X, although different 5′ UTRs are regulated differently.

Lentiviral transduction can lead to differential expression of the exogenous construct across cells. We used the BFP signal, which is a proxy for the expression of DDX3X-FLAG, to investigate the effect of DDX3X expression level on the HART ratio.

Notably, higher BFP levels in DDX3X-FLAG-BFP expressing cells correlated with a reduction in the difference of the HART ratio between auxin and DMSO treated cells, indicating dosage sensitivity (Figure 3.9 C). In contrast, increasing levels of DDX3X mutants either had no effect (38-44ala) or diminished the HART ratio (R534H and R534H/38-44ala) (Figure 3.9 C). These results indicate dosage sensitivity of DDX3X and suggest dominant repression of DDX3X-dependent translation by inactive, pathogenic DDX3X mutants.

We also investigated the effect of DDX3X mutants on cellular growth. We first tested whether the N and C-termini of DDX3X were important for cell growth through rescue experiments. While exogenous full length DDX3X rescued cell-growth defects due to the loss of endogenous DDX3X, neither helicase defective mutant DDX3X R534H nor the functional core DDX3X 132-607 did (Figure 3.9 D and Figure 3.10 A). DDX3X 38-44ala and R534H containing cells did not rescue the cell growth defect caused by the loss of endogenous DDX3X, unlike cells infected with WT DDX3X (Figure 3.9 D). DDX3X 38-44ala exhibited a similar growth phenotype to DDX3X 132-602, a truncation which preserves the functional core but removes the N and C-termini (Figure 3.10 A). These data suggest that both helicase function and the association with the ribosome are crucial to DDX3X function in proliferation.

Our data shows that the 38-44 residues of DDX3X contribute to its interaction with the translational machinery. This interaction, whether direct with the ribosome or mediated by other factors, is important for DDX3X's role in unwinding secondary structures in the 5′ UTR of a subset of human mRNAs and regulate translation (Figure 3.9 E).

METHODS

Molecular cloning

DNA amplification was obtained by PCR with either KAPA HiFi HotStart ReadyMix (Roche) or Q5 High-Fidelity 2X Master Mix (New England Biosystems #M0492) following manufacturer protocol unless otherwise noted. PCR products were digested with 1 µL DpnI (NEB #R0176L) for 1 hour and purified by agarose gel extraction (MinElute Gel Extraction Kit, Qiagen #28606). Plasmid constructs were created by Gibson cloning with NEBuilder HiFi DNA Assembly Master Mix (NEB #E2621L) or Gibson Assembly Master Mix (NEB E2611L). Assembled plasmids were transformed into Mach1 competent cells (Invitrogen #C862003) or STBL3 (from Q3 Macrolab at University of California, Berkeley) for amplification and were purified with QIAprep miniprep (Qiagen #27104).

DNA sequences

The bidirectional promoter lentiviral plasmid backbone for HART was a gift of the Goodarzi lab and published in Amendola et. al, 2005. The 5′ UTRs of RAC1, HMBS, ODC1, and RPLP1, and control were taken from plasmids from previous work (Calviello et al., 2021). Deletions in RAC1 and ODC1 were achieved by Gibson cloning. The mutated d4 ornithine decarboxylase (ODC) degron fused to mCherry was inserted via primers with Gibson cloning based on the published sequence:

(AGCCATGGCTTCCCGCCGGAGGTGGAGGAGCAGGATGATGGCGCGCTGCCCAT

GTCTTGTGCCCAGGAGAGCGGGATGGACCGTCACCCTGCAGCCTGTGCTTCTGCT

AGGATCAATGTG) (Yen et al., 2008). Gibson cloning was used to insert all the HART elements into the lentivirus UCOE-SFFV backbone. The final HART construct is: PuroR-T24-eGFP-[control5′ UTR]-miniCMV-hPGK-[DDX3X-sensitive5′ UTR]-mCherry-d4ODCdegron.

Plasmids were deposited on Addgene. Plasmid IDs:

KW54_HART_ODC1 #207398

KW57_HART_RAC1 #207399

KW63_HART_RAC1_PuroR #207400

KW78_HART_ODC1_PuroR #207401.

Lentiviral DDX3X constructs were created by inserting the DDX3X sequence from previous work into the UCOE-SFFV backbone (gift from the James K Nuñez lab) via Gibson cloning. Lentivirus packaging plasmids included gag/pol, REV, TAT, and VSVG (gift from the Weissman lab). Gibson cloning was also employed to generate the various mutations via primers containing said mutations. BFP and Puromycin resistance sequences were taken from pHR-SFFV-dCas9-BFP-KRAB (Addgene # 46911) and Twist respectively. The final DDX3X lentiviral construct sequence is: UCOE-SSFV-DDX3X-3xFLAG-2xP2A-TagBFP-PuromycinR

Cell culture

HCT116 cells were cultured in McCoy's 5A media (Gibco #16600082) and 10% FBS (Avantor #97068-085) and 1X Penicillin-Streptomycin Solution (Corning #30002CI).

HEK 293T cells were cultured in DMEM with 4.5 g / L glucose, L-glutamine & sodium pyruvate (Corning #10-0130CV) and 10% FBS (Avantor #97068-085) and 1X Penicillin-Streptomycin Solution (Corning #30002CI). Cells were cultured at 37 °C in 5% CO_2. Cell passage was done with trypsin (Corning #25-053-CI). Cells were washed with 1X PBS pH 7.4 (Gibco #70011044) before media change and passaging.

Lentivirus packaging and infection

For packaging lentivirus, HEK 293T cells were kept at confluency below 90% for several passages. On day 1, HEK 293T cells were plated at $1.2X10^6$ cells/well in 6 well plates. On day 2 cells were transfected with lentiviral DNA following the Mirus-LT1 (Mirus MIR 2300) transfection protocol. Briefly, 6 µL transfection reagent Mirus-LT1 were mixed with 250 µL Opti-MEM (Thermo Fischer #31985062) and incubated at room temperature for 15 minutes. 1.5 µg of the desired lentiviral DNA with 0.1 µg gag/pol, REV, and TAT packaging plasmids and 0.2 µg VSVG packaging plasmid (for a total of 2 µg of DNA) were added to the Opti-MEM mix. The mix was incubated at room temperature for 15 minutes, and then gently added to the HEK 293T cells dropwise. On day 4, the virus-containing supernatant was harvested by gentle pipetting and filtered with a low protein binding syringe filter (0.22 µm, EDM Millipore # SLGV033RB). The virus was frozen at -80 °C for long-term storage or transduced directly into the desired cells.

Cells to be transduced were plated in 24 well plates at $0.168x10^6$ cells/well on day 1. On day 2, the lentivirus supernatant collected previously was added to the cells. Different amounts of virus, ranging from 5 to 500 µL was added to each well together with

8ug/mL polybrene (EMD Millipore TR-1003-G). The plates were spun down for 2 hours at 1000 RPM at 37 °C. On day 4, cells were sorted as described below. The appropriate amount of virus was determined by sorting cells from wells with infection rates below 30%.

Cells in Figures 1 and 3 were transduced with HART constructs containing the indicated DDX3X-sensitive 5′ UTR. Cells in Figure 3.7 were transduced with DDX3X constructs. Cells in Figure 3.9 were transduced both with the indicated HART and DDX3X constructs.

Flow cytometry

For cells transduced with the HART constructs in Figures 1 and 3, FACS was used to sort cells positive for both eGFP and mCherry. For cells transduced with the DDX3X constructs in Figure 3.7 , cells positive for BFP were sorted. For cells transduced with both HART and DDX3X constructs in Figure 3.9 , cells positive for eGFP, mCherry, and BFP were sorted.

FACS was performed using Fortessa SORP to measure the florescent signal of eGFP (488nm 50mW laser, Blue B or Blue C), mCherry (561nm. 50mW laser, YG C detector) and BFP (405nm 100mW laser, Violet F detector). Untransduced cells were used as negative controls for gating after filtering for single cells.

Sorted cells were used for the HART experiments in Figures 1, 3, and 5. Cells were plated in 24-well plates at 0.168×10^6 cells/well with 2 mL of media. 500 mM Auxin (Indole-3-acetic acid, RPI # I54000-25) in DMSO (Corning #25950CQC) or DMSO alone were added at a 1:1000 dilution to the media. After 48 hours, cells were trypsinized with 200

µL trypsin and resuspended with 200 µL media. Cells were then flowed with a Fortessa X20 Dual SORP. Untransduced cells were used as negative controls for gating after filtering for single cells. Cells were gated as single cells and double positive for eGFP (488nm 60mW laser, Blue C detector) and mCherry (561nm 50mW laser, YG C detector) for Figures 1 and 3, and in as triple negative for eGFP, mCherry, and BFP 405nm 100mW laser, Violet F detector) in Figure 3.9 . The raw value of the three channels was exported. The ratio of mCherry/eGFP was calculated as the HART redout.

Cell growth curves

Cells were plated in opaque 96-well plates at 5000 cells per well. Cell number was measured at the indicated time intervals with CellTiter-Glo® Luminescent Cell Viability Assay (Promega #G7571) and following manufacturer's instructions.

RNA folding prediction

RNA folding predictions were computed using the ViennaRNA Package (Version 2.5.1) (Lorenz et al., 2011; Zuker & Stiegler, 1981).

SHAPE-MaP

SHAPE-MaP was conducted as described (Smola et al., 2015; Smola & Weeks, 2018). First, we *in vitro* transcribed RNA as described (Wilkins et al., 2022). RAC1 and ODC1 5′ UTRs were placed under control of a T7 promoter and in front of luciferase ORF and transcribed using T7 polymerase (Calviello et al., 2021; Wilkins et al., 2022). For

Shape-MaP, 1000 ng of the transcribed RNA in 12 µL water was denatured at 95 °C for 2 min and then snap cooled on ice for 2 min. 6 µL of the 3.3x folding buffer (333 mM HEPES pH 8.0, 333 mM NaCl, 33 mM $MgCl_2$) were added to each sample and the RNA was folded at 37 °C for 20 min. For the unfolded control, 1000 ng RNA was placed in 10 µL formamide, 2 µL 10x DC buffer (500 mM HEPES (pH 8.0), 40 mM EDTA), 6 µL water and denatured at 95 °C for 2 min.

For RNA modification, 1 µL of either 2M NAI (Sigma-Aldrich #03-310) in DMSO or DMSO alone was added to the RNA and mixed. The folded RNA was incubated 15 min at 37 °C, while the unfolded RNA was incubated 15 min at 60 °C. Added 2 µL 100 mM DTT to all tubes to quench the reaction. Added water to volume of 50 µL and cleaned up the RNA (Zymo RNA clean and concentrator -5 # R1013) and eluted in 15 µL water.

For reverse transcription, added 1.5 µL 200 ng/µL random reverse transcription primers to the 15 µL RNA tubes. Incubated at 65 °C for 10 min, then 4 °C 2 min. Prepared fresh MaP buffer by mixing equal volumes 5x MaP prebuffer (250 mM Tris (pH 8.0), 375 mM KCl, 50 mM DTT, 2.5 mM dNTP each) and 30 mM $MnCl_2$. Added 12 µL 2.5x MaP buffer to the RNA tubes and mixed and incubated at 25 °C for 2 min. Added 1 µL Superscript II reverse transcriptase (Thermo Fischer Scientific # 18064014) and incubated at 25 °C for 10 min, then at 42 °C for 90 min, then 10 cycles of 50 °C 2 min and 42 °C 2 min, and then 70 °C for 10 min to deactivate the reverse transcriptase. Placed on ice and then purified using Zymo DNA clean and concentrator kit -5 (Zymo #D4004) following cDNA protocol. The cDNA was then amplified by PCR and sequenced using Amplicon-EZ (Azenta Lifesciences). ShapeMapper and SuperFold packaged were used

to analyze the data, convert it into mutational profiles, create SHAPE reactivity plots, and model RNA secondary structures. VARNA software was used for the automated drawing, visualization and annotation of the secondary structures (Darty et al., 2009).

For the *in cell* Shape-map, HART-ODC1 and HART-RAC1 cells were grown to ~80% confluency in 24-well plates. Cells were washed with PBS. Added 150µL 300 mM NAI in DMSO in PBS to each well and added the same volume of DMSO in PBS to control cells. Incubated at 37 °C for 30 min. Added 200 μL quench solution (700 mM 2-mercaptoethanol in 1x PBS, made immediately before use) for 2 min. Washed cells with PBS and collected into a tube. Spun down and pelleted cells and washed once with PBS. Extracted RNA using Direct-zol RNA Miniprep Kits (Zymo #R2050) following manufacturer's instructions (including DNA degradation) and resuspended in 88 µL water. Reverse transcription, library amplification, sequencing, and data analysis were achieved as described above for the *in vitro* protocol.

NMR spectroscopy

Isotope labeled His-MBP tagged S. cerevisiae eIF4E was expressed in BL21-star E. coli grown in M9 minimal media with 15N ammonium sulfate as the sole nitrogen source. Induction was performed by addition of 1 mM IPTG when the cultures reached an OD of 0.5 and overnight incubation at 16 °C. Bacteria were lysed by sonication in lysis buffer containing 500 mM NaCl, 0.5% NP-40 (Igepal), 10 mM Imidazole, 20 mM HEPES pH 7.5, 10 mM 2-mercaptoethanol, clarified by centrifugation at 40,000 g, and the clarified lysate was applied to nickel resin (Qiagen) pre-equilibrated in wash buffer (500 mM NaCl,

20 mM Imidazole, 10 mM 2-mercaptoethanol, and 20 mM HEPES pH 7.5). After three washes in wash buffer, purified protein was eluted in elution buffer containing 500 mM NaCl, 250 mM Imidazole, 100 mM Na2SO4, 50 mM sodium phosphate buffer at pH 7.5, and 10 mM 2-mercaptoethanol. Protein was then dialyzed into two liters of buffer containing 20 mM HEPES pH 7.5, 125 mM KCl, and 0.5 mM TCEP overnight at 4 °C while simultaneously the affinity tags were cleaved through addition of 1:40 w/w tev protease. Dialyzed protein was applied to m7G cap resin (GE Healthcare) equilibrated in dialysis buffer and eluted using dialysis buffer supplemented with 0.1 mM m7GDP (Edery et al., 1988). Purified eIF4E protein was exchanged into 50 mM phosphate pH 6.5 and 50 mM KCl using a desalting column (Gross et al., 2003), concentrated to 200 µM, and m7GTP was added to 250 µM. DDX3 33-51 peptide (ASKGRYIPPHLRNREATKGAA) was synthesized by the HHMI Mass Spectrometry Facility at UC Berkeley and dissolved at 50 mM in water, while 4E-BP1 peptide (RIIYDRKFLMECRNSPV; amino acids 51-67) was synthesized by Elim Bio and dissolved at 50 mM in DMSO. Peptides were added to a final concentration of 1 mM. 15N HSQCs were acquired at 298 K using the 900 MHz spectrometer at the Central California 900 MHz NMR facility at UC Berkeley using 10% D2O as a lock signal. Spectra were overlaid using UCSF Sparky.

Immunoprecipitations

For Figure 3.7 , HEK293T cells transduced with DDX3X WT and mutants were washed with cold PBS (Gibco #10010049) and lysed in 500 µL of ice-cold immunoprecipitation buffer (40 mM HEPES–KOH (pH 7.5), 100 mM KCl, 1 mM EDTA, 10

mM β-glycerophosphate, 10 mM NaF, 2 mM Na3VO4, 0.4% NP-40 and 1 mM PMSF). The lysates were passaged 5 times through a 25 gauge needle and centrifuged to remove the nuclei. RNAse A (5 µg/ml, Quiagen # 19101) was added to the whole cell extracts (WCE) and incubated on ice for 15 min. WCEs were pre-cleared with Mouse IgG-Agarose resin (Sigma-Aldrich #A0919) for 2 hours at 4 °C and then incubated with anti-Flag M2 affinity gel (Millipore Sigma # A2220) for 1.5 hours at 4 °C under continuous rotation. The beads were collected and washed five times with the same immunoprecipitation buffer, and the bead–bound proteins were resolved by SDS-PAGE and analyzed by Western blotting.

For Figure 3.8 , HEK293T cells transduced with DDX3X WT and mutants were washed with cold PBS, collected, and lysed in NP-40 buffer (150 mM NaCL, 1% IGEPAL, 50 mM Tris-Cl p.H. 7.5) with protease inhibitor (04693132001, Roche, cOmplete™, EDTA-free Protease Inhibitor Cocktail). Pipetted up and down, don't vortex. Samplez were placed 45 min on rotor in cold room and then spun down in centrifuge at 4700rpm for 2 min. The supernatant was transferred to new tubes and treated with 1µL MNAse/200 µL lysate for 30 min on the rotor at RT. RNAsin, 4x the amount of MNAse, was used to stop the reaction for 15 min at RT. Anti-FLAG® M2 Magnetic Beads were added and used to precipitate FLAG according to protocol (M8823, Millipore). Elution was achieved with 3X FLAG® peptide (F4799, Sigma-Aldrich,). Briefly, 30 µL of 150 ng/µL FLAG peptide (in TBS with protease inhibitor) was added to the tube and placed on rotor for 30 min. The supernatant was collected and resolved by SDS-PAGE and analyzed by Western blotting.

Western blotting

Primary antibodies used in this study include rabbit polyclonal anti-DDX3X(custom made by Genemed Synthesis using peptide ENALGLDQQFAGLDLNSSDNQS; Figure 3.7), anti-actin HRP (Santa Cruz Biotechnology, sc-47778), anti-FLAG HRP (Sigma, A8592), anti-eIF4A1 antibody (ab31217), anti-eIF4E antibody (Cell signaling technologies #9742), anti-ribosomal protein S11/RPS11 (ab175213).

Microscopy

For microscopy in Figure 3.1 , HCT116 degron cells transduced with HART-ODC1 or HART-RAC1 were plated in a 384 well plate (Perkin Elmer #6057302) and were treated with AUX or DMSO for 96 hours. Media was removed and 50 µL of the 4% PFA in PBS was added to each well for 15 min and incubated at RT. PFA solution was removed and the cells were washed with 100 µL PBS three times using a BioTek EL406. Cells were incubated with 50 µL 1X DAPI (Biotium #40043) in PBS for 5 min at RT. Cells were washed with 100 µL PBS three times using a BioTek EL406 and imaged using a InCell Analyzer 2000 (GE), taking three pictures for well. HART ratio was calculated as the ratio between the mCherry and GFP channels.

For microscopy in Figure 3.7 , HEK293T cells were grown in 96 well plates. When they reached 70% confluency media was removed and cells were washed once with PBS. 50 μL of 4% paraformaldehyde in PBS was added to the well for 10 min at room

temperature. Cells were washed three times with ice-cold PBS and then incubated for 10 min in PBS containing 0.1% Triton X-100 at 4 °C by rocking. Cells were washed in PBS three times for 5 min at 4 °C by rocking and then incubated with 1% BSA PBST solution for 30 min at 4 °C by rocking. Cells were incubated in diluted antibody (ANTI-FLAG, 1:1000, Sigma Aldrich #F1804) in 1% BSA PBST overnight at 4C by rocking. Cells were washed in PBS three times for 5 min at 4 °C by rocking and then incubated by rocking with secondary antibody (Goat-anti-Mouse 488, 1:2000, Invitrogen #A-11008) in 1% BSA PBST for 1 hour at room temperature in the dark. Cells were washed in PBS three times for 5 min at 4 °C by rocking in the dark. 1X DRAQ7 (Thermo Fisher Scientific #D15106). in PBS was added to the for 15 min by rocking, followed by one wash with PBS. Images were taken with a confocal microscope at a 20X-40X magnification.

DISCUSSION

In this chapter we develop and use translational reporters to investigate the activity of DDX3X. DDX3X-sensitive 5′ UTRs were selected among transcripts whose ribosome density went down upon loss of DDX3X and whose 5′ UTR was shown to be sensitive to DDX3X in validation assays (Calviello et al., 2021). We chose the ODC1 and RAC1 5′ UTRs as they were among the most DDX3X-sensitive in both *in vitro* and *in cell* assays. They also provide diversity in length, at 511 bp vs 197 bp respectively. Notably, HART data replicated the previous assays, with translation of ODC1 and RAC1 5′ UTRs shown to be sensitive to the loss of DDX3X unlike the RPLP1 5′ UTR (Calviello et al., 2021). Being embedded into the cell as DNA via lentiviral transduction, reporters undergo

several steps of the RNA metabolism that are known to be regulated by DDX3X, including mRNA preprocessing and export, before it undergoes translation initiation. This potentially limits HART's ability to isolate translation initiation as source of the 5′ UTRs' DDX3X's dependency. On the other hand, the alignment between HART and in *in vitro* and in cell assays, which are performed with *in vitro* transcribed and capped mRNA, suggest that the DDX3X-sensitive step is translation initiation.

To promote translation of eGFP in HART and act as an internal control, we selected a short 8bp 5′ UTR whose size makes it unlikely to form complex secondary structures that might depend on DDX3X for unwinding before proper translation. Additionally, the lack of change of eGFP signal between auxin and DMSO conditions in HART (Figure 3.2 C) suggests that the loss of DDX3X does not affect its translation. In addition to its likely lack of complex secondary structures, there could be other reasons that make it insensitive to permutations in DDX3X. Very short 5′ UTRs have been identified as promoting translation both in a cap dependent and independent manners (Trainor & Shcherbik, 2021). Additionally, even in the context of cap dependent translation, they have been observed to direct translation in a ribosome scanning free manner (Elfakess et al., 2011; Haimov et al., 2015). For example, the Translation Initiator of Short 5′ UTR (TISU) is a regulatory that has a median length of 12 nucleotides and is required for a cap-dependent, scanning-free mechanism of translation initiation on 5′ UTRs with fewer than 30 nucleotides (Elfakess et al., 2011). Notably, TISU function does not require eIF4A, suggesting that some short 5′ UTRs lack the need for DEAD-box helicases (Sinvani et al., 2015). Similarly, cap-assisted translation without scanning was reported for the histone H4 mRNA, which is notable for directing translation in a wide

variety of eukaryotic cells (Dasmahapatra et al., 1987; Martin et al., 2011; Trainor & Shcherbik, 2021). It is possible that this extremely short 5′ UTR avoids DDX3X dependency by initiating translation without ribosome scanning or by cap independent mechanisms altogether, hence without the need for unwinding of complex structures. Further work into the mechanism of translation on very short 5′ UTRs is still needed to understand this phenomenon. Taken together, and in with conjunction with HART's reproducibility in microscopy (Figure 3.1 E), the data suggests that HART is a reliable and versatile reporter for the activity of DDX3X in translation initiation.

One crucial aspect of DDX3X regulation is what structures and features make a 5′ UTR dependent on DDX3X for translation. We used HART to dissect DDX3X-sensitive 5′ UTRs. Both the RAC1 and ODC1 5′ UTRs have high GC content and are predicted by SHAPE-MaP to possess complex secondary structures. This is in line with previous data suggesting high GC content as a marker of DDX3X sensitivity (Calviello et al., 2021; Oh et al., 2016) as well data in yeast, where repression of Ded1p activity leads to accumulation of organized RNA structures in 5′ UTRs (Guenther et al., 2018). Elaborate RNA secondary and tertiary structures can sterically block scanning the scanning ribosome, which possesses no intrinsic unwinding activity and relies on helicases such as DDX3X (Leppek et al., 2018).

Our work suggests that the RAC1 5′ UTR contains a large stem loop which relies on DDX3X for unwinding. Disruption of this structure with deletions of nucleotides 1-39 and 40-78 decreases sensitivity to DDX3X (Figure 3.5 B) and produces 5′ UTRs with lower predicted free energy and structural complexity. In particular, the HART ratio in the 40-78 deletion construct is unaffected by DDX3X loss. Another possibility is that this stem

loop regulates uORF usage. Secondary structures in the 5′ UTRs can also increase ribosome dwelling time and promote translation on sub-optimal upstream start codons (Hinnebusch et al., 2016; Kozak, 1991). The RAC1 5′ UTRs features a CTG near cognate start codon in position 28, right upstream of the stem loop (Figure 3.5 B). In the absence of DDX3X, the stem loop might direct translation towards the uCTG, which might negatively affect translation of the main ORF. This dependence on DDX3X would be diminished in the 1-39 and 40-78 deletion constructs. Overall, the data suggests that sensitivity to DDX3X in RAC1 and ODC1 5′ UTRs is conferred by complex secondary structures.

We envision two models of DDX3X unwinding 5′ UTRs structures during ribosome scanning. In the *trans* model, DDX3X unwinds structures ahead of and untethered from the scanning ribosome and associated translational machinery. In the *cis* mode, DDX3X unwinds the RNA while tethered or bound, similarly to how eIF4A which associates with the ribosome during scanning (Brito Querido et al., 2020). To differentiate between these two models, we investigated the potential binding of DDX3X to the translational machinery. We showed that full length DDX3X, but not its helicase core alone, can immunoprecipitate the translation machinery (Figure 3.8 A), suggesting an interaction between the terminal domains of DDX3X and the ribosome. Notably, these termini are highly conserved from yeast to human across the Ded1/DDX3X subfamily, but are not withing the wider DEAD box family (Floor, Condon, et al., 2016; Sharma & Jankowsky, 2014). Both DDX3X and Ded1 have been suggested to bind to helix 16 of the 18S of the smaller subunit of the ribosome (Calviello et al., 2021; Guenther et al., 2018). We

reasoned that if this interaction with the ribosome or associated factors is specific to the subfamily, the residues mediating it are likely to be found in the termini.

To determine which residues mediate an interaction between DDX3X and the translation machinery, we made targeted alanine substitutions to several conserved regions in DDX3X termini. Immunoprecipitation showed the 38-44ala mutation lost interaction with ribosomal protein RPS11 and several translation initiation factors, which were instead pulled down by DDX3X WT in an RNA-independent way. While it was previously identified as an eIF4E binding region, NMR data showed that the 38-44 residues of DDX3X did not bind directly to eIF4E (Figure 3.7 E-F). This can be explained by the fact that 38-44 region of DDX3X is similar to the canonical eIF4E binding region found in 4EBP and eIF4G but differs in its last residue, which is a hydrophobic amino acid in the canonical sequence but an arginine in DDX3X (Richter & Sonenberg, 2005; Sachs & Varani, 2000; von der Haar et al., 2004). 38-44 could residues mediate binding to the translational machinery via other factors. Previous work has also suggested that DDX3X interacts with eIF4G (Ayalew et al., 2016; Gong et al., 2021; Soto-Rifo et al., 2012; Soto-Rifo & Ohlmann, 2013), with direct binding observed between positions 682-1086 of eIF4G (Soto-Rifo et al., 2012). Direct binding to yeast eIF4G, 4A and 4E was also seen in Ded1 (Guenther et al., 2018; Gulay et al., 2020; Hilliker et al., 2011), suggesting interaction between DDX3X and the eIF4F complex (Ryan & Schröder, 2022). We suggest that the 38-44 residues of DDX3X contribute, at least partially, to the interaction with the ribosome, although whether this interaction is direct or mediate by other factors in the translational machinery needs further study (Figure 3.9 E).

We next investigated the importance of the interaction with translational machinery on DDX3X's functional role. Using HART to measure translational activity on both RAC1 and ODC1 5′ UTRs, we determined that exogenous DDX3X WT can rescue the loss of endogenous DDX3X (Figure 3.9 A), in a dose dependent manner (Figure 3.9 C). Conversely DDX3X R534H, a mutant deficient in its RNA unwinding ability, is unable to rescue translation activity and acts as a dominant negative, in line with previous studies (Calviello et al., 2021; Floor, Condon, et al., 2016; Oh et al., 2016). DDX3X 38-44ala acts as a dominant negative in HART-ODC1 but not in HART-RAC1, where it fails simply to rescue loss of endogenous DDX3X. The difference in behavior might be due to ODC1's length, more complex structure and higher free energy, or specific structural features. Further studies are necessary to understand how DDX3X behaves with different structures. Notably, the double mutant 38-44ala/R534H follows the 38-44ala pattern. This suggests that detaching DDX3X from the translational machinery is upstream of helicase deficient mutations, underscoring the importance of this interaction for DDX3X translational role.

DDX3X's role in translation has also been linked to promoting cell growth, possibly through the translation regulation of G1/S-specific cyclin E1 (Lai et al., 2010). Our data showed that helicase defective DDX3X is deficient in promoting cell growth (Figure 3.9), in line with what observed in a previous study (Lai et al., 2010), as are also DDX3X 38-44ala and DDX3X 132-607 (Figure 3.9 A, Figure 3.10 A), further suggesting the importance of the translational machinery interaction. Our data shows how HART can be used to investigate translational dynamics of DDX3X in translation, in particular suggesting that DDX3X acts in cis with respect to the ribosome and associated factors

during translation initiation. Additionally, HART can measure the effect of mutations on DDX3X's ability to promote translation on sensitive 5′ UTRs.

DDX3X's behaves like a specialized helicase. Unlike eIF4A, that is necessary for the translation of the majority of human transcripts, both DDX3X and Ded1 regulate only a subset of translation of atypically long and structured 5′ UTRs (Calviello et al., 2021; Oh et al., 2016; Sen et al., 2016). Ded1 has a higher unwinding activity than eIF4A, which may position Ded1/DDX3X as a specialist helicase required to unwind particularly complex structures (Gao et al., 2016). Additionally, the interaction between DDX3X and the ribosome outlined here could also play a role in Ded1/DDX3X's specialization. Taken together with previous data, we have shown that DDX3X, whether directly or indirectly, binds the helix 16 of the small subunit of the ribosome (Calviello et al., 2021). This location could be a hub of mRNA regulation, as other helicases such as DHX29 have also been shown to bind here. Understanding the dynamics of of this hub, including the timing and competition among helicases for ribosome binding and mRNA unwinding, will yield fruitful insight on mRNA regulation.

In addition to its role in dissecting specific 5′ UTRs sensitivities and DDX3X mutant effect, we anticipate HART to be useful in several other settings. Its reliability as a 5′ UTR-based reporter of function in translation initiation can be employed in conjunction with large naturally occurring or artificial 5′ UTR libraries to gain a granular and large-scale characterization of DDX3X regulation. Alternatively, HART's readout in both flow cytometry and microscopy setting can be employed to screen for drugs that alter DDX3X behavior or rescue DDX3X or mutation. The lentiviral transduction delivery of HART enables measurement of DDX3X-dependent translation *in vivo*. Finally, by choosing the

proper control and experimental 5′ UTRs, it can be adapted to measure the activity of any other helicase or translation factor in addition to DDX3X. HART's reliability and flexibility can prove a useful tool to study translation in diverse settings, and advance both the understanding of human diseases and fundamental biology.

ACKNOWLEDGMENTS

We thank all members of the Floor Lab for their invaluable support, expertise, and feedback. We are indebted to the UCSF Parnassus Flow Cytometry CoLab staff for their technical assistance and expertise (RRID:SCR_018206). Research reported here was supported in part by the DRC Center Grant NIH P30 DK063720 and by the NIH S10 Instrumentation Grant S10 1S10OD021822-01. This work was supported by the DDX3X Foundation (to S.N.F.) and the National Institutes of Health R35GM149255 (to S.N.F.) and R01NS120667 (to S.N.F.) and the California Tobacco-Related Disease Research Grants Program 27KT-0003 (to SNF) and T30DT1004 (to KCW). S.N.F. is a Pew Scholar in the Biomedical Sciences, supported by The Pew Charitable Trusts. We thank David King for help with peptide synthesis and general advice.

AUTHOR CONTRIBUTIONS

Conceptualization, K.C.W. and S.N.F.; Investigation, K.C.W., T.S., S.G., J.R.D., S.N.F. Writing – K.C.W. and S.N.F.; Funding Acquisition, K.C.W., S.N.F.; Supervision, S.N.F.

FIGURES

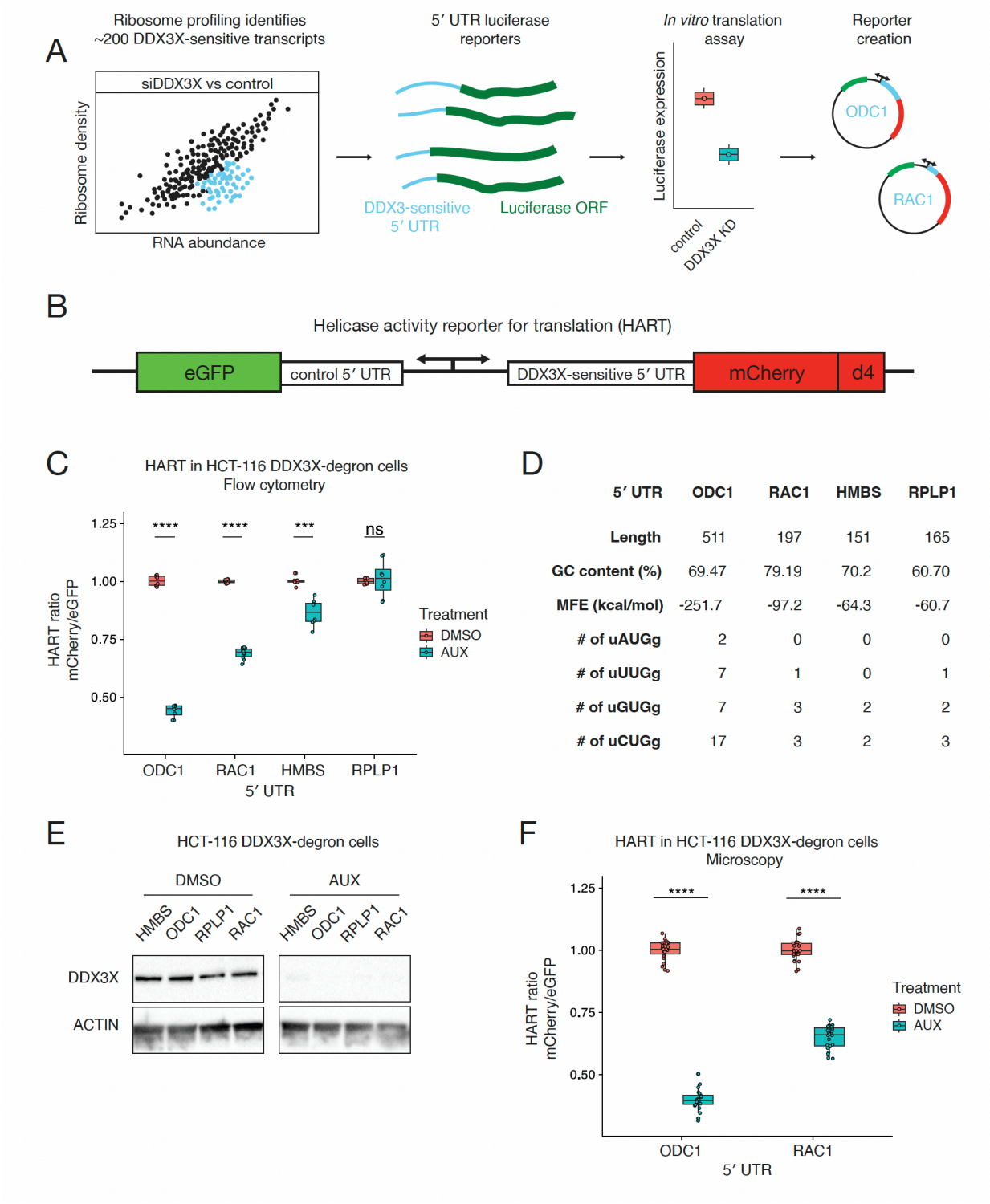

5′ UTR	ODC1	RAC1	HMBS	RPLP1
Length	511	197	151	165
GC content (%)	69.47	79.19	70.2	60.70
MFE (kcal/mol)	-251.7	-97.2	-64.3	-60.7
# of uAUGg	2	0	0	0
# of uUUGg	7	1	0	1
# of uGUGg	7	3	2	2
# of uCUGg	17	3	2	3

Figure 3.1 The helicase activity reporter for translation (HART) employs DDX3X-sensitive 5′ UTRs to measure the translational activity of DDX3X. (A) Selection of DDX3X-sensitive 5′ UTRs for HART. Validated DDX3X-sensitive untranslated regions from prior ribosome profiling and in vitro translation, as well as negative controls, were cloned into the HART reporter. (B) Diagram of HART. HART is constructed around a bidirectional promoter, with one arm directing the transcription of a control 5′ UTR and EGFP, and the other arm featuring a DDX3X-sensitive 5′ UTR followed by mCherry. An ornithine decarboxylase (ODC) degron (d4) shortens the mCherry half-life. The HART ratio (mCherry/EGFP) can be used to measure the translational activity of DDX3X. (C) HART ratio in HCT-116 degron cells analyzed with flow cytometry. HCT-116 degron cells were lentivirally transduced with HART constructs with indicated 5′ UTRs upstream of mCherry. After 48 hours from the addition of either DMSO or auxin, which induces degradation of endogenous DDX3X, the fluorescent signal of cells was measured by fluorescent cytometry. The ratio of mCherry/EGFP was calculated for each cell and averaged across replicate wells. Statistical significance was determined by unpaired *t*-test: ns: p > 0.05, *: p <= 0.05, **: p <= 0.01, ***: p <= 0.001, ****: p <= 0.0001. (D) Table of features for the 5′ UTRs from C. Features catalogued include length, GC content, RNA minimum free energy (MFE) prediction using the ViennaRNA Package (Lorenz et al., 2011), and the number of upstream AUGs and near cognate codons. (E) Western blot for cells in A. HCT-116 degron cells were treated with either auxin or DMSO, and then lysates were collected and resolved by SDS-page and used for western blotting with antibodies against actin and DDX3X. (F) HART ratio in HCT-116 degron cells analyzed by microscopy. HCT-116 degron cells were transduced with HART construct for ODC1 or RAC1. After 48 hours from the addition of either DMSO or auxin the cells were fixed and imaged using an InCell Analyzer 2000. The ratio of mCherry/EGFP was calculated for each cell and averaged across replicate wells. Statistical significance was determined by unpaired *t*-test: ns: p > 0.05, *: p <= 0.05, **: p <= 0.01, ***: p <= 0.001, ****: p <= 0.0001.

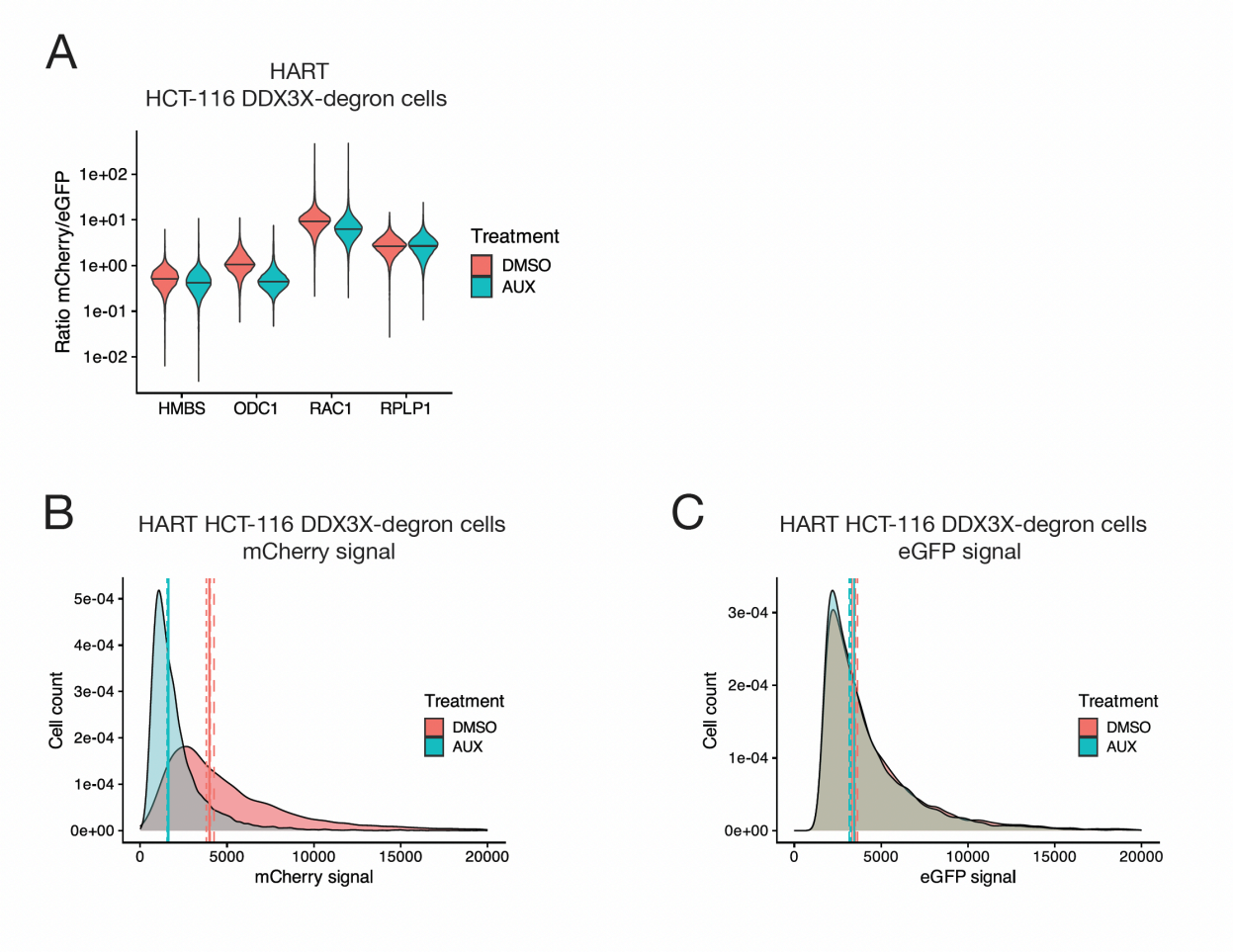

Figure 3.2 HART signal is driven by DDX3X-sensitivity (A) Violin plot for HART ratio in HCT-116 degron cells analyzed with flow cytometry for the experiment in Figure 3.1 B. HCT-116 degron cells were lentivirally transduced with HART constructs with various 5′ UTRs in front of mCherry. After 48 hours from the addition of either DMSO or auxin, which induces degradation of endogenous DDX3X, the fluorescent signal cells was measured by fluorescent cytometry. The ratio of mCherry/EGFP was calculated for each cell and plotted as a violin plot. **(B)** Flow cytometry data for the mCherry channel for experiment in Figure 3.1 B. The raw data for the 561nm 50mW laser, YG C detector (corresponding to mCherry) for each cell was plotted and the mean for each replicate well was calculated and plotted as a vertical line. **(C)** Flow cytometry data for the EGFP channel for cells in Figure 3.1 B. The raw data for the 488nm 60mW laser, Blue C detector (corresponding to EGFP) for each cell was plotted and the mean for each replicate well was calculated and plotted as a vertical line.

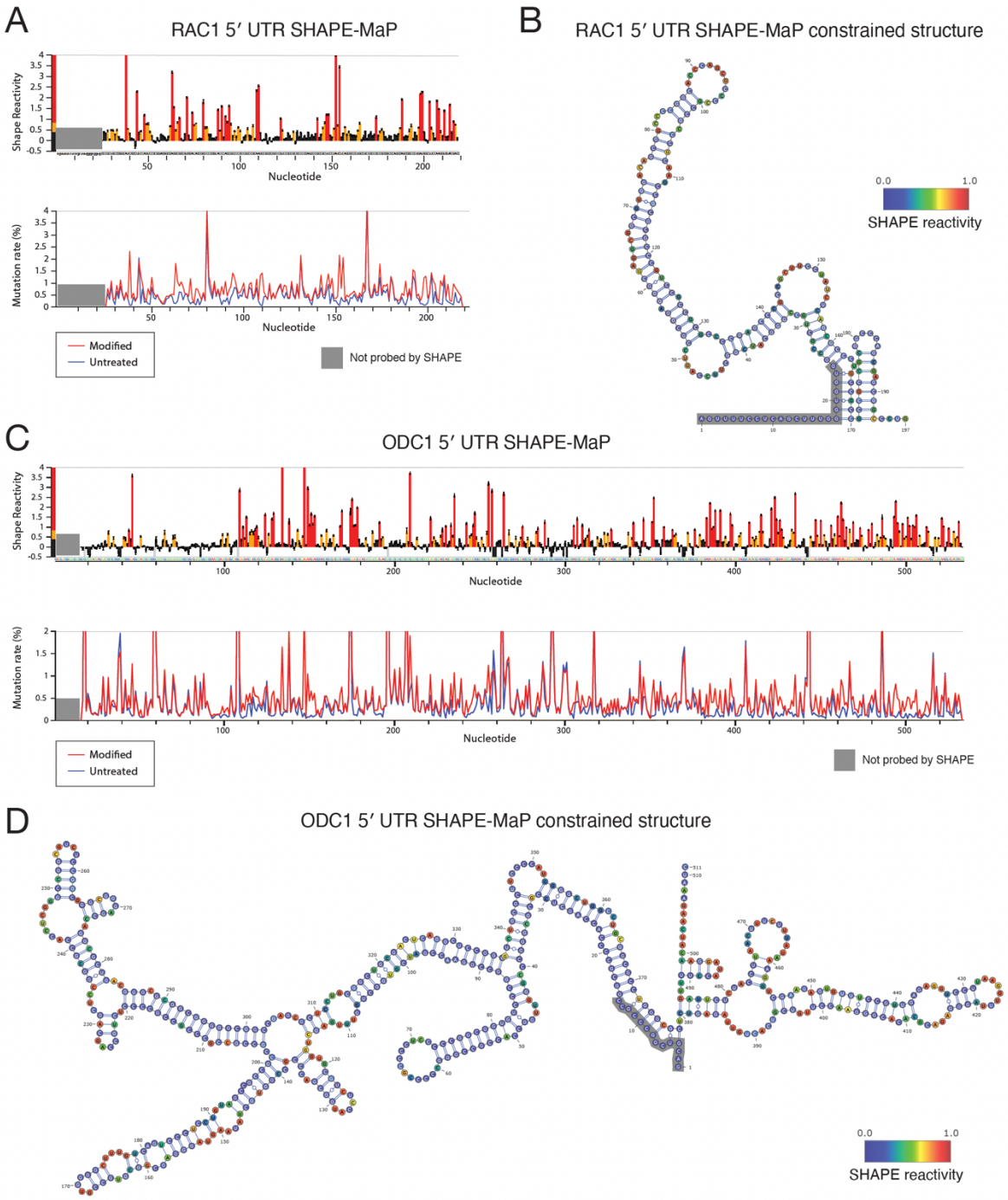
A
RAC1 5′ UTR SHAPE-MaP
Shape Reactivity
Nucleotide
Mutation rate (%)
Modified
Untreated
Not probed by SHAPE
B
RAC1 5′ UTR SHAPE-MaP constrained structure
0.0
1.0
SHAPE reactivity
C
ODC1 5′ UTR SHAPE-MaP
Shape Reactivity
Nucleotide
Mutation rate (%)
Modified
Untreated
Not probed by SHAPE
D
ODC1 5′ UTR SHAPE-MaP constrained structure
0.0
1.0
SHAPE reactivity

Figure 3.3 DDX3X sensitive 5′ UTRs are highly structured. (A) SHAPE-map reactivity and mutation rate for the 5′ UTR of RAC1 *in vitro*. *In vitro* transcribed mRNA containing the 5′ UTR of RAC1 and the open reading frame of luciferase was probed with 200 mM NAI or DMSO control for SHAPE-map. The RNA was reverse transcribed, sequenced, and analyzed to obtain mutation profiles and SHAPE reactivity with the ShapeMapper tool. **(B)** Diagram of the structure of the RAC1 5′ UTR *in vitro*, based on data from Figure 3.3 A and computed with ShapeMapper 2.1.3. (Busan & Weeks, 2018) **(C)** SHAPE-map reactivity and mutation rate for the 5′ UTR of RAC1 *in vitro*. In vitro transcribed mRNA containing the 5′ UTR of ODC1 and the open reading frame of luciferase was probed with 200 mM NAI or DMSO control for SHAPE-map. The RNA was reverse transcribed and sequenced. The mutation rate was calculated at each position for both treated and control samples. The shape reactivity was calculated based on the difference in mutation rate. **(D)** Diagram of the structure of the ODC1 5′ UTR *in vitro*, based on data from Figure 3.3 C and computed with ShapeMapper 2.1.3. (Busan & Weeks, 2018).

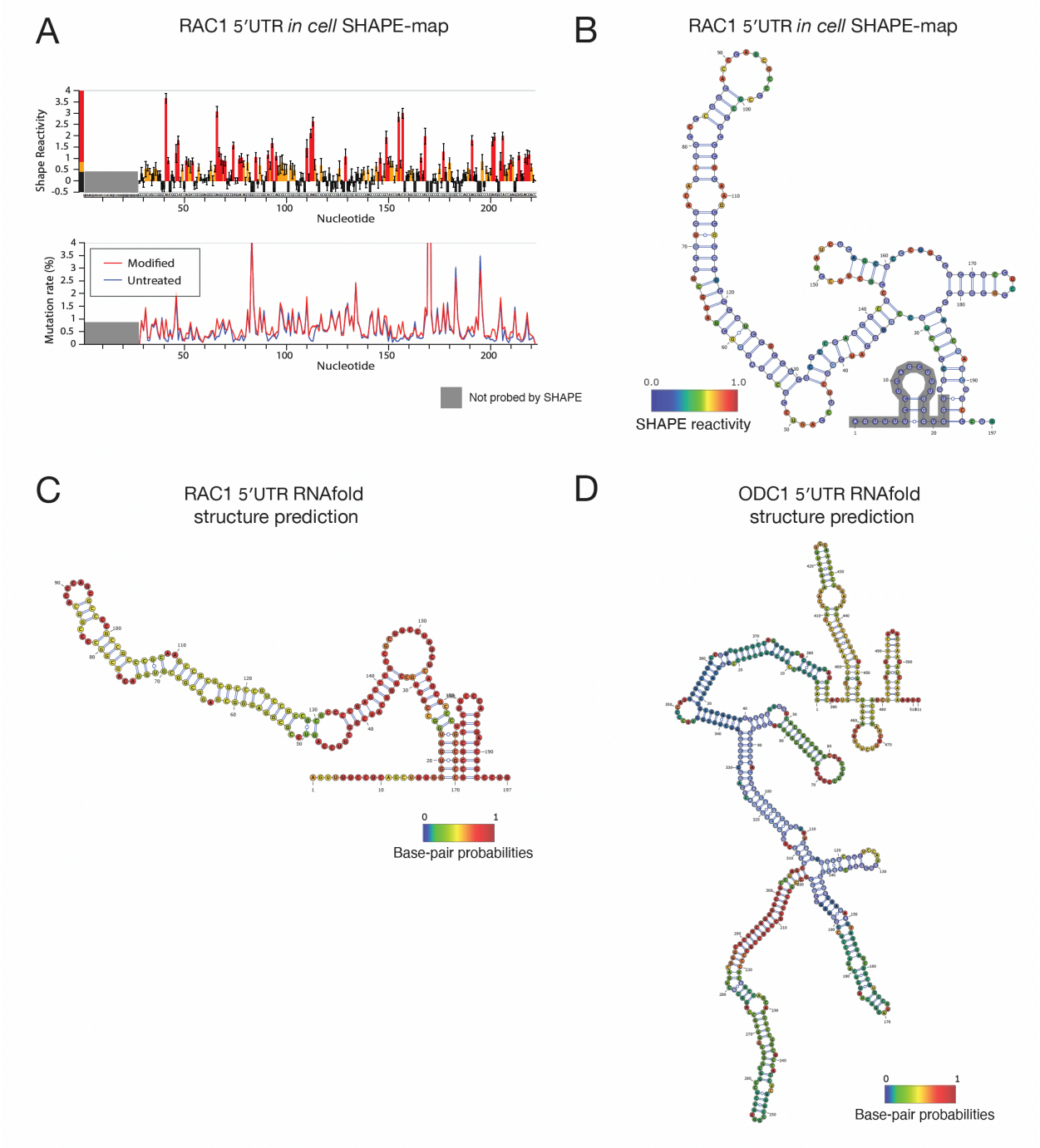
A
RAC1 5′UTR *in cell* SHAPE-map
Shape Reactivity
Nucleotide
Mutation rate (%)
Modified
Untreated
Not probed by SHAPE
B
RAC1 5′UTR *in cell* SHAPE-map
0.0
1.0
SHAPE reactivity
C
RAC1 5′UTR RNAfold
structure prediction
0
1
Base-pair probabilities
D
ODC1 5′UTR RNAfold
structure prediction
0
1
Base-pair probabilities

Figure 3.4 In cell Shape-MaP data and RNA folding predictions for DDX3X sensitive 5′ UTRs (A) SHAPE-map reactivity and mutation rate for the 5′ UTR of RAC1 *in cell*. Cells were treated with 300 mM NAI in PBS or control for 20 min before quenching the reaction and extracting the RNA. The RNA was reverse transcribed, sequenced, and analyzed to obtain mutation profiles and SHAPE reactivity with the ShapeMapper tool. **(B)** Diagram of the structure of the RAC1 5′ UTR *in cell*, based on data from Figure 3.4 A and computed with ShapeMapper 2.1.3. (Busan & Weeks, 2018) **(C-D)** RNA folding minimum free energy prediction of the structures of the 5′ UTRs of RAC1 (C) and ODC1 (D) using the ViennaRNA Package (Lorenz et al., 2011). The minimum free energy for the RAC1 structure is -97.20 kcal/mol and for the ODC1 is -251.70 kcal/mol.

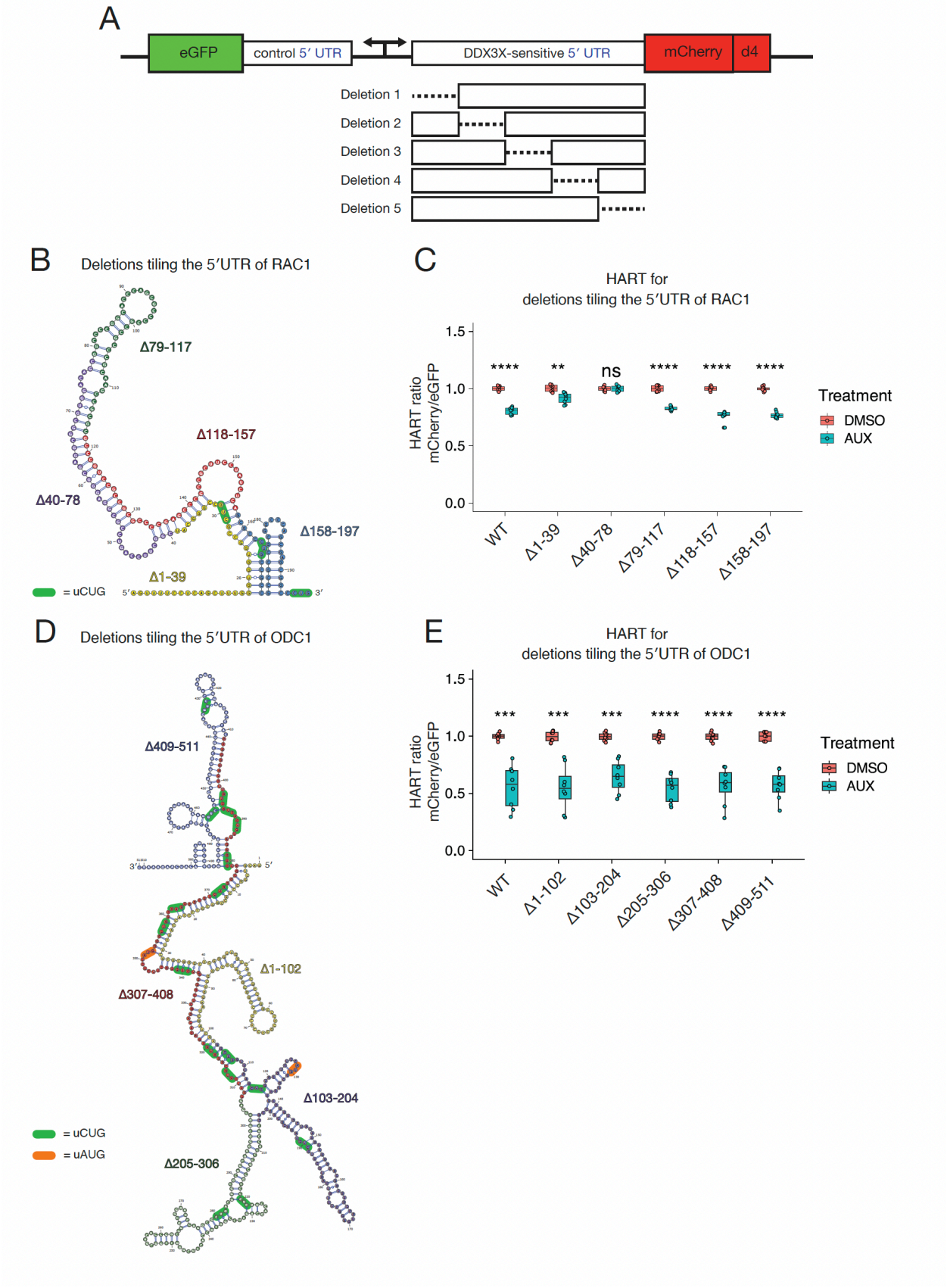
A
eGFP
control 5′ UTR
DDX3X-sensitive 5′ UTR
mCherry
d4
Deletion 1
Deletion 2
Deletion 3
Deletion 4
Deletion 5
B
Deletions tiling the 5′UTR of RAC1
Δ79-117
Δ118-157
Δ40-78
Δ158-197
Δ1-39
= uCUG
5′
3′
C
HART for
deletions tiling the 5′UTR of RAC1
HART ratio
mCherry/eGFP
1.5
1.0
0.5
0.0
****
**
ns
****
****
****
WT
Δ1-39
Δ40-78
Δ79-117
Δ118-157
Δ158-197
Treatment
DMSO
AUX
D
Deletions tiling the 5′UTR of ODC1
Δ409-511
3′
5′
Δ1-102
Δ307-408
Δ103-204
= uCUG
= uAUG
Δ205-306
E
HART for
deletions tiling the 5′UTR of ODC1
HART ratio
mCherry/eGFP
1.5
1.0
0.5
0.0
***
***
***
****
****
****
WT
Δ1-102
Δ103-204
Δ205-306
Δ307-408
Δ409-511
Treatment
DMSO
AUX

Figure 3.5 Dissection of RAC1 and ODC1 DDX3X-sensitivity. (A) Schematic of the HART construct with deletions tiling the DDX3X-sensitive 5′ UTR. **(B)** Diagram of the structure of RAC1 with the deletions highlighted. **(C)** HART data for panel B. HART constructs containing RAC1 5′ UTR or five deletion mutants were inserted via lentivirus into HCT116 degron cells. The cells were treated with auxin to induce loss of endogenous DDX3X or DMSO control for 48 hours, and the HART ratio (mCherry/EGFP) was measured by flow cytometry**. (D)** Diagram of the structure of ODC1 with the deletions highlighted. **(E)** Same experiment as in C, but with ODC1 constructs from D.

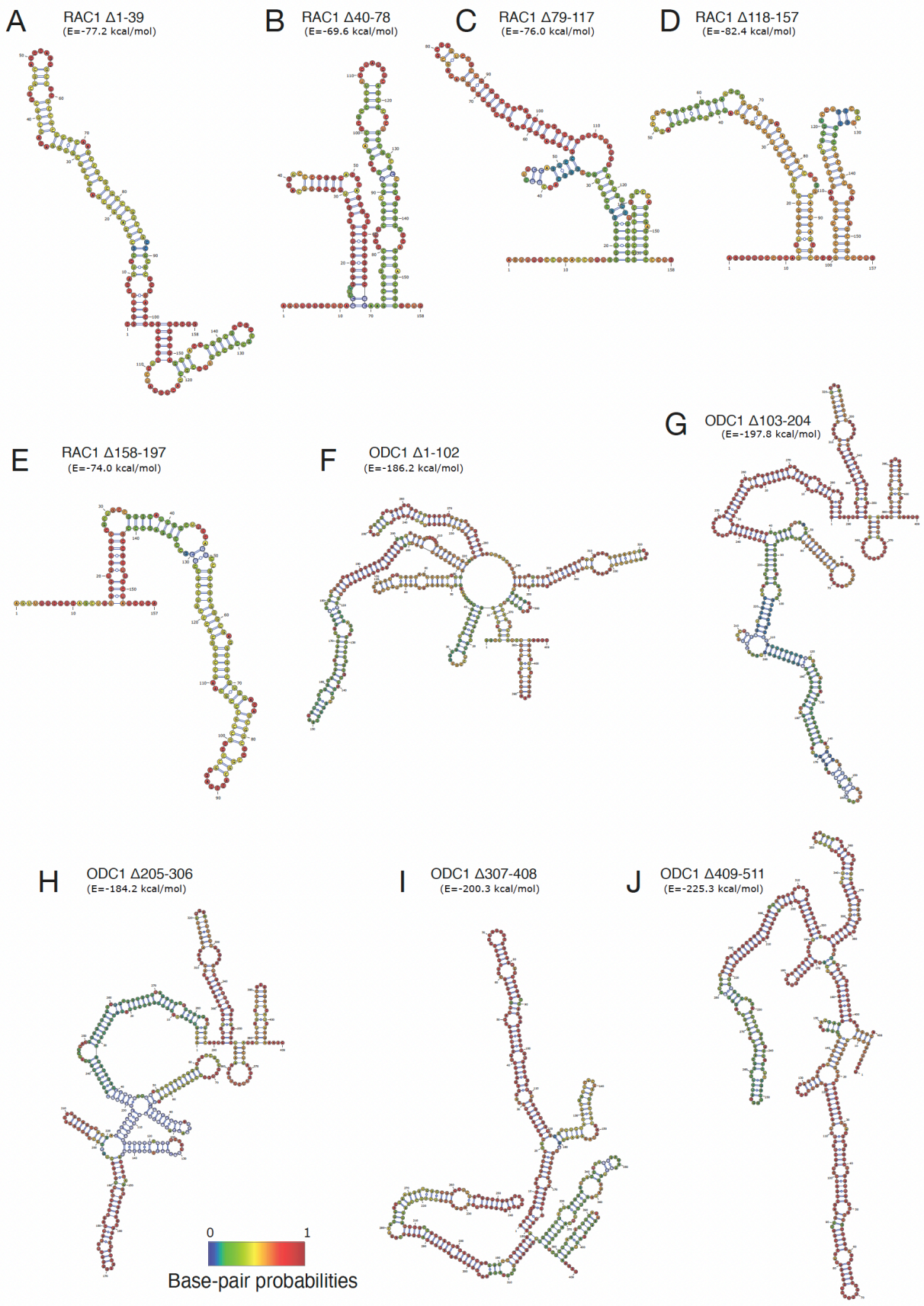
A
RAC1 Δ1-39
(E=-77.2 kcal/mol)
B
RAC1 Δ40-78
(E=-69.6 kcal/mol)
C
RAC1 Δ79-117
(E=-76.0 kcal/mol)
D
RAC1 Δ118-157
(E=-82.4 kcal/mol)
E
RAC1 Δ158-197
(E=-74.0 kcal/mol)
F
ODC1 Δ1-102
(E=-186.2 kcal/mol)
G
ODC1 Δ103-204
(E=-197.8 kcal/mol)
H
ODC1 Δ205-306
(E=-184.2 kcal/mol)
I
ODC1 Δ307-408
(E=-200.3 kcal/mol)
J
ODC1 Δ409-511
(E=-225.3 kcal/mol)
0
1
Base-pair probabilities

Figure 3.6 RNA folding minimum free energy prediction of the structures containing tiled deletions of DDX3X sensitive 5′ UTRs (A-E) RNA folding minimum free energy prediction of the structures of the 5′ UTR of RAC1 containing the deletions used in Figure 3.5 B-C using the ViennaRNA Package (Lorenz et al., 2011). The predicted minimum free energies for the RAC1 deletion constructs are: -77.20 kcal/mol for Δ1-39 -77.20 kcal/mol, -69.60 kcal/mol for Δ40-78, -76.00 kcal/mol for Δ79-117, -82.40 kcal/mol for Δ118-157, -74.00 kcal/mol for Δ158-197. **(F-J)** RNA folding minimum free energy prediction of the structures of the 5′ UTR of ODC1 containing the deletions used in Figure 3.5 D-E using the ViennaRNA Package (Lorenz et al., 2011). The predicted minimum free energies for the ODC1 deletion constructs are: -186.20 kcal/mol for Δ1-102, -197.80 kcal/mol for Δ103-204, -184.20 kcal/mol for Δ205-306, -200.30 kcal/mol for Δ307-408, -225.30 kcal/mol for Δ409-511.

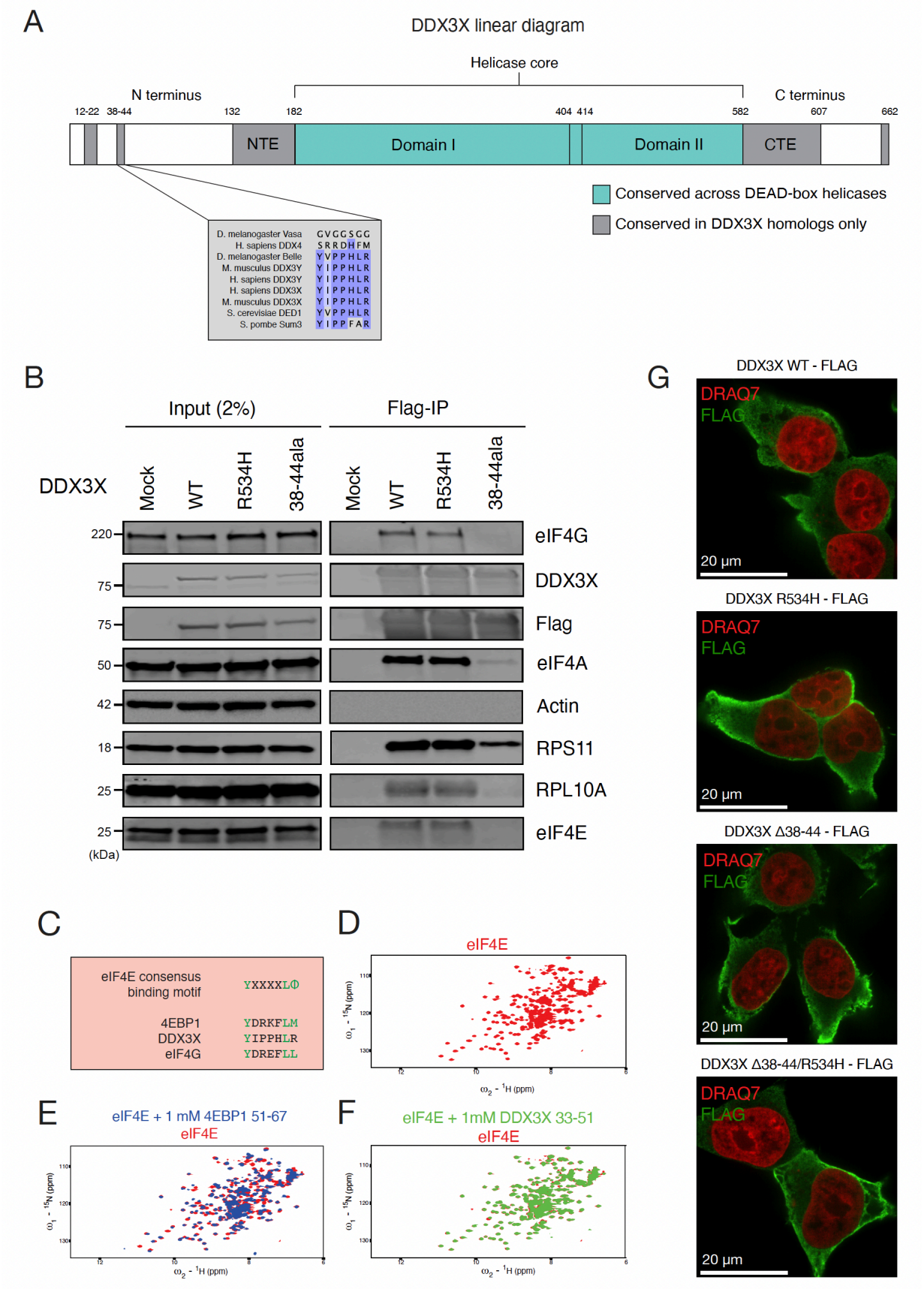
A
DDX3X linear diagram
Helicase core
N terminus
C terminus
12-22
38-44
132
182
404
414
582
607
662
NTE
Domain I
Domain II
CTE
Conserved across DEAD-box helicases
Conserved in DDX3X homologs only
D. melanogaster Vasa G V G G S G G
H. sapiens DDX4 S R R D H F M
D. melanogaster Belle Y V P P H L R
M. musculus DDX3Y Y I P P H L R
H. sapiens DDX3Y Y I P P H L R
H. sapiens DDX3X Y I P P H L R
M. musculus DDX3X Y I P P H L R
S. cerevisiae DED1 Y V P P H L R
S. pombe Sum3 Y I P P F A R
B
Input (2%)
Flag-IP
DDX3X
Mock
WT
R534H
38-44ala
220
75
75
50
42
18
25
25
(kDa)
eIF4G
DDX3X
Flag
eIF4A
Actin
RPS11
RPL10A
eIF4E
C
eIF4E consensus binding motif
YXXXXLΦ
4EBP1 YDRKFLM
DDX3X YIPPHLR
eIF4G YDREFLL
D
eIF4E
E
eIF4E + 1 mM 4EBP1 51-67
eIF4E
F
eIF4E + 1mM DDX3X 33-51
eIF4E
G
DDX3X WT - FLAG
DDX3X R534H - FLAG
DDX3X Δ38-44 - FLAG
DDX3X Δ38-44/R534H - FLAG
DRAQ7
FLAG
20 μm

Figure 3.7 DDX3X interacts with the translational machinery via the 38-44 residues. **(A)** Diagram of the DDX3X protein structure. DDX3X contains a helicase core, highly conserved across the DEAD-box helicase protein family, composed of two RecA-like domains, denoted as Domain I and Domain II (denoted in blue). In addition to the helicase core, the functional core of the protein also includes the NTE and CTE, which have been shown to be necessary for the RNA unwinding activity of DDX3X. Outside of the functional core there are the N and C termini, which are less conserved across the protein family, but contained regions conserved across the Ded1/DDX3X subfamily (denoted in gray). **(B)** DDX3X co-immunoprecipitation with translation machinery proteins. HEK 293T cells were transduced with FLAG tagged DDX3X WT, R534H, or 38-44ala. Immunoprecipitation was conducted for FLAG and immunoblotted for ribosome-related proteins and controls. **(C)** Comparison of eIF4E-binding-like motifs. The consensus eIF4E interacting protein motif is compared to the motifs in 4EBP1 and in DDX3X **(D)** ^{15}N HSQC spectrum for m7G bound eIF4E (in red) alone. **(E)** HSQC spectra of m7G bound eIF4E alone (in red) and with the addition of 1mM 4EBP1 peptide (blue) **(F)** HSQC spectra of m7G bound eIF4E alone (in red) and with the addition of 1 mM DDX3X peptide (green). **(G)** Immunofluorescence for DDX3X WT and mutants. Images are representative of N > 10 cells. HEK 293T cells were transduced with DDX3X-FLAG construct, fixed, and stained for anti-DDX3X and the nuclear marker DRAQ7 (Figure 3.7 G).

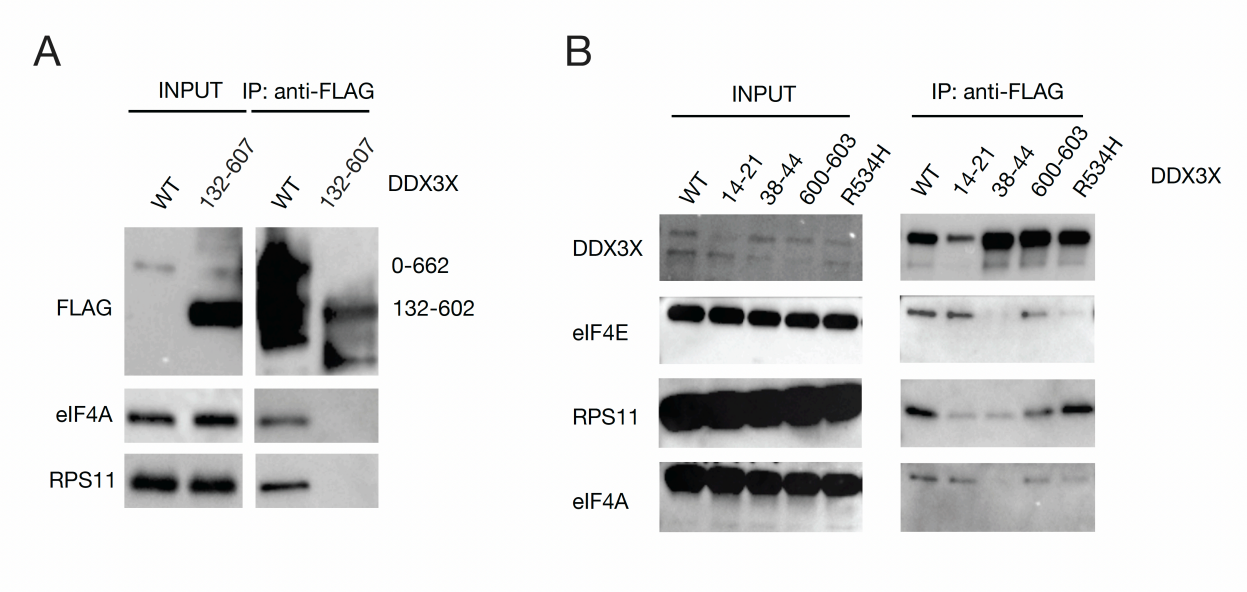

Figure 3.8 Immunprecipitation of DDX3X truncations and mutants with translational factors (A) DDX3X WT and 132-607 immunoprecipitation. HEK293t cells were lentivirally transduced with FLAG tagged DDX3X WT or 132-607, which represents its functional helicase core. Immunoprecipitation was conducted for FLAG and run on western blot, staining for ribosome-related proteins and controls. **(B)** Immunoprecipitation of DDX3X mutants. HEK293t cells were lentivirally transduced with FLAG tagged DDX3X WT or several mutants, including the helicase defective mutant R534H and three mutations in conserved sites in the N- and C-termini. Immunoprecipitation was conducted for FLAG and run on western blot, staining for ribosome-related proteins and controls.

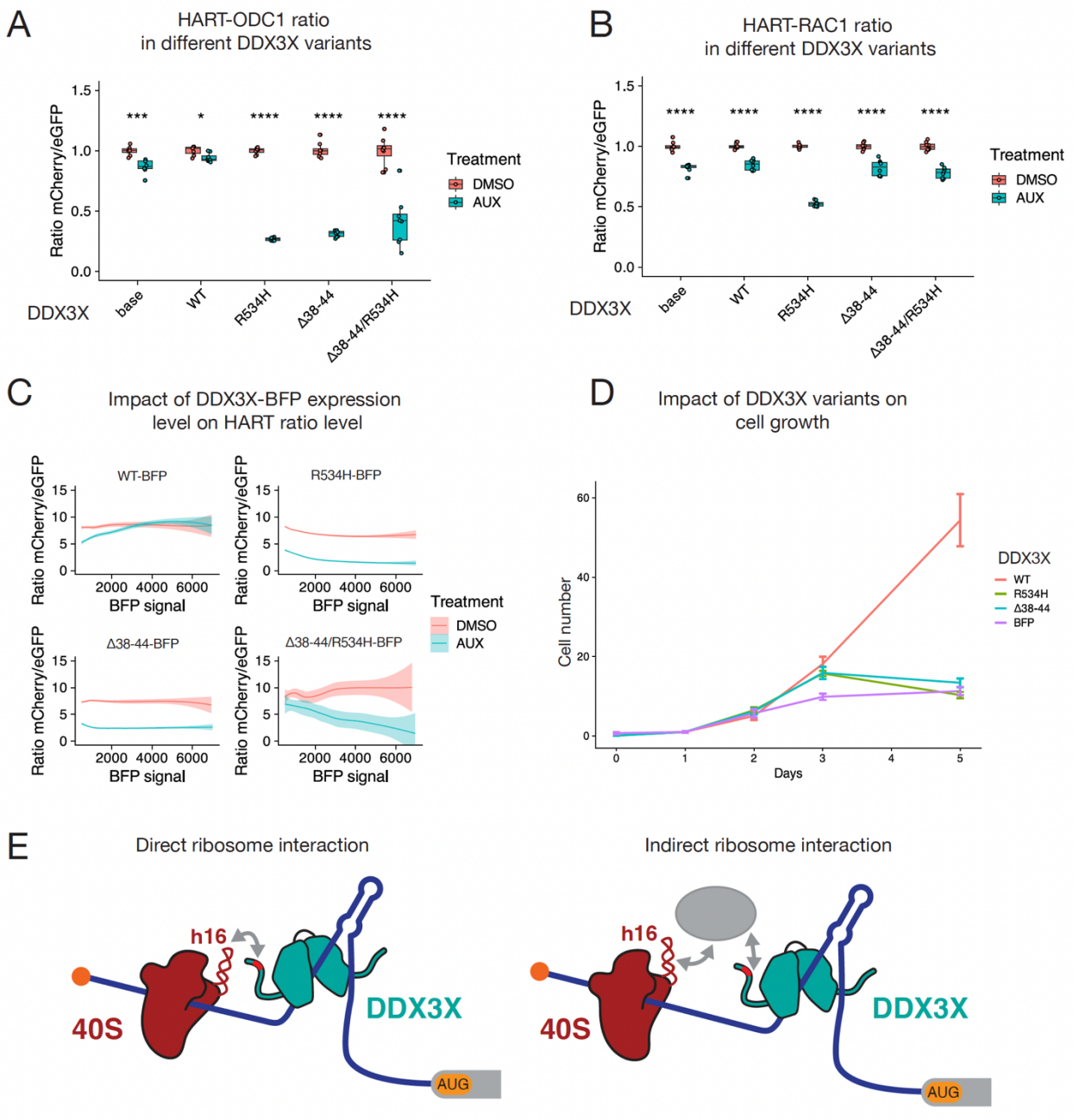
A
HART-ODC1 ratio
in different DDX3X variants
Ratio mCherry/eGFP
1.5
1.0
0.5
0.0
***
*
****
****
****
DDX3X
base
WT
R534H
Δ38-44
Δ38-44/R534H
Treatment
DMSO
AUX
B
HART-RAC1 ratio
in different DDX3X variants
Ratio mCherry/eGFP
1.5
1.0
0.5
0.0
****
****
****
****
****
DDX3X
base
WT
R534H
Δ38-44
Δ38-44/R534H
Treatment
DMSO
AUX
C
Impact of DDX3X-BFP expression
level on HART ratio level
WT-BFP
R534H-BFP
Δ38-44-BFP
Δ38-44/R534H-BFP
Ratio mCherry/eGFP
15
10
5
0
2000 4000 6000
BFP signal
Treatment
DMSO
AUX
D
Impact of DDX3X variants on
cell growth
Cell number
60
40
20
0
0
1
2
3
4
5
Days
DDX3X
WT
R534H
Δ38-44
BFP
E
Direct ribosome interaction
h16
40S
DDX3X
AUG
Indirect ribosome interaction
h16
40S
DDX3X
AUG

Figure 3.9 DDX3X 38-44ala cannot rescue translational or cell growth defects caused by the loss of DDX3X. (A-B) HART data for indicated DDX3X mutants. HCT116 degron cells were transduced with the HART-ODC1 **(A)** or HART-RAC1 **(B)** construct and different variants of DDX3X-FLAG-BFP, either WT, helicase defective R534H, 38-44ala, or the double mutant R534H/38-44ala. Cells were treated with auxin to induce loss of the endogenous DDX3X via a degron tag. After 48 hours flow cytometry was used to measure fluorescence levels, and the HART ratio (mCherry/EGFP) was calculated. Statistical significance was determined by unpaired *t*-test: ns: p > 0.05, *: p <= 0.05, **: p <= 0.01, ***: p <= 0.001, ****: p <= 0.0001. **(C)** Relationship between DDX3X-FLAG-BFP levels and HART ratio. Flow cytometry was used to measure EGFP and mCherry levels, which constitute the HART ratio, and BFP, which is a proxy for the level of DDX3X-FLAG-BFP expression. **(D)** Cell growth curve for DDX3X variants. HCT116 degron cells were transduced with DDX3X WT, R534H, 38-44ala or BFP control. After auxin was added to degrade endogenous DDX3X, CellTiter Glo was used to measure cell number and plot cell growth. **(E)** Model of DDX3X functioning in translation and its relation to the ribosome. The 38-44 residues of DDX3X (shown in red) contribute to its interaction with the translational machinery. Helix 16 has been previously identified as mediating this association, but it is unknown whether this interaction happens directly between DDX3X and the ribosome (left) or via intermediary protein(s) such as the components of the eIF4F complex (shown in grey). Our data shows that association between DDX3X and the translational machinery plays a crucial role in DDX3X's role of unwinding 5′ UTRs to allow ribosome scanning and promote translation of a subset of human mRNAs.

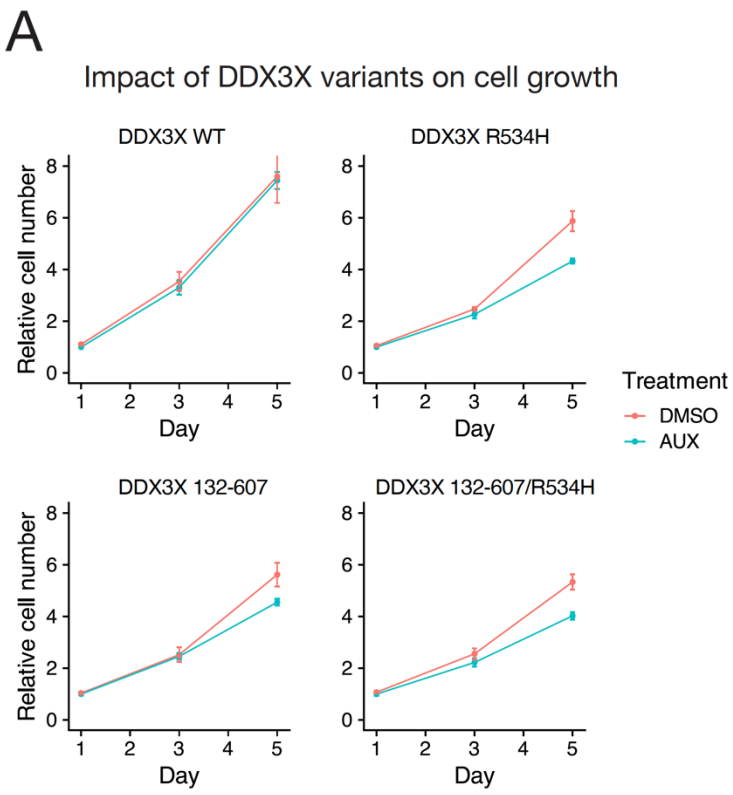

Figure 3.10 DDX3X 38-44ala cannot rescue cell growth defects (A) Cell growth curves for DDX3X variants. HCT116 degron cells where lentivirally transduced with exogenous DDX3X WT and mutants. Auxin was added to induce loss of endogenous DDX3X and cell number was measured over time with CellTiter Glo.

CONCLUDING REMARKS

Summary

The process of translation initiation, a crucial and tightly regulated step in protein synthesis, is influenced by helicases that interact with and modulate the 5' untranslated region (5′ UTR) and its structural features. These helicases unwind complex secondary structures like hairpins and g-quadruplexes, and influence uORF selection, ensuring proper regulation of ribosome scanning. Investigating the impact of helicases on translation provides deeper insights into their role as proteome regulators in both normal and diseased states. The second chapter of this dissertation outlines methods for studying helicase effects on mRNA translation initiation using in vitro transcribed luciferase 5′ UTR reporters. Two assays are described: an *in vitro* approach using cell-free lysate and an in cell approach with living cells. While the in vitro method offers precision, the in cell approach provides physiological relevance. For example, these assays showed how medulloblastoma-associated mutation R534H in DDX3X lead to decrease translation on DDX3X-sensitive reporters, suggesting a potential avenue through which mutated DDX3X leads dysfunction in a cancer setting. In addition to its application on DDX3X and similar helicases in relation to 5′ UTRs, this protocol is adaptable to explore other mRNA features and can be used to study the translational role of various factors, including RNA binding proteins, as well as the perturbation and effects caused by chemical compounds.

This third chapter or this dissertation focuses on investigating DDX3X's mRNA targets and what renders them sensitive to loss of DDX3X translation, as well as the

interaction between DDX3X and the rest of the translational machinery. Complex secondary structures were identified in the 5′ UTRs sensitive to DDX3X, and the removal of certain structures resulted in a reduction of DDX3X, suggesting that DDX3X is required for the unwinding of certain transcripts ahead of ribosome scanning. The interaction between the ribosome and DDX3X during scanning is itself incompletely. The data in this dissertation shows that the 38-44 residues of DDX3X contribute, at least partially, to the interaction with the ribosome, although whether this interaction could be either direct or mediate by other factors in the translational machinery. Experiments with HART showed that the DDX3X interaction with the translational machinery is necessary for its role in promoting translation initiation. Overall, DDX3X acts to unwind complex mRNA structures to allow for ribosome scanning across the 5′ UTR while associating with the translational machinery.

Future Directions

Gaining an understanding of interaction between DDX3X and the translational machinery will provide an insight into the dynamics of the complex but crucial interplay of different helicases and translation factors during ribosome scanning. Methods like FRET can elucidate the timing of association and disassociation of DDX3X from the ribosomal complex and might provide insight into the collaborative or competitive nature of binding to the ribosome between DDX3X and other helicases such as eIF4A and DHX29. Future studies are required to understand if any other DDX3X residues also contribute to association with the translational machinery. Further, understanding whether this association is direct between DDX3X and the ribosomal helix 16, or whether it is mediated

by eIF4G. Tools such as cryo-EM or mass spectroscopy, in conjunction with the purification of specific regions of DDX3X, can help detect direct binding with the ribosomal proteins or rRNA or with specific translation factors.

Another avenue to gain a more granular view of DDX3X's mechanism of action is to gain a deeper understanding of how the 5′ UTR structures identified in RAC1 and ODC1 contribute to sensitivity to DDX3X. Additional and larger deletions of the ODC1 may reveal if the loss of large structures also causes the reporter to lose DDX3X-sensitivity as in the case for RAC1, or whether it is due to other factors. Mutations of uAUGs and uCTGs could also lead to changes in DDX3X-sensitivity that can illuminate the role of DDX3X in regulating uORF usage and hence influence elongation initiation on the main ORF. Finally, to determine whether the deletions in RAC1 that cause the loss in sensitivity are indeed due to loss of structure and not specific sequences, insertions containing similar structures but different sequences could be re-inserted to rescue loss of DDX3X-sensitivity.

In addition to its role in dissecting specific 5′ UTRs DDX3X-sensitivities, I anticipate HART to be useful in several other settings, both for the study of DDX3X and of other helicases or translational factors. The lentiviral transduction delivery of HART, as well as its robust expression by *in vivo* tested bidirectional promoter construct, enables measurement of DDX3X-dependent translation *in vivo*. HART may be hence applied to several other models of biological function and pathogenesis, in diverse cellular lines and model systems.

HART can be employed in conjunction with Fluorescence-activated Cell Sorting to identify mutations, both in the 5′ UTR and in DDX3X itself, that alter the HART ratio. For

example, HART cells transfected with plasmids containing a deep mutational library of DDX3X and sorter with FACS based on the HART ratio could identify mutations in DDX3X that lead to high or low translation of DDX3X-sensitive transcripts. This can help obtain a gradual understanding of which residues of DDX3X contribute to its translational activity, as well as correlating mutations found in diseases with phenotypic defects at the translational initiation levels.

Its reliability as a 5′ UTR-based reporter of functional attributes in translation initiation can be effectively harnessed in tandem with expansive libraries of both naturally occurring and synthetically engineered 5′ UTRs. This combined approach facilitates a comprehensive and expansive profiling of DDX3X-mediated regulation. The synthetic 5′ UTR repertoire, comprising diverse structural variants, lengths, and sequence motifs, can serve as a broad canvas for a large-scale screening aimed at discerning structural and contextual determinants impacting DDX3X sensitivity. In a parallel vein, integration of a library of naturally occurring genomic 5′ UTRs into the HART can yield invaluable insights into the landscape of transcripts reliant on DDX3X for proficient translation. This approach offers the prospect of uncovering yet unrecognized DDX3X-sensitive transcripts, as well as the possibility of implementing in different cellular lines and models to uncover DDX3X-sensitive transcripts that manifest distinct sensitivities contingent upon diverse contexts, encompassing divergent tissue types or physiological states.

Alternatively, the versatile readout capabilities of HART, spanning both flow cytometric and microscopy, can be employed to screen for drugs and other bioactive compounds capable of modulating the behavior of DDX3X or rescuing its loss or malfunction. HART expressing cells could be grown in conjunction with loss or mutation

of DDX3X and treated with drug libraries and followed by HART ratio readout in a high-throughput format. Candidates that rescue the HART ratio might be restoring the translation phenotype by compensation or direct targeting DDX3X, and could undergo further validation and open the possibility of finding drugs treating DDX3X-related diseases.

Finally, by choosing the proper control and experimental 5′ UTRs or other sequences, HART can be adapted to measure the activity of any other helicase or translation factor in addition to DDX3X. The experiments described in this dissertation, as well as those envisioned in the future direction section, could potentially be adapted to study many other modulators of translation and their effects on regulating 5′ UTR as well as several other mRNA features such as 3′ UTRs. In conclusion, HART possess the potential to become a tool for the effective investigation of the underlying mechanisms of human mRNA translation.

REFERENCES

Acker, M. G., Kolitz, S. E., Mitchell, S. F., Nanda, J. S., & Lorsch, J. R. (2007). Reconstitution of yeast translation initiation. *Methods in Enzymology*, *430*, 111–145. https://doi.org/10.1016/S0076-6879(07)30006-2

Aitken, C. E., Beznosková, P., Vlčkova, V., Chiu, W.-L., Zhou, F., Valášek, L. S., Hinnebusch, A. G., & Lorsch, J. R. (2016). Eukaryotic translation initiation factor 3 plays distinct roles at the mRNA entry and exit channels of the ribosomal preinitiation complex. *ELife*, *5*, e20934. https://doi.org/10.7554/eLife.20934

Amendola, M., Venneri, M. A., Biffi, A., Vigna, E., & Naldini, L. (2005). Coordinate dual-gene transgenesis by lentiviral vectors carrying synthetic bidirectional promoters. *Nature Biotechnology*, *23*(1), Article 1. https://doi.org/10.1038/nbt1049

Andreou, A. Z., & Klostermeier, D. (2013). The DEAD-box helicase eIF4A. *RNA Biology*, *10*(1), 19–32. https://doi.org/10.4161/rna.21966

Andrisani, O., Liu, Q., Kehn, P., Leitner, W. W., Moon, K., Vazquez-Maldonado, N., Fingerman, I., & Gale, M. (2022). Biological functions of DEAD/DEAH-box RNA helicases in health and disease. *Nature Immunology*, *23*(3), Article 3. https://doi.org/10.1038/s41590-022-01149-7

Arrowsmith, C. H., Audia, J. E., Austin, C., Baell, J., Bennett, J., Blagg, J., Bountra, C., Brennan, P. E., Brown, P. J., Bunnage, M. E., Buser-Doepner, C., Campbell, R. M., Carter, A. J., Cohen, P., Copeland, R. A., Cravatt, B., Dahlin, J. L., Dhanak, D., Edwards, A. M., … Zuercher, W. J. (2015). The promise and peril of chemical probes. *Nature Chemical Biology*, *11*(8), 536–541. https://doi.org/10.1038/nchembio.1867

Aryanpur, P. P., Renner, D. M., Rodela, E., Mittelmeier, T. M., Byrd, A., & Bolger, T. A. (2019). The DEAD-box RNA helicase Ded1 has a role in the translational response to TORC1 inhibition. *Molecular Biology of the Cell*, *30*(17), 2171–2184. https://doi.org/10.1091/mbc.E18-11-0702

Ayalew, L. E., Patel, A. K., Gaba, A., Islam, A., & Tikoo, S. K. (2016). Bovine Adenovirus-3 pVIII Suppresses Cap-Dependent mRNA Translation Possibly by Interfering with the Recruitment of DDX3 and Translation Initiation Factors to the mRNA Cap. *Frontiers in Microbiology*, *7*, 2119. https://doi.org/10.3389/fmicb.2016.02119

Bai, Y., Zhou, K., & Doudna, J. A. (2013). Hepatitis C virus 3'UTR regulates viral translation through direct interactions with the host translation machinery. *Nucleic Acids Research*, *41*(16), 7861–7874. https://doi.org/10.1093/nar/gkt543

Bhat, M., Robichaud, N., Hulea, L., Sonenberg, N., Pelletier, J., & Topisirovic, I. (2015). Targeting the translation machinery in cancer. *Nature Reviews Drug Discovery*, *14*(4), 261–278. https://doi.org/10.1038/nrd4505

Blagden, S. P., & Willis, A. E. (2011). The biological and therapeutic relevance of mRNA translation in cancer. *Nature Reviews Clinical Oncology*, *8*(5), Article 5. https://doi.org/10.1038/nrclinonc.2011.16

Bohnsack, K. E., Yi, S., Venus, S., Jankowsky, E., & Bohnsack, M. T. (2023). Cellular functions of eukaryotic RNA helicases and their links to human diseases. *Nature Reviews Molecular Cell Biology*, 1–21. https://doi.org/10.1038/s41580-023-00628-5

Bourgeois, C. F., Mortreux, F., & Auboeuf, D. (2016). The multiple functions of RNA helicases as drivers and regulators of gene expression. *Nature Reviews Molecular Cell Biology*, *17*(7), 426–438. https://doi.org/10.1038/nrm.2016.50

Brito Querido, J., Sokabe, M., Kraatz, S., Gordiyenko, Y., Skehel, J. M., Fraser, C. S., & Ramakrishnan, V. (2020). Structure of a human 48S translational initiation complex. *Science*, *369*(6508), 1220–1227. https://doi.org/10.1126/science.aba4904

Busan, S., & Weeks, K. M. (2018). Accurate detection of chemical modifications in RNA by mutational profiling (MaP) with ShapeMapper 2. *RNA (New York, N.Y.)*, *24*(2), 143–148. https://doi.org/10.1261/rna.061945.117

Buttgereit, F., & Brand, M. D. (1995). A hierarchy of ATP-consuming processes in mammalian cells. *The Biochemical Journal*, *312 (Pt 1)*(Pt 1), 163–167. https://doi.org/10.1042/bj3120163

Cai, W., Xiong Chen, Z., Rane, G., Satendra Singh, S., Choo, Z., Wang, C., Yuan, Y., Zea Tan, T., Arfuso, F., Yap, C. T., Pongor, L. S., Yang, H., Lee, M. B., Cher Goh, B., Sethi, G., Benoukraf, T., Tergaonkar, V., & Prem Kumar, A. (2017). Wanted DEAD/H or Alive: Helicases Winding Up in Cancers. *JNCI: Journal of the National Cancer Institute*, *109*(6), djw278. https://doi.org/10.1093/jnci/djw278

Calviello, L., Venkataramanan, S., Rogowski, K. J., Wyler, E., Wilkins, K., Tejura, M., Thai, B., Krol, J., Filipowicz, W., Landthaler, M., & Floor, S. N. (2021). DDX3 depletion represses translation of mRNAs with complex 5’ UTRs. *Nucleic Acids Research*, *49*(9), 5336–5350. https://doi.org/10.1093/nar/gkab287

Calvo, S. E., Pagliarini, D. J., & Mootha, V. K. (2009). Upstream open reading frames cause widespread reduction of protein expression and are polymorphic among humans. *Proceedings of the National Academy of Sciences*, *106*(18), 7507–7512. https://doi.org/10.1073/pnas.0810916106

Chao, C.-H., Chen, C.-M., Cheng, P.-L., Shih, J.-W., Tsou, A.-P., & Lee, Y.-H. W. (2006). DDX3, a DEAD box RNA helicase with tumor growth-suppressive property and transcriptional regulation activity of the p21waf1/cip1 promoter, is a candidate tumor suppressor. *Cancer Research*, *66*(13), 6579–6588. https://doi.org/10.1158/0008-5472.CAN-05-2415

Chen, C.-Y., Chan, C.-H., Chen, C.-M., Tsai, Y.-S., Tsai, T.-Y., Wu Lee, Y.-H., & You, L.-R. (2016). Targeted inactivation of murine Ddx3x: Essential roles of Ddx3x in placentation and embryogenesis. *Human Molecular Genetics*, *25*(14), 2905–2922. https://doi.org/10.1093/hmg/ddw143

Chen, H.-H., Yu, H.-I., Cho, W.-C., & Tarn, W.-Y. (2015). DDX3 modulates cell adhesion and motility and cancer cell metastasis via Rac1-mediated signaling pathway. *Oncogene*, *34*(21), 2790–2800. https://doi.org/10.1038/onc.2014.190

Chen, H.-H., Yu, H.-I., Yang, M.-H., & Tarn, W.-Y. (2018). DDX3 Activates CBC-eIF3–Mediated Translation of uORF-Containing Oncogenic mRNAs to Promote Metastasis in HNSCC. *Cancer Research*, *78*(16), 4512–4523. https://doi.org/10.1158/0008-5472.CAN-18-0282

Chong, S. (2014). Overview of Cell-Free Protein Synthesis: Historic Landmarks, Commercial Systems, and Expanding Applications. *Current Protocols in*

Molecular Biology / Edited by Frederick M. Ausubel ... [et Al.], *108*, 16.30.1-16.30.11. https://doi.org/10.1002/0471142727.mb1630s108

Darty, K., Denise, A., & Ponty, Y. (2009). VARNA: Interactive drawing and editing of the RNA secondary structure. *Bioinformatics*, *25*(15), 1974–1975. https://doi.org/10.1093/bioinformatics/btp250

Dasmahapatra, B., Rozhon, E. J., & Schwartz, J. (1987). PBD7, a novel cell-free expression vector with efficient translation initiation signal. *Nucleic Acids Research*, *15*(9), 3933. https://doi.org/10.1093/nar/15.9.3933

De Colibus, L., Stunnenberg, M., & Geijtenbeek, T. B. H. (2022). DDX3X structural analysis: Implications in the pharmacology and innate immunity. *Current Research in Immunology*, *3*, 100–109. https://doi.org/10.1016/j.crimmu.2022.05.002

Dieterich, D. C., Hodas, J. J. L., Gouzer, G., Shadrin, I. Y., Ngo, J. T., Triller, A., Tirrell, D. A., & Schuman, E. M. (2010). In situ visualization and dynamics of newly synthesized proteins in rat hippocampal neurons. *Nature Neuroscience*, *13*(7), 897–905. https://doi.org/10.1038/nn.2580

Edery, I., Altmann, M., & Sonenberg, N. (1988). High-level synthesis in Escherichia coli of functional cap-binding eukaryotic initiation factor eIF-4E and affinity purification using a simplified cap-analog resin. *Gene*, *74*(2), 517–525. https://doi.org/10.1016/0378-1119(88)90184-9

Elfakess, R., Sinvani, H., Haimov, O., Svitkin, Y., Sonenberg, N., & Dikstein, R. (2011). Unique translation initiation of mRNAs-containing TISU element. *Nucleic Acids Research*, *39*(17), 7598–7609. https://doi.org/10.1093/nar/gkr484

Epling, L. B., Grace, C. R., Lowe, B. R., Partridge, J. F., & Enemark, E. J. (2015). Cancer-associated mutants of RNA helicase DDX3X are defective in RNA-stimulated ATP hydrolysis. *Journal of Molecular Biology*, *427*(9), 1779–1796. https://doi.org/10.1016/j.jmb.2015.02.015

Fairman-Williams, M. E., Guenther, U.-P., & Jankowsky, E. (2010). SF1 and SF2 helicases: Family matters. *Current Opinion in Structural Biology*, *20*(3), 313–324. https://doi.org/10.1016/j.sbi.2010.03.011

Floor, S. N., Barkovich, K. J., Condon, K. J., Shokat, K. M., & Doudna, J. A. (2016). Analog sensitive chemical inhibition of the DEAD-box protein DDX3. *Protein Science: A Publication of the Protein Society*, *25*(3), 638–649. https://doi.org/10.1002/pro.2857

Floor, S. N., Condon, K. J., Sharma, D., Jankowsky, E., & Doudna, J. A. (2016). Autoinhibitory Interdomain Interactions and Subfamily-specific Extensions Redefine the Catalytic Core of the Human DEAD-box Protein DDX3. *The Journal of Biological Chemistry*, *291*(5), 2412–2421. https://doi.org/10.1074/jbc.M115.700625

Floor, S. N., & Doudna, J. A. (2016). Tunable protein synthesis by transcript isoforms in human cells. *ELife*, *5*, e10921. https://doi.org/10.7554/eLife.10921

Fuller-Pace, F. V. (2013a). DEAD box RNA helicase functions in cancer. *RNA Biology*, *10*(1), 121–132. https://doi.org/10.4161/rna.23312

Fuller-Pace, F. V. (2013b). DEAD box RNA helicase functions in cancer. *RNA Biology*, *10*(1), 121–132. https://doi.org/10.4161/rna.23312

Gadek, M., Sherr, E. H., & Floor, S. N. (2023). The variant landscape and function of DDX3X in cancer and neurodevelopmental disorders. *Trends in Molecular Medicine*, *0*(0). https://doi.org/10.1016/j.molmed.2023.06.003

Galicia-Vázquez, G., Cencic, R., Robert, F., Agenor, A. Q., & Pelletier, J. (2012). A cellular response linking eIF4AI activity to eIF4AII transcription. *RNA (New York, N.Y.)*, *18*(7), 1373–1384. https://doi.org/10.1261/rna.033209.112

Gao, Z., Putnam, A. A., Bowers, H. A., Guenther, U.-P., Ye, X., Kindsfather, A., Hilliker, A. K., & Jankowsky, E. (2016). Coupling between the DEAD-box RNA helicases Ded1p and eIF4A. *ELife*, *5*, e16408. https://doi.org/10.7554/eLife.16408

Gebauer, F., & Hentze, M. W. (2004). Molecular mechanisms of translational control. *Nature Reviews Molecular Cell Biology*, *5*(10), Article 10. https://doi.org/10.1038/nrm1488

Gong, C., Krupka, J. A., Gao, J., Grigoropoulos, N. F., Giotopoulos, G., Asby, R., Screen, M., Usheva, Z., Cucco, F., Barrans, S., Painter, D., Zaini, N. B. M., Haupl, B., Bornelöv, S., Ruiz De Los Mozos, I., Meng, W., Zhou, P., Blain, A. E., Forde, S., … Hodson, D. J. (2021). Sequential inverse dysregulation of the RNA helicases DDX3X and DDX3Y facilitates MYC-driven lymphomagenesis. *Molecular Cell*, *81*(19), 4059-4075.e11. https://doi.org/10.1016/j.molcel.2021.07.041

Goodman, C. A., Pierre, P., & Hornberger, T. A. (2012). Imaging of protein synthesis with puromycin. *Proceedings of the National Academy of Sciences of the United States of America*, *109*(17), E989. https://doi.org/10.1073/pnas.1202000109

Gross, J. D., Moerke, N. J., von der Haar, T., Lugovskoy, A. A., Sachs, A. B., McCarthy, J. E. G., & Wagner, G. (2003). Ribosome loading onto the mRNA cap is driven by conformational coupling between eIF4G and eIF4E. *Cell*, *115*(6), 739–750. https://doi.org/10.1016/s0092-8674(03)00975-9

Guenther, U.-P., Weinberg, D. E., Zubradt, M. M., Tedeschi, F. A., Stawicki, B. N., Zagore, L. L., Brar, G. A., Licatalosi, D. D., Bartel, D. P., Weissman, J. S., & Jankowsky, E. (2018). The helicase Ded1p controls use of near-cognate translation initiation codons in 5' UTRs. *Nature*, *559*(7712), 130–134. https://doi.org/10.1038/s41586-018-0258-0

Gulay, S., Gupta, N., Lorsch, J. R., & Hinnebusch, A. G. (2020). Distinct interactions of eIF4A and eIF4E with RNA helicase Ded1 stimulate translation in vivo. *ELife*, *9*, e58243. https://doi.org/10.7554/eLife.58243

Gupta, N., Lorsch, J. R., & Hinnebusch, A. G. (2018). Yeast Ded1 promotes 48S translation pre-initiation complex assembly in an mRNA-specific and eIF4F-dependent manner. *ELife*, *7*, e38892. https://doi.org/10.7554/eLife.38892

Haimov, O., Sinvani, H., & Dikstein, R. (2015). Cap-dependent, scanning-free translation initiation mechanisms. *Biochimica et Biophysica Acta (BBA) - Gene Regulatory Mechanisms*, *1849*(11), 1313–1318. https://doi.org/10.1016/j.bbagrm.2015.09.006

Hao, P., Yu, J., Ward, R., Liu, Y., Hao, Q., An, S., & Xu, T. (2020). Eukaryotic translation initiation factors as promising targets in cancer therapy. *Cell Communication and Signaling*, *18*(1), 175. https://doi.org/10.1186/s12964-020-00607-9

Harms, U., Andreou, A. Z., Gubaev, A., & Klostermeier, D. (2014). EIF4B, eIF4G and RNA regulate eIF4A activity in translation initiation by modulating the eIF4A conformational cycle. *Nucleic Acids Research*, *42*(12), 7911–7922. https://doi.org/10.1093/nar/gku440

Heaton, S. M., Gorry, P. R., & Borg, N. A. (2023). DExD/H-box helicases in HIV-1 replication and their inhibition. *Trends in Microbiology*, *31*(4), 393–404. https://doi.org/10.1016/j.tim.2022.11.001

Heerma van Voss, M. R., van Kempen, P. M. W., Noorlag, R., van Diest, P. J., Willems, S. M., & Raman, V. (2015). DDX3 has divergent roles in head and neck squamous cell carcinomas in smoking versus non-smoking patients. *Oral Diseases*, *21*(2), 270–271. https://doi.org/10.1111/odi.12299

Hernández-Díaz, T., Valiente-Echeverría, F., & Soto-Rifo, R. (2021). RNA Helicase DDX3: A Double-Edged Sword for Viral Replication and Immune Signaling. *Microorganisms*, *9*(6), 1206. https://doi.org/10.3390/microorganisms9061206

Hershey, J. W. B., Sonenberg, N., & Mathews, M. B. (2019). Principles of Translational Control. *Cold Spring Harbor Perspectives in Biology*, *11*(9), a032607. https://doi.org/10.1101/cshperspect.a032607

Hilbert, M., Karow, A. R., & Klostermeier, D. (2009). The mechanism of ATP-dependent RNA unwinding by DEAD box proteins. *Biological Chemistry*, *390*(12), 1237–1250. https://doi.org/10.1515/BC.2009.135

Hilliker, A., Gao, Z., Jankowsky, E., & Parker, R. (2011). The DEAD-box protein Ded1 modulates translation by the formation and resolution of an eIF4F-mRNA

complex. *Molecular Cell*, *43*(6), 962–972. https://doi.org/10.1016/j.molcel.2011.08.008

Hinnebusch, A. G., Ivanov, I. P., & Sonenberg, N. (2016). Translational control by 5'-untranslated regions of eukaryotic mRNAs. *Science (New York, N.Y.)*, *352*(6292), 1413–1416. https://doi.org/10.1126/science.aad9868

Hk, L., Rt, M., Hd, H., Ch, C., Ya, C., Yw, C., Lr, Y., Cm, C., & Yh, L. (2016). DDX3 Represses Stemness by Epigenetically Modulating Tumor-suppressive miRNAs in Hepatocellular Carcinoma. *Scientific Reports*, *6*. https://doi.org/10.1038/srep28637

Hoye, M. L., Calviello, L., Poff, A. J., Ejimogu, N.-E., Newman, C. R., Montgomery, M. D., Ou, J., Floor, S. N., & Silver, D. L. (2022). Aberrant cortical development is driven by impaired cell cycle and translational control in a DDX3X syndrome model. *ELife*, *11*, e78203. https://doi.org/10.7554/eLife.78203

Ingolia, N. T., Hussmann, J. A., & Weissman, J. S. (2019). Ribosome Profiling: Global Views of Translation. *Cold Spring Harbor Perspectives in Biology*, *11*(5), a032698. https://doi.org/10.1101/cshperspect.a032698

Iwasaki, S., Floor, S. N., & Ingolia, N. T. (2016). Rocaglates convert DEAD-box protein eIF4A into a sequence-selective translational repressor. *Nature*, *534*(7608), 558–561. https://doi.org/10.1038/nature17978

Jishi, A., Qi, X., & Miranda, H. C. (2021). Implications of mRNA translation dysregulation for neurological disorders. *Seminars in Cell & Developmental Biology*, *114*, 11–19. https://doi.org/10.1016/j.semcdb.2020.09.005

Joshi, B., Cameron, A., & Jagus, R. (2004). Characterization of mammalian eIF4E-family members. *European Journal of Biochemistry*, *271*(11), 2189–2203. https://doi.org/10.1111/j.1432-1033.2004.04149.x

Kafri, M., Metzl-Raz, E., Jona, G., & Barkai, N. (2016). The Cost of Protein Production. *Cell Reports*, *14*(1), 22–31. https://doi.org/10.1016/j.celrep.2015.12.015

Kozak, M. (1990). Downstream secondary structure facilitates recognition of initiator codons by eukaryotic ribosomes. *Proceedings of the National Academy of Sciences*, *87*(21), 8301–8305. https://doi.org/10.1073/pnas.87.21.8301

Kozak, M. (1991). Structural features in eukaryotic mRNAs that modulate the initiation of translation. *The Journal of Biological Chemistry*, *266*(30), 19867–19870.

Kozak, M. (2002). Pushing the limits of the scanning mechanism for initiation of translation. *Gene*, *299*(1), 1–34. https://doi.org/10.1016/S0378-1119(02)01056-9

Kumar, P., Hellen, C. U. T., & Pestova, T. V. (2016). Toward the mechanism of eIF4F-mediated ribosomal attachment to mammalian capped mRNAs. *Genes & Development*, *30*(13), 1573–1588. https://doi.org/10.1101/gad.282418.116

Kwon, J., Choi, H., & Han, C. (2022). A Dual Role of DDX3X in dsRNA-Derived Innate Immune Signaling. *Frontiers in Molecular Biosciences*, *9*, 912727. https://doi.org/10.3389/fmolb.2022.912727

Lai, M.-C., Chang, W.-C., Shieh, S.-Y., & Tarn, W.-Y. (2010). DDX3 Regulates Cell Growth through Translational Control of Cyclin E1. *Molecular and Cellular Biology*, *30*(22), 5444–5453. https://doi.org/10.1128/MCB.00560-10

Lai, M.-C., Lee, Y.-H. W., & Tarn, W.-Y. (2008). The DEAD-Box RNA Helicase DDX3 Associates with Export Messenger Ribonucleoproteins as well asTip-associated

Protein and Participates in Translational Control. *Molecular Biology of the Cell*, *19*(9), 3847–3858. https://doi.org/10.1091/mbc.E07-12-1264

Lai, M.-C., Sun, H. S., Wang, S.-W., & Tarn, W.-Y. (2016). DDX3 functions in antiviral innate immunity through translational control of PACT. *The FEBS Journal*, *283*(1), 88–101. https://doi.org/10.1111/febs.13553

Lee, A. S. Y., Kranzusch, P. J., & Cate, J. H. D. (2015). EIF3 targets cell-proliferation messenger RNAs for translational activation or repression. *Nature*, *522*(7554), 111–114. https://doi.org/10.1038/nature14267

Lee, C.-H., Lin, S.-H., Yang, S.-F., Yang, S.-M., Chen, M.-K., Lee, H., Ko, J.-L., Chen, C.-J., & Yeh, K.-T. (2014). Low/negative expression of DDX3 might predict poor prognosis in non-smoker patients with oral cancer. *Oral Diseases*, *20*(1), 76–83. https://doi.org/10.1111/odi.12076

Lee, L. J., Papadopoli, D., Jewer, M., del Rincon, S., Topisirovic, I., Lawrence, M. G., & Postovit, L.-M. (2021). Cancer Plasticity: The Role of mRNA Translation. *Trends in Cancer*, *7*(2), 134–145. https://doi.org/10.1016/j.trecan.2020.09.005

Lennox, A. L., Hoye, M. L., Jiang, R., Johnson-Kerner, B. L., Suit, L. A., Venkataramanan, S., Sheehan, C. J., Alsina, F. C., Fregeau, B., Aldinger, K. A., Moey, C., Lobach, I., Afenjar, A., Babovic-Vuksanovic, D., Bézieau, S., Blackburn, P. R., Bunt, J., Burglen, L., Campeau, P. M., … Sherr, E. H. (2020). Pathogenic DDX3X mutations impair RNA metabolism and neurogenesis during fetal cortical development. *Neuron*, *106*(3), 404-420.e8. https://doi.org/10.1016/j.neuron.2020.01.042

Leppek, K., Das, R., & Barna, M. (2018). Functional 5’ UTR mRNA structures in eukaryotic translation regulation and how to find them. *Nature Reviews. Molecular Cell Biology*, *19*(3), 158–174. https://doi.org/10.1038/nrm.2017.103

Levy, T., Siper, P. M., Lerman, B., Halpern, D., Zweifach, J., Belani, P., Thurm, A., Kleefstra, T., Berry-Kravis, E., Buxbaum, J. D., & Grice, D. E. (2023). DDX3X Syndrome: Summary of Findings and Recommendations for Evaluation and Care. *Pediatric Neurology*, *138*, 87–94. https://doi.org/10.1016/j.pediatrneurol.2022.10.009

Linder, P., & Jankowsky, E. (2011). From unwinding to clamping—The DEAD box RNA helicase family. *Nature Reviews Molecular Cell Biology*, *12*(8), 505–516. https://doi.org/10.1038/nrm3154

Lorenz, R., Bernhart, S. H., Höner zu Siederdissen, C., Tafer, H., Flamm, C., Stadler, P. F., & Hofacker, I. L. (2011). ViennaRNA Package 2.0. *Algorithms for Molecular Biology*, *6*(1), 26. https://doi.org/10.1186/1748-7188-6-26

Marintchev, A., Edmonds, K. A., Marintcheva, B., Hendrickson, E., Oberer, M., Suzuki, C., Herdy, B., Sonenberg, N., & Wagner, G. (2009). Topology and Regulation of the Human eIF4A/4G/4H Helicase Complex in Translation Initiation. *Cell*, *136*(3), 447–460. https://doi.org/10.1016/j.cell.2009.01.014

Martin, F., Barends, S., Jaeger, S., Schaeffer, L., Prongidi-Fix, L., & Eriani, G. (2011). Cap-assisted internal initiation of translation of histone H4. *Molecular Cell*, *41*(2), 197–209. https://doi.org/10.1016/j.molcel.2010.12.019

Merz, C., Urlaub, H., Will, C. L., & Lührmann, R. (2007). Protein composition of human mRNPs spliced in vitro and differential requirements for mRNP protein recruitment. *RNA*, *13*(1), 116–128. https://doi.org/10.1261/rna.336807

Mitschka, S., & Mayr, C. (2021). Endogenous p53 expression in human and mouse is not regulated by its 3′UTR. *ELife*, *10*, e65700. https://doi.org/10.7554/eLife.65700

Mitschka, S., & Mayr, C. (2022). Context-specific regulation and function of mRNA alternative polyadenylation. *Nature Reviews Molecular Cell Biology*, *23*(12), Article 12. https://doi.org/10.1038/s41580-022-00507-5

Mo, J., Liang, H., Su, C., Li, P., Chen, J., & Zhang, B. (2021). DDX3X: Structure, physiologic functions and cancer. *Molecular Cancer*, *20*(1), 38. https://doi.org/10.1186/s12943-021-01325-7

Murat, P., Marsico, G., Herdy, B., Ghanbarian, A., Portella, G., & Balasubramanian, S. (2018). RNA G-quadruplexes at upstream open reading frames cause DHX36- and DHX9-dependent translation of human mRNAs. *Genome Biology*, *19*(1), 229. https://doi.org/10.1186/s13059-018-1602-2

Naineni, S. K., Itoua Maïga, R., Cencic, R., Putnam, A. A., Amador, L. A., Rodriguez, A. D., Jankowsky, E., & Pelletier, J. (2020). A comparative study of small molecules targeting eIF4A. *RNA*, *26*(5), 541–549. https://doi.org/10.1261/rna.072884.119

Nashchekin, D., Zhao, J., Visa, N., & Daneholt, B. (2006). A novel Ded1-like RNA helicase interacts with the Y-box protein ctYB-1 in nuclear mRNP particles and in polysomes. *The Journal of Biological Chemistry*, *281*(20), 14263–14272. https://doi.org/10.1074/jbc.M600262200

Natsume, T., Kiyomitsu, T., Saga, Y., & Kanemaki, M. T. (2016). Rapid Protein Depletion in Human Cells by Auxin-Inducible Degron Tagging with Short Homology Donors. *Cell Reports*, *15*(1), 210–218. https://doi.org/10.1016/j.celrep.2016.03.001

Nussbacher, J. K., & Yeo, G. W. (2018). Systematic Discovery of RNA Binding Proteins that Regulate MicroRNA Levels. *Molecular Cell*, *69*(6), 1005-1016.e7. https://doi.org/10.1016/j.molcel.2018.02.012

Oh, S., Flynn, R. A., Floor, S. N., Purzner, J., Martin, L., Do, B. T., Schubert, S., Vaka, D., Morrissy, S., Li, Y., Kool, M., Hovestadt, V., Jones, D. T. W., Northcott, P. A., Risch, T., Warnatz, H.-J., Yaspo, M.-L., Adams, C. M., Leib, R. D., … Cho, Y.-J. (2016). Medulloblastoma-associated DDX3 variant selectively alters the translational response to stress. *Oncotarget*, *7*(19), 28169–28182. https://doi.org/10.18632/oncotarget.8612

Parsyan, A., Shahbazian, D., Martineau, Y., Petroulakis, E., Alain, T., Larsson, O., Mathonnet, G., Tettweiler, G., Hellen, C. U., Pestova, T. V., Svitkin, Y. V., & Sonenberg, N. (2009). The helicase protein DHX29 promotes translation initiation, cell proliferation, and tumorigenesis. *Proceedings of the National Academy of Sciences*, *106*(52), 22217–22222. https://doi.org/10.1073/pnas.0909773106

Parsyan, A., Svitkin, Y., Shahbazian, D., Gkogkas, C., Lasko, P., Merrick, W. C., & Sonenberg, N. (2011). mRNA helicases: The tacticians of translational control. *Nature Reviews Molecular Cell Biology*, *12*(4), 235–245. https://doi.org/10.1038/nrm3083

Perfetto, M., Xu, X., Lu, C., Shi, Y., Yousaf, N., Li, J., Yien, Y. Y., & Wei, S. (2021). The RNA helicase DDX3 induces neural crest by promoting AKT activity. *Development (Cambridge, England)*, *148*(2), dev184341. https://doi.org/10.1242/dev.184341

Pestova, T. V., & Kolupaeva, V. G. (2002). The roles of individual eukaryotic translation initiation factors in ribosomal scanning and initiation codon selection. *Genes & Development*, *16*(22), 2906–2922. https://doi.org/10.1101/gad.1020902

Phung, B., Cieśla, M., Sanna, A., Guzzi, N., Beneventi, G., Cao Thi Ngoc, P., Lauss, M., Cabrita, R., Cordero, E., Bosch, A., Rosengren, F., Häkkinen, J., Griewank, K., Paschen, A., Harbst, K., Olsson, H., Ingvar, C., Carneiro, A., Tsao, H., … Jönsson, G. (2019). The X-Linked DDX3X RNA Helicase Dictates Translation Reprogramming and Metastasis in Melanoma. *Cell Reports*, *27*(12), 3573-3586.e7. https://doi.org/10.1016/j.celrep.2019.05.069

Pisarev, A. V., Shirokikh, N. E., & Hellen, C. U. T. (2005). Translation initiation by factor-independent binding of eukaryotic ribosomes to internal ribosomal entry sites. *Comptes Rendus Biologies*, *328*(7), 589–605. https://doi.org/10.1016/j.crvi.2005.02.004

Pisareva, V. P., Pisarev, A. V., Komar, A. A., Hellen, C. U. T., & Pestova, T. V. (2008). Translation initiation on mammalian mRNAs with structured 5'UTRs requires DExH-box protein DHX29. *Cell*, *135*(7), 1237–1250. https://doi.org/10.1016/j.cell.2008.10.037

Rao, S., Lungu, C., Crespo, R., Steijaert, T. H., Gorska, A., Palstra, R.-J., Prins, H. A. B., van Ijcken, W., Mueller, Y. M., van Kampen, J. J. A., Verbon, A., Katsikis, P.

D., Boucher, C. A. B., Rokx, C., Gruters, R. A., & Mahmoudi, T. (2021). Selective cell death in HIV-1-infected cells by DDX3 inhibitors leads to depletion of the inducible reservoir. *Nature Communications*, *12*(1), Article 1. https://doi.org/10.1038/s41467-021-22608-z

Richter, J. D., & Sonenberg, N. (2005). Regulation of cap-dependent translation by eIF4E inhibitory proteins. *Nature*, *433*(7025), 477–480. https://doi.org/10.1038/nature03205

Rio, D. C. (Ed.). (2011). *RNA: A laboratory manual*. Cold Spring Harbor Laboratory Press.

Rio, D. C. (2013). Expression and purification of active recombinant T7 RNA polymerase from E. coli. *Cold Spring Harbor Protocols*, *2013*(11), pdb.prot078527. https://doi.org/10.1101/pdb.prot078527

Rio, D. C. (2015). Denaturation and Electrophoresis of RNA with Glyoxal. *Cold Spring Harbor Protocols*, *2015*(2), pdb.prot081000. https://doi.org/10.1101/pdb.prot081000

Rolfe, D. F., & Brown, G. C. (1997). Cellular energy utilization and molecular origin of standard metabolic rate in mammals. *Physiological Reviews*, *77*(3), 731–758. https://doi.org/10.1152/physrev.1997.77.3.731

Roux, P. P., & Topisirovic, I. (2018). Signaling Pathways Involved in the Regulation of mRNA Translation. *Molecular and Cellular Biology*, *38*(12), e00070-18. https://doi.org/10.1128/MCB.00070-18

Ryan, C. S., & Schröder, M. (2022). The human DEAD-box helicase DDX3X as a regulator of mRNA translation. *Frontiers in Cell and Developmental Biology*, *10*. https://www.frontiersin.org/articles/10.3389/fcell.2022.1033684

Sachs, A. B., & Varani, G. (2000). Eukaryotic translation initiation: There are (at least) two sides to every story. *Nature Structural Biology*, *7*(5), 356–361. https://doi.org/10.1038/75120

Saikruang, W., Ang Yan Ping, L., Abe, H., Kasumba, D. M., Kato, H., & Fujita, T. (2022). The RNA helicase DDX3 promotes IFNB transcription via enhancing IRF-3/p300 holocomplex binding to the IFNB promoter. *Scientific Reports*, *12*(1), Article 1. https://doi.org/10.1038/s41598-022-07876-z

Samir, P., & Kanneganti, T.-D. (2022). DEAD/H-Box Helicases in Immunity, Inflammation, Cell Differentiation, and Cell Death and Disease. *Cells*, *11*(10), 1608. https://doi.org/10.3390/cells11101608

Samir, P., Kesavardhana, S., Patmore, D. M., Gingras, S., Malireddi, R. K. S., Karki, R., Guy, C. S., Briard, B., Place, D. E., Bhattacharya, A., Sharma, B. R., Nourse, A., King, S. V., Pitre, A., Burton, A. R., Pelletier, S., Gilbertson, R. J., & Kanneganti, T.-D. (2019). DDX3X acts as a live-or-die checkpoint in stressed cells by regulating NLRP3 inflammasome. *Nature*, *573*(7775), 590–594. https://doi.org/10.1038/s41586-019-1551-2

Sarkar, M., & Ghosh, M. K. (2016). DEAD box RNA helicases: Crucial regulators of gene expression and oncogenesis. *Frontiers in Bioscience-Landmark*, *21*(2), Article 2. https://doi.org/10.2741/4386

Sauer, M., Juranek, S. A., Marks, J., De Magis, A., Kazemier, H. G., Hilbig, D., Benhalevy, D., Wang, X., Hafner, M., & Paeschke, K. (2019). DHX36 prevents the accumulation of translationally inactive mRNAs with G4-structures in untranslated regions. *Nature Communications*, *10*(1), 2421. https://doi.org/10.1038/s41467-019-10432-5

Secchi, M., Lodola, C., Garbelli, A., Bione, S., & Maga, G. (2022). DEAD-Box RNA Helicases DDX3X and DDX5 as Oncogenes or Oncosuppressors: A Network Perspective. *Cancers*, *14*(15), 3820. https://doi.org/10.3390/cancers14153820

Sen, N. D., Zhou, F., Harris, M. S., Ingolia, N. T., & Hinnebusch, A. G. (2016). EIF4B stimulates translation of long mRNAs with structured 5' UTRs and low closed-loop potential but weak dependence on eIF4G. *Proceedings of the National Academy of Sciences of the United States of America*, *113*(38), 10464–10472. https://doi.org/10.1073/pnas.1612398113

Sen, N. D., Zhou, F., Ingolia, N. T., & Hinnebusch, A. G. (2015). Genome-wide analysis of translational efficiency reveals distinct but overlapping functions of yeast DEAD-box RNA helicases Ded1 and eIF4A. *Genome Research*, *25*(8), 1196–1205. https://doi.org/10.1101/gr.191601.115

Sengoku, T., Nureki, O., Nakamura, A., Kobayashi, S., & Yokoyama, S. (2006). Structural Basis for RNA Unwinding by the DEAD-Box Protein Drosophila Vasa. *Cell*, *125*(2), 287–300. https://doi.org/10.1016/j.cell.2006.01.054

Sharma, D., & Jankowsky, E. (2014). The Ded1/DDX3 subfamily of DEAD-box RNA helicases. *Critical Reviews in Biochemistry and Molecular Biology*, *49*(4), 343–360. https://doi.org/10.3109/10409238.2014.931339

Shih, J.-W., Tsai, T.-Y., Chao, C.-H., & Wu Lee, Y.-H. (2008). Candidate tumor suppressor DDX3 RNA helicase specifically represses cap-dependent translation by acting as an eIF4E inhibitory protein. *Oncogene*, *27*(5), 700–714. https://doi.org/10.1038/sj.onc.1210687

Shih, J.-W., Wang, W.-T., Tsai, T.-Y., Kuo, C.-Y., Li, H.-K., & Wu Lee, Y.-H. (2012). Critical roles of RNA helicase DDX3 and its interactions with eIF4E/PABP1 in stress granule assembly and stress response. *The Biochemical Journal*, *441*(1), 119–129. https://doi.org/10.1042/BJ20110739

Sinvani, H., Haimov, O., Svitkin, Y., Sonenberg, N., Tamarkin-Ben-Harush, A., Viollet, B., & Dikstein, R. (2015). Translational tolerance of mitochondrial genes to metabolic energy stress involves TISU and eIF1-eIF4GI cooperation in start codon selection. *Cell Metabolism*, *21*(3), 479–492. https://doi.org/10.1016/j.cmet.2015.02.010

Smola, M. J., Rice, G. M., Busan, S., Siegfried, N. A., & Weeks, K. M. (2015). Selective 2′-hydroxyl acylation analyzed by primer extension and mutational profiling (SHAPE-MaP) for direct, versatile and accurate RNA structure analysis. *Nature Protocols*, *10*(11), Article 11. https://doi.org/10.1038/nprot.2015.103

Smola, M. J., & Weeks, K. M. (2018). In-cell RNA structure probing with SHAPE-MaP. *Nature Protocols*, *13*(6), Article 6. https://doi.org/10.1038/nprot.2018.010

Sonenberg, N., & Hinnebusch, A. G. (2009). Regulation of translation initiation in eukaryotes: Mechanisms and biological targets. *Cell*, *136*(4), 731–745. https://doi.org/10.1016/j.cell.2009.01.042

Song, H., & Ji, X. (2019). The mechanism of RNA duplex recognition and unwinding by DEAD-box helicase DDX3X. *Nature Communications*, *10*(1), Article 1. https://doi.org/10.1038/s41467-019-11083-2

Sonneveld, S., Verhagen, B. M. P., & Tanenbaum, M. E. (2020). Heterogeneity in mRNA Translation. *Trends in Cell Biology*, *30*(8), 606–618. https://doi.org/10.1016/j.tcb.2020.04.008

Soto-Rifo, R., & Ohlmann, T. (2013). The role of the DEAD-box RNA helicase DDX3 in mRNA metabolism. *WIREs RNA*, *4*(4), 369–385. https://doi.org/10.1002/wrna.1165

Soto-Rifo, R., Rubilar, P. S., Limousin, T., de Breyne, S., Décimo, D., & Ohlmann, T. (2012). DEAD-box protein DDX3 associates with eIF4F to promote translation of selected mRNAs. *The EMBO Journal*, *31*(18), 3745–3756. https://doi.org/10.1038/emboj.2012.220

Soto-Rifo, R., Rubilar, P. S., & Ohlmann, T. (2013). The DEAD-box helicase DDX3 substitutes for the cap-binding protein eIF4E to promote compartmentalized translation initiation of the HIV-1 genomic RNA. *Nucleic Acids Research*, *41*(12), 6286–6299. https://doi.org/10.1093/nar/gkt306

Soulat, D., Bürckstümmer, T., Westermayer, S., Goncalves, A., Bauch, A., Stefanovic, A., Hantschel, O., Bennett, K. L., Decker, T., & Superti-Furga, G. (2008). The DEAD-box helicase DDX3X is a critical component of the TANK-binding kinase 1-dependent innate immune response. *The EMBO Journal*, *27*(15), 2135–2146. https://doi.org/10.1038/emboj.2008.126

Stransky, N., Egloff, A. M., Tward, A. D., Kostic, A. D., Cibulskis, K., Sivachenko, A., Kryukov, G. V., Lawrence, M. S., Sougnez, C., McKenna, A., Shefler, E., Ramos, A. H., Stojanov, P., Carter, S. L., Voet, D., Cortés, M. L., Auclair, D., Berger, M. F., Saksena, G., … Grandis, J. R. (2011). The mutational landscape of head and neck squamous cell carcinoma. *Science (New York, N.Y.)*, *333*(6046), 1157–1160. https://doi.org/10.1126/science.1208130

Sweeney, T. R., Dhote, V., Guca, E., Hellen, C. U. T., Hashem, Y., & Pestova, T. V. (2021). Functional role and ribosomal position of the unique N-terminal region of DHX29, a factor required for initiation on structured mammalian mRNAs. *Nucleic Acids Research*, *49*(22), 12955–12969. https://doi.org/10.1093/nar/gkab1192

Szappanos, D., Tschismarov, R., Perlot, T., Westermayer, S., Fischer, K., Platanitis, E., Kallinger, F., Novatchkova, M., Lassnig, C., Müller, M., Sexl, V., Bennett, K. L., Foong-Sobis, M., Penninger, J. M., & Decker, T. (2018). The RNA helicase DDX3X is an essential mediator of innate antimicrobial immunity. *PLoS Pathogens*, *14*(11), e1007397. https://doi.org/10.1371/journal.ppat.1007397

Tabassum, S., & Ghosh, M. K. (2023). DEAD-box RNA helicases with special reference to p68: Unwinding their biology, versatility, and therapeutic opportunity in cancer. *Genes & Diseases*, *10*(4), 1220–1241. https://doi.org/10.1016/j.gendis.2022.02.008

Tanner, N. K., & Linder, P. (2001). DExD/H Box RNA Helicases: From Generic Motors to Specific Dissociation Functions. *Molecular Cell*, *8*(2), 251–262. https://doi.org/10.1016/S1097-2765(01)00329-X

Taschuk, F., & Cherry, S. (2020). DEAD-Box Helicases: Sensors, Regulators, and Effectors for Antiviral Defense. *Viruses*, *12*(2), 181. https://doi.org/10.3390/v12020181

Trainor, B. M., & Shcherbik, N. (2021). Short and Sweet: Viral 5`-UTR as a Canonical and Non-Canonical Translation Initiation Switch. *Journal of Cellular Immunology*, *3*(5), 296–304. https://doi.org/10.33696/immunology.3.110

Tsai, T.-Y., Wang, W.-T., Li, H.-K., Chen, W.-J., Tsai, Y.-H., Chao, C.-H., & Wu Lee, Y.-H. (2017). RNA helicase DDX3 maintains lipid homeostasis through upregulation of the microsomal triglyceride transfer protein by interacting with HNF4 and SHP. *Scientific Reports*, *7*(1), Article 1. https://doi.org/10.1038/srep41452

Valentin-Vega, Y. A., Wang, Y.-D., Parker, M., Patmore, D. M., Kanagaraj, A., Moore, J., Rusch, M., Finkelstein, D., Ellison, D. W., Gilbertson, R. J., Zhang, J., Kim, H. J., & Taylor, J. P. (2016). Cancer-associated DDX3X mutations drive stress granule assembly and impair global translation. *Scientific Reports*, *6*, 25996. https://doi.org/10.1038/srep25996

van Voss, M. R. H., van Diest, P. J., & Raman, V. (2017). Targeting RNA helicases in cancer: The translation trap. *Biochimica et Biophysica Acta*, *1868*(2), 510–520. https://doi.org/10.1016/j.bbcan.2017.09.006

Venkataramanan, S., Gadek, M., Calviello, L., Wilkins, K., & Floor, S. N. (2021). DDX3X and DDX3Y are redundant in protein synthesis. *RNA*, *27*(12), 1577–1588. https://doi.org/10.1261/rna.078926.121

von der Haar, T., Gross, J. D., Wagner, G., & McCarthy, J. E. G. (2004). The mRNA cap-binding protein eIF4E in post-transcriptional gene expression. *Nature Structural & Molecular Biology*, *11*(6), 503–511. https://doi.org/10.1038/nsmb779

Weis, K., & Hondele, M. (2022). The Role of DEAD-Box ATPases in Gene Expression and the Regulation of RNA–Protein Condensates. *Annual Review of Biochemistry*, *91*(1), 197–219. https://doi.org/10.1146/annurev-biochem-032620-105429

Wilkie, G. S., Dickson, K. S., & Gray, N. K. (2003). Regulation of mRNA translation by 5′- and 3′-UTR-binding factors. *Trends in Biochemical Sciences*, *28*(4), 182–188. https://doi.org/10.1016/S0968-0004(03)00051-3

Wilkins, K. C., Venkataramanan, S., & Floor, S. N. (2022). Lysate and cell-based assays to probe the translational role of RNA helicases. In *Methods in Enzymology*. Academic Press. https://doi.org/10.1016/bs.mie.2022.03.032

Wurm, J. P., Glowacz, K.-A., & Sprangers, R. (2021). Structural basis for the activation of the DEAD-box RNA helicase DbpA by the nascent ribosome. *Proceedings of the National Academy of Sciences*, *118*(35), e2105961118. https://doi.org/10.1073/pnas.2105961118

Yedavalli, V. S. R. K., Neuveut, C., Chi, Y., Kleiman, L., & Jeang, K.-T. (2004). Requirement of DDX3 DEAD Box RNA Helicase for HIV-1 Rev-RRE Export Function. *Cell*, *119*(3), 381–392. https://doi.org/10.1016/j.cell.2004.09.029

Zhao, L., Mao, Y., Zhao, Y., & He, Y. (2016). DDX3X promotes the biogenesis of a subset of miRNAs and the potential roles they played in cancer development. *Scientific Reports*, *6*, 32739. https://doi.org/10.1038/srep32739

Zhao, L., Mao, Y., Zhou, J., Zhao, Y., Cao, Y., & Chen, X. (2016). Multifunctional DDX3: Dual roles in various cancer development and its related signaling pathways. *American Journal of Cancer Research*, *6*(2), 387–402.

Zhou, Z., Licklider, L. J., Gygi, S. P., & Reed, R. (2002). Comprehensive proteomic analysis of the human spliceosome. *Nature*, *419*(6903), Article 6903. https://doi.org/10.1038/nature01031

Zuker, M., & Stiegler, P. (1981). Optimal computer folding of large RNA sequences using thermodynamics and auxiliary information. *Nucleic Acids Research*, *9*(1), 133–148.

Publishing Agreement

It is the policy of the University to encourage open access and broad distribution of all theses, dissertations, and manuscripts. The Graduate Division will facilitate the distribution of UCSF theses, dissertations, and manuscripts to the UCSF Library for open access and distribution. UCSF will make such theses, dissertations, and manuscripts accessible to the public and will take reasonable steps to preserve these works in perpetuity.

I hereby grant the non-exclusive, perpetual right to The Regents of the University of California to reproduce, publicly display, distribute, preserve, and publish copies of my thesis, dissertation, or manuscript in any form or media, now existing or later derived, including access online for teaching, research, and public service purposes.

DocuSigned by:
B4F066BD57B2428...
Author Signature

8/21/2023
Date